

**ANALYSIS OF TRENDS AND  
VARIABILITY OF WATER LEVELS**

*Santamaria/05*

**Dissertation**

**Sara Santamaria Aguilar**



# **ANALYSIS OF TRENDS AND VARIABILITY OF WATER LEVELS**

**Dissertation**

in fulfilment of the requirements for the Degree “Dr. rer. Nat.”  
of the Faculty of Mathematics and Natural Sciences  
at the Christian-Albrechts University of Kiel

submitted by

**Sara Santamaria Aguilar**

Kiel, November 2020

**About the cover picture:**

The cover picture is a painting of the artist Julian Santamaria. It is part of the collection "Mi mar" and depicts a calm Cantabrian Sea at the Comillas coast (Spain).

**First Examiner: Prof. Dr. Athanasios T. Vafeidis**

**Second Examiner: Prof. Dr.-Ing. Arne Arns**

Date of oral examination: 5<sup>th</sup> February 2021

gez. Prof. Dr. Frank Kempken



## **Erklärung**

Hiermit erkläre ich, dass ich die vorliegende Dissertation, abgesehen von der Beratung durch meine Betreuer, nach Inhalt und Form selbständig verfasst habe und keine weiteren Quellen und Hilfsmittel als die hier angegebenen verwendet habe. Diese Arbeit hat weder ganz noch in Teilen bereits an anderer Stelle im Rahmen eines Prüfungsverfahrens vorgelegen. Als kumulative Dissertation sind Kapitel 2 bis 4 wie zu Beginn der Kapitel vermerkt in den genannten Zeitschriften veröffentlicht. Ich erkläre, dass die vorliegende Arbeit unter Einhaltung der Regeln guter wissenschaftlicher Praxis der Deutschen Forschungsgemeinschaft entstanden ist. Weiterhin versichere ich hiermit, dass mir bisher kein akademischer Grad entzogen wurde.

Kiel, 2020



## Acknowledgments

Finally, I am reaching the crest of the last wave of the Ph.D. degree and completing this important chapter of my career and life. While working on this thesis, I had the opportunity to increase my knowledge about tides, surges, statistics, coasts, etc., and I have grown as a person. However, none of this would have been possible without the support of many people I would like to acknowledge.

First, I would like to thank Nassos for giving me the opportunity to do the Ph.D. and allowing me to choose the topics. He has been a great supervisor - in fact, I would not imagine a better one - who supported me in many ways, from guidance and many technical discussions about the topics of this thesis (which probably caused him some headaches) to relaxed chats about any aspect of life. Σας ευχαριστώ Nassos for being a great researcher and person to learn from (and for the coffee machine).

I would also like to express my gratitude to all the co-authors of the papers that this cumulative thesis comprises. Arne Arns, who believed in my first research idea of this thesis, received me in Siegen and provided data and technical support to develop it. Mark Schuerch, who was my colleague during the first three years and helped me develop the research ideas of this thesis. Silvina Carretero, who provided the *Argentinian* expert knowledge for the second chapter of this thesis.

I want to thank all my colleagues of the Coastal Risks and Sea-Level Rise research group for all their support during these years (both inside and outside of university), the technical discussions even though I have been working on different topics, the funny lunches and coffee breaks, the great trips to conferences and “non-conferences” and after-work drinks. Many thanks to Leigh (best “adopted” officemate, with whom I can discuss technical issues but also have a lot of fun), Claudia (with whom I had great times during our amazing trips, including long conversations with nice cocktails and food on paradise beaches), Joshua, Lena, Bente, Jana, Maureen (who helped with the design of some graphs of this thesis but also became a good friend), Sunna (“*my best student*”), Jan (who was a great officemate, patiently listened to all my technical problems and provided support), and Tobias, for creating this great environment and team!

A particular important support for me was that of my friends, who became my family in Kiel, and, in particular, my *Familia Latina*, which like all good Latin families has many

members (I won't list them so I don't miss any), and with whom I have spent more than "*19 dias y 500 noches*".

Obviously, the greatest thanks go to my parents and my sister, because without them I would not be who I am today. Thanks mum & dad for supporting me on my way, instilling a passion for science in me, and providing unconditional love. Thanks in particular to my dad, who has been asking me since day one when I will finish this thesis. Many thanks to Elisa for always being there for me, I love you *mucho* sister.

*Gracias!*

# Table of Contents

Erklärung.....	iii
Acknowledgments .....	v
Table of Contents.....	vii
List of Tables.....	ix
List of Figures.....	x
List of Acronyms.....	xiii
Summary.....	xv
Zusammenfassung.....	xvii
<b>Chapter 1. General Introduction.....</b>	<b>1</b>
1.1. Tides .....	6
1.1.1. Non-astronomical tidal changes.....	9
1.2. Storm surges.....	11
1.2.1. Non-tidal residual, skew surge and tide-surge interaction .....	12
1.2.2. Long-term variability of storm surges .....	15
1.3. Objectives and outline of the thesis .....	16
<b>Chapter 2. Long-term trends and variability of water levels and tides in Buenos Aires and Mar del Plata, Argentina.....</b>	<b>21</b>
Abstract.....	23
Keywords .....	23
2.1. Introduction.....	23
2.2. Data.....	26
2.3. Methods .....	28
2.3.1. Percentile Analysis .....	28
2.3.2. Tidal Analysis .....	29
2.4. Results .....	31
2.4.1. Percentile Analysis .....	31
2.4.2. Tidal Analysis .....	34
2.5. Discussion .....	39
2.5.1. Percentile Analysis .....	39
2.5.2. Tidal Analysis .....	41
2.6. Conclusions.....	45
Acknowledgments .....	46
<b>Chapter 3. Sea-level rise impacts on the temporal and spatial variability of extreme water levels: A case study for St. Peter-Ording, Germany.....</b>	<b>47</b>
Abstract.....	49
Key Points.....	49
3.1. Introduction.....	49
3.2. Study area and Data.....	52
3.2.1. Study area .....	52
3.2.2. Data.....	54
3.3. Methods .....	57
3.3.1. Correction of numerically simulated water levels .....	57
3.3.2. Analysis of temporal and spatial variability of storm WLS .....	60

3.3.3. Accounting for effects of storm WL Variability .....	61
3.4. Results and Discussion .....	63
3.4.1. Temporal and spatial variability of extreme WLs.....	63
3.4.2. Implications of storm WL variability on overflow rates and fullness .....	69
3.5. Conclusions.....	73
Acknowledgments .....	74
<b>Chapter 4. Are extreme skew surges independent of high waters in mixed tidal regimes? .....</b>	<b>75</b>
Abstract.....	77
Plain Language Summary .....	77
Key Points.....	77
4.1. Introduction.....	78
4.2. Tide-gauge data .....	79
4.3. Methods .....	80
4.4. Results and Discussion .....	83
4.4.1. Seasonal Effects.....	87
4.4.2. Dependence Analysis for LHWs and HHWs .....	89
4.5. Conclusions.....	92
Acknowledgments .....	93
<b>Chapter 5. Summary and general conclusions .....</b>	<b>95</b>
5.1. Answers to Research Questions.....	99
<b>Chapter 6. Implications for research and further work.....</b>	<b>99</b>
<b>References.....</b>	<b>109</b>
<b>Appendix A .....</b>	<b>123</b>
<b>Appendix B .....</b>	<b>125</b>
Sensitivity test of the multi-linear regression model to different data sampling methods.....	125
<b>Appendix C .....</b>	<b>127</b>

## List of Tables

Table 2.1 Description, period, and source of the Climate Indices. ....	28
Table 2.2 Trends (mm y <sup>-1</sup> ) of the WL, RedM, Tide (reduced to their median) and Residual annual percentile series of Buenos Aires and Mar del Plata.....	32
Table 3.1 Characteristics of the Different Sections of the Dike-Ring Protecting St. Peter-Ording and Design WLs for 2020 <sup>a</sup> .....	57
Table 4.1 Relative Frequency (in Percentage) of Extreme Skew Surges at lower high water .....	89

## List of Figures

Figure 1.1 Components of extreme WLs .....	4
Figure 1.2 Tidal curve and high water levels of the mixed semidiurnal regime of Buenos Aires.....	8
Figure 1.3 Diagram defining the skew surge and the NTR.....	14
Figure 2.1 Diagram of the tidal levels and phases of the tidal curve analyzed .....	30
Figure 2.2 Series of (A) WL percentile series at Buenos Aires (top: 99.5th; bottom: 0.05th), (B) Residual 99.5th (orange) and 0.05th (blue) percentile series at Buenos Aires, (C) WL percentile series at Mar del Plata (top: 99.5th; bottom: 0.05th), and (D) Residual 99.5 <sup>th</sup> (orange) and 0.05 <sup>th</sup> (blue) percentile series at Mar del Plata. ....	33
Figure 2.3 Correlation between climate indices, river runoff and the reduced (to median and tide) annual percentiles of Buenos Aires and Mar del Plata.....	34
Figure 2.4 Linear trends of Annual HHW, LLW, and GDTR of Buenos Aires (Left) and Mar del Plata (Right). ....	35
Figure 2.5 Ratio of the annual mean ebb and flood duration of Buenos Aires (Upper) and Mar del Plata (Lower). ....	36
Figure 2.6 Variability and linear trends of the amplitude and phase of the main tidal constituents of Buenos Aires (only significant trends are shown) .....	37
Figure 2.7 Variability and linear trends of the amplitude and phase of the main tidal constituents of Mar del Plata .....	38
Figure 2.8 Comparison of the MSL (19-y running average) and the GDTR of (A) Buenos Aires and (C) Mar del Plata; scatter MSL and GDTR of (B) Buenos Aires and (D) Mar del Plata. ....	42
Figure 2.9 Comparison of the Paraná runoff (19-y running average) and the GDTR of Buenos Aires.....	43
Figure 3.1 Location of the study area (upper left map) in the North Sea; bathymetry of the study area showing tide-gauge stations (as orange dots) and St. Peter-Ording locations (as pink dots) are shown in the upper right map. Sections of the dike-ring of St. Peter-Ording (modified from <a href="http://www.FLOODsite.net">www.FLOODsite.net</a> ) and locations of numerically simulated WLs (lower map). ....	53
Figure 3.2 Conceptual diagram of WLs transfer and correction methodology: (a) Fitting the transfer models (multiple-linear regression) using the simulated WLs of the three gauged sites to each of the 13 St. Peter-Ording locations. (b) Transferring the observed WLs from the gauged sites to each of the 13 St. Peter-Ording locations using the transfer models. (c) Correction of the simulated WLs of each St. Peter-Ording location: the linear regression fitted to simulated (y axis) and transferred (x axis) WLs of one location is shown in the left graph; scatter of uncorrected simulated WLs versus transferred WLs (blue) and corrected simulated WLs versus transferred WLs (red) are shown in the right plot. ....	56
Figure 3.3 Normalized set of hindcast events (light blue lines) and SLR scenarios (pink lines): (a) RCP 4.5 scenario, (b) RCP 8.5 scenario, and (c) RCP 8.5 HE scenario; and upper, mean and lower envelopes (dark blue	

lines for the Hindcast scenario and red lines for the SLR scenarios) at location 6.....	59
Figure 3.4 GPDs fitted for the different locations and scenarios: (a) hindcast, (b) RCP 4.5, (c) RCP 8.5, and (d) RCP 8.5 HE.....	61
Figure 3.5 Return WLs of the four events: (a) T = 200 year; (b) T = 500 year, (c) T = 1000 year, and (d) T = 10,000 year, at each St. Peter-Ording location. ....	62
Figure 3.6 Spatial-temporal differences of the 5th percentile envelope (relative WLs in %) between (a) the RCP 4.5 scenario and the hindcast, (b) the RCP 8.5 scenario and the hindcast, and (c) the RCP 8.5 HE scenario and the hindcast. Positive values (red) represent an increase of the relative WL in the SLR scenarios (blue a decrease). ....	64
Figure 3.7 Spatial-temporal difference of the mean envelope (relative WLs in %) between (a) the RCP 4.5 scenario and the hindcast, (b) the RCP 8.5 scenario and the hindcast, and (c) the RCP 8.5 HE scenario and the hindcast. Positive values (red) represent an increase of the relative WL in the SLR scenarios (blue a decrease). ....	65
Figure 3.8 Spatial-temporal differences of the 95th percentile envelope (relative WLs in %) between (a) the RCP 4.5 scenario and the hindcast, (b) the RCP 8.5 scenario and the hindcast, and (c) the RCP 8.5 HE scenario and the hindcast. Positive values (red) represent an increase of the relative WL in the SLR scenarios (blue a decrease). ....	67
Figure 3.9 Spatial and temporal variability (standard deviation) of the normalized set of events from the hindcast scenario. ....	68
Figure 3.10 Differences of variability between (a) the RCP 4.5 scenarios and the hindcast, (b) the RCP 8.5 scenario and the hindcast, and (c) the RCP 8.5 HE scenario and the hindcast. Positive values (red) represent an increase of the variability in the SLR scenarios (blue a decrease). ....	69
Figure 3.11 Overflow rates obtained for the (a) T = 200 year, (b) T = 500 year, (c) T = 1000 year, and (d) T = 10,000 year storm-peak heights of the RCP 8.5 HE scenario and the normalized WL curves of all scenarios .....	70
Figure 3.12 Differences in fullness obtained between the WL curves of the hindcast and the three SLR scenarios of the (a) T = 200 year, (b) T = 500 year, (c) T = 1000 year, and (d) T = 10,000 year events of the RCP 8.5 HE scenario. ....	71
Figure 4.1 (a) Map showing the location of the tide-gauge sites and (b) length of the tide-gauge records .....	80
Figure 4.2 Tidal water levels of (a) Antofagasta and (b) Buenos Aires. Scatter plots of both samples of extreme skew surges (note that all values of the POT sample are also included in the Ex. Sample) and their associated high waters (HWs) for (c) Antofagasta and (d) Buenos Aires. Histograms of HWs associated to the two extreme skew samples and probability distribution function of all HWs of (e) Antofagasta and (f) Buenos Aires. Similar figures for the other tide-gauge sites can be found in Appendix C. ....	84
Figure 4.3 Regional maps showing the width of the continental shelf of the study areas.....	85
Figure 4.4 Results of the dependence analysis obtained for all tide-gauges and extreme samples. Dependent = rejection of the null hypothesis of the Anderson-Darling test (0.05 significant level. The results for $\alpha = 0.01$ can be found in Figure C.8 in Appendix C). Independent = the null	

hypothesis cannot be rejected. The null hypothesis is that HWs associated to the extreme skew sample are drawn from the same distribution as all HWs. (These results can also be found in Table C.3 in Appendix C). HW = high water; PDF = probability distribution function. ....86

Figure 4.5 PDF and weighted PDF of all HWs, and histograms of HWs associated to the two extremes samples of (1) Bella bella, (2) Antofagasta, (3) St. Petersburg, (4) Key West, (5) Buenos Aires, (6) Mar del Plata, (7) Trieste, (8) Venice, (9) Salalah, (10) Carnarvon, (11) Saigo, (12) Sakai, (13) Omaezaki, (14) Murotomisaki, and (15) Uwajima. HW = high water; PDF = probability distribution function. ....88

Figure 4.6 Histograms of the LHWs (left panels) and HHWs (right panels) associated to the two extreme skew surge samples and PDFs of all LHWs and HHWs. Stations' names that are in bold show a dependency (at 0.05 and 0.01 significant level, excluding both POT samples of Sakai, POT sample of St. Petersburg, and Key West that only show dependency at 0.05 level). HHW = higher high water; LHW = lower high water; PDF = probability distribution function. ....91

## List of Acronyms

ENSO	El Niño Southern Oscillation
GDTR	Greater Diurnal Tidal Range
GESLA	Global Extreme Sea Level Analysis
HE	High End
HHW	Higher High Water
HLW	Higher Low Water
HW	High Water
HWP	High Water Peak
LDTR	Lesser Diurnal Tidal Range
LHW	Lower High Water
LLW	Lower Low Water
LW	Low Water
LWP	Low Water Peak
MHW	Mean High Water
MLW	Mean Low Water
MSL	Mean Sea Level
MTR	Mean Tidal Range
NHN	Normalhöhennull (German ordnance datum)
NTR	Non-Tidal Residual
PDF	Probability Distribution Function
POT	Peaks Over a Threshold
PSMSL	Permanent Service for Mean Sea Level
RCP	Representative Concentration Pathway
RdIP	Rio de la Plata
RedM	Reduced to Median
SAM	Southern Annual Mode
SAODI	South Atlantic Ocean Dipole Index
SHN	Servicio Hidrografico Naval
SLR	Sea-Level Rise
SOI	Southern Oscillation Index
std	Standard deviation
WL	Water Level



## Summary

Knowledge about the magnitude and frequency of extreme water levels is essential for assessing the risk of coastal flooding, which is the major coastal hazard worldwide. In the last years, significant effort has been directed to analyzing extreme water levels and their potential future changes under climate change. This thesis aims to contribute to this field by analyzing the historical variability of water levels and their components (i.e. tides and surges) at different temporal and spatial scales, and the potential effects of sea-level rise on the short-term variability of storm surges. Knowledge of both long and short term variability of water levels is required for reducing the uncertainties associated with the estimation of the likelihood of extreme water levels for flood impact assessments.

Specifically, this thesis investigates long-term trends and inter-annual variability of water levels, tides and surges at two of the longest tide-gauge records of the southern hemisphere: Buenos Aires and Mar del Plata (Argentina). Over the last century, both water level series show an increasing trend caused by the rise of the mean sea-level, but also a decrease of the tidal amplitude. In the case of Buenos Aires, the changes in the tides are likely to be caused by the long-term changes in river discharge, as indicated by the high correlation observed between these two variables. In addition, river discharge is also highly correlated to the inter-annual variability of the extremes. Therefore, climate change induced changes in river discharge can in turn result in changes in the tides and storm surges at the Rio de la Plata estuary.

Regarding the short-term variability of extreme water levels, two aspects are investigated in this thesis: namely the variability of the water level curve and the tide-surge interaction. The latter causes a dependency between the tide and the surge component, complicating their separation and posterior combination and thus the assessment of the water level curve evolution. To overcome this issue of tide-surge interaction, the skew surge parameter has been defined and shown to be independent on the high tidal level in semidiurnal regimes. Mixed semidiurnal regimes are characterized by a higher variability of high tidal levels, which can cause a dependency between the tide and the skew surge. This is statistically investigated for 15 sites worldwide, finding that half of these sites show a dependency between high tidal levels and extreme skew surges, and thus not any extreme skew surge can occur at any high tidal level. The skew surge does not contain information of the temporal evolution of the storm surge (water level curve), which is required as input of flood models. The

uncertainties related to not accounting for the variability of the water curve when assessing coastal flooding is investigated for a coastal stretch of the German Bight. The high variability found at times around the water level peaks, when overflow/overtopping is more likely, can lead to a threefold increase of the total overflow volumes between events. Sea-level rise produces an increase of the water levels at times around the water level peaks, and this increase is relatively larger for low to moderate sea-level rise scenarios. Therefore, neglecting the variability of the water level curve can introduce large uncertainties in flood assessments and thus using the skew surge parameter might not be recommended when assessing coastal flooding.

The results presented here provide important information about the long and short term variability of tides and storm surges that can be used for reducing uncertainties when estimating future extreme water levels and their associated coastal flood risk.

## Zusammenfassung

Überflutungen stellen derzeit die größte Gefahr für niedrig gelegene Küstenregionen dar. Um das Risiko von Überflutungen zu erfassen, sind Kenntnisse über das Ausmaß und die Häufigkeit von Extremwasserständen unerlässlich. In den letzten Jahren wurde erhebliche Ressourcen in die Erforschung extremer Wasserstände und der möglichen zukünftigen Veränderungen unter dem Einfluss des Klimawandels investiert. Ziel dieser Dissertation ist es, einen Beitrag zum besseren Verständnis eben dieses Themenfeldes zu leisten. Hierzu wird die historische Variabilität von Wasserständen und ihrer Komponenten (z.B. Gezeiten und Sturmfluten) auf verschiedenen zeitlichen und räumlichen Skalen analysiert sowie die möglichen Auswirkungen des Meeresspiegelanstiegs auf die kurzzeitige Variabilität untersucht. Die Kenntnis der lang- und kurzzeitigen Variabilität des Wasserstands ist essentiell um Unsicherheiten bei der Abschätzung von Eintrittswahrscheinlichkeiten bestimmter Extremwasserstände für die Bewertung möglicher Auswirkungen von Überflutungsereignissen erfassen zu können. .

Genauer untersucht diese Dissertation die langfristigen Trends und die interannuelle Wasserstandsvariabilität, sowie Gezeiten und Sturmfluten an zwei der am längsten verfügbaren Tidepegelzeitreihen in der südlichen Hemisphäre: Buenos Aires und Mar del Plata (Argentinien). Über das letzte Jahrhundert zeigen beide Pegelzeitreihen einen beschleunigten Anstieg aufgrund des mittleren Meeresspiegelanstiegs, aber auch eine Verringerung des Tidenhubs. Im Falle von Buenos Aires lassen sich die Veränderungen der Gezeiten wahrscheinlich auf die langfristigen Veränderungen des Flussabflusses zurückführen, was durch die hohe Korrelation beider Parameter verdeutlicht wird. Darüber hinaus ist der Flussabfluss ebenfalls stark mit der interannuellen Variabilität von Extremereignissen korreliert. Es lässt sich daher sagen, dass durch den Klimawandel hervorgerufene Veränderungen im Abflussverhalten zu Veränderungen von Gezeiten und Sturmfluten im Rio de la Plata Ästuar führen.

Im Hinblick auf die kurzzeitige Variabilität von Extremwasserständen werden in dieser Arbeit zwei Aspekte untersucht: nämlich die Variabilität der Wasserstandskurve (des Hydrographen) und die Interaktion zwischen Gezeiten und Sturmfluten (engl. Tide-surge-interaction). Letztere verursacht eine Abhängigkeit zwischen der Gezeiten- und Sturmflutkomponente, was sowohl deren Separation als auch die spätere Zusammenführung beider Parameter erschwert und damit auch die Analyse des Hydrographen. Um das Problem der Gezeiten-Sturmflut-Interaktion zu lösen wurde

zunächst der schiefe Sturmflutparameter (engl. Skew surge parameter) definiert und seine Unabhängigkeit von Scheitelwasserständen in semidiurnalen Gebieten gezeigt. Im Gegensatz dazu sind gemischte semidiurnale Regime durch eine erhöhte Variabilität von Scheitelwasserständen charakterisiert, was durchaus zu einer Abhängigkeit zwischen der Gezeit und dem skew surge führt. Dies wurde statistisch für 15 Pegelstandorte weltweit untersucht, wobei festgestellt wurde, dass die Hälfte dieser Standorte eine Abhängigkeit zwischen Scheitelwasserständen und extremen skew surges aufweisen. Dies bedeutet, dass nicht jeder extreme skew surge zu jedem Tidehochwasserstand auftreten kann. Der skew surge enthält keine Informationen zur zeitlichen Entwicklung einer Sturmflut (Wasserstandskurve), welche allerdings als Randbedingung zur Eingabe in Überflutungsmodelle benötigt wird. Die Unsicherheiten in Bezug auf die nicht Berücksichtigung der Variabilität des Hydrographen bei der Bewertung von Küstenüberflutungen werden für einen Küstenabschnitt der Deutschen Bucht untersucht. So konnte gezeigt werden, dass die hohe Variabilität des Hydrographen, die zu Zeiten der Tidehochwasserstände festgestellt wird, wenn das Auftreten von Überflutungen wahrscheinlicher ist, zu einer Verdreifachung im Überflutungswasservolumen führen kann. Der Meeresspiegelanstieg verursacht zusätzlich erhöhte Scheitelwasserstände und dieser Anstieg ist vergleichsweise hoch für niedrige und mittlere Meeresspiegelanstiegsszenarien. Aus diesem Grund kann eine Vernachlässigung der Variabilität des Hydrographen große Unsicherheiten in den Folgenabschätzungen von Überflutungen hervorrufen, so dass die Verwendung des skew surge Parameters bei der Beurteilung von Küstenüberflutungen möglicherweise nicht zu empfehlen ist.

Die in dieser Arbeit gezeigten Ergebnisse liefern wichtige Informationen über die langzeitliche und kurzzeitige Variabilität von Gezeiten und Sturmfluten, die zur Verringerung der Unsicherheiten bei der Abschätzung zukünftiger extremer Wasserstände und des damit verbundenen Überflutungsrisikos an Küsten verwendet werden können.

Chapter 1.

## **General Introduction**



Flooding from storm surges is the major hazard for low-lying coastal regions worldwide (Wong et al., 2014), causing annually an average of more than 8000 fatalities and affecting 1,5 million people globally (Bouwer and Jonkman, 2018). For assessing the risk associated with storm surges, knowledge about their magnitude and frequency of occurrence is essential. However, storm surges show a high level of natural variability at different temporal and spatial scales (e.g. Idier et al., 2019; Woodworth et al., 2019), which complicates their analysis and introduces large uncertainties in the estimation of their occurrence probability (Marcos et al., 2015; Wahl and Chambers, 2015). In addition, climate change can alter the historical variability of storm surges due to changes in storminess and sea-level rise (hereafter SLR; e.g. Vitousek et al., 2017). This thesis focuses on the analysis of the historical variability of storm surges at different temporal and spatial scales that still remains unknown, but is required for reducing the uncertainties associated with the estimation of the occurrence probability of storm surges for flood impact assessments. In addition, it addresses the potential effects of SLR on the short-term variability of storm surges.

Different definitions of storm surge can be found in the literature. In some cases, the term is used to denote the combination of the tide and large surge events (including also the interactions between both), whereas in other cases it only refers to large surge events (Figure 1.1).<sup>1</sup> Tides can be defined as the periodic movement of the sea-level caused by the gravitational forces of the moon and sun and the inertia of the Earth rotation, whereas the surge component is the variation of the sea-level caused by meteorological forcing (i.e. winds and air pressure). The water level baseline, over which these two components build upon, is the mean sea level (MSL), which is the average of the sea level over a specific period of time (from month to years). The MSL calculated over 19 years is frequently used as national survey datums (Pugh and Woodworth, 2014). The water level (WL) defined by the sum of these three components and their interactions is commonly termed in the literature as “still water level” or in some cases “total water level”, although the latter often includes the wind waves’ contribution.

Coastal WLs show variability at different spatial and temporal scales due to different forcing mechanisms and effects of coastal characteristics such as bathymetry and coastline shape (see e.g. Woodworth et al., 2019). Tides show the largest variability at daily and half-daily time scales, but also have shorter and longer periodicities, whose

---

<sup>1</sup> In this thesis, the first definition of storm surge is used in Chapter 3, whereas in the other Chapters the term is only used to refer to the surge component.

magnitude can be significant. Although the variability of the tides has always been assumed known, with the periodicity related to astronomic motions, several studies made in the last years have reported secular trends in the tidal levels and constituents, comparable in magnitude to MSL trends. These trends seem not to be related to astronomic motions in most coastal regions of the world (see Mawdsley et al., 2015 for a global assessment). A detailed discussion about the trends observed in tidal levels and constituents is included in subsection 1.1.1 of this chapter and Chapter 2.

Surges are included within the short-time variability of the sea-level, comprising several hours to days, but they are also affected by mid to long term processes such as seasonal, inter-annual and secular variability of the meteorological forcing. This variability of the meteorological forcing also induces changes of the MSL, variability of which is driven by a variety of mechanisms including ocean circulation changes, ice melting and variations in steric height (Woodworth et al., 2019).



Figure 1.1 Components of extreme WLS (source: AIR Worldwide)

Focusing on coastal flooding, hazards emerge when large positive surges (i.e. storm surges) coincide with high tidal levels, and specifically with the larger tidal high waters that occur during spring tides (Figure 1.1). These combinations are “rare” due to the large natural variability of the tides and surges previously mentioned. In fact, only few storm surges have been measured in the majority of coastal gauged sites as the length

of WL records rarely exceed 100 years (Marcos et al., 2019). Therefore, it is virtually certain that larger storm surges will occur in the future, compared to those measured in the past (Dangendorf et al., 2016). In addition to the limitation of the length of the records, sites with an operational tide gauge are scarce and unevenly distributed around the world, as tide gauges are mostly concentrated at the coasts of Europe and North America (Marcos et al., 2019). Limitations related to the temporal and spatial availability of WL records are commonly overcome by generating WL hindcasts using hydrodynamic numerical models forced with atmospheric reanalysis (e.g. Arns et al., 2013a).

In order to assess the risk of coastal flooding at any site, the first step needed is to estimate the occurrence probability of these “rare” hazard events, which might lead to damages. A wide range of hazard scenarios, from high-probability of occurrence and low-consequences to low-probability and high-consequences, is required to account for uncertainties in flood risk assessments (Nicholls et al., 2014; Hinkel et al., 2015). The occurrence probability of extreme WLs is commonly estimated using models based on the extreme value theory (see Jonathan & Ewans, 2013 for a review). However, there is no standard approach to conduct extreme value analysis for coastal flood assessments and thus many different models are commonly used (see e.g. Wahl et al., 2017). These approaches range from direct univariate to more complex multivariate models including different variables (e.g. modelling separately the tide and the surge components), producing therefore different estimates of return WLs (e.g. Haigh et al., 2010a; Wahl et al., 2012; Arns et al., 2013b). From a statistical perspective, the tide and surge component should be modelled separately due to their different nature, the latter being stochastic and the former periodic. However, non-linear interactions between these two components complicate their separation and posterior combination. These non-linear interactions, as well as their effects on the analysis of extreme storm surges, are described and discussed in more detail in subsection 1.2.1 of this chapter and chapter 4.

Classical extreme value models are based on the assumption that extreme WLs are stationary and independent (Coles, 2001). However, this assumption is not satisfied due to the WL variability at the different time scales mentioned before, which introduces a serial dependency between WLs of the same event as well as between events due to trends (e.g. rise of the MSL) and meteorological cycles (e.g. seasonality, inter-annual variability related to climate modes). This serial dependency should be removed before conducting the extreme value analysis (e.g. by de-trending and de-

clustering) or included in the model (e.g. non-stationary models; Marcos & Woodworth, 2017; Menéndez & Woodworth, 2010). In addition, known variability related to climate modes (e.g. ENSO) can be used as a covariate for improving return WL estimates (e.g. Wahl & Chambers, 2016). The majority of the extreme value models used to estimate return WLs focus only on the peaks of the extreme WL events due to the assumption of independent and stationary data, losing therefore the information about the temporal variability of the storm surge curve (also known as hydrograph). Nevertheless, the storm surge curve is required as boundary conditions for hydrodynamic flood modelling and the use of a unique design storm surge curve is a common practice (see e.g. Vousdoukas et al., 2016). However, little is known about the uncertainties introduced in flood assessments due to the variability of the curve of storm surges (Quinn et al., 2014), which is further discussed in subsection 1.2.1 and chapter 3 of this thesis.

In addition to the natural variability, WL extremes are affected by climate change induced changes such as SLR and potential changes in storminess, which must also be considered within flood risk assessments. SLR will at least increase the baseline of the other WL components, but numerical simulations show that it can also produce non-linear amplifications on the tides and surges (Arns et al., 2017). Therefore, knowledge about the natural and climate change induced variability of the different components of the sea-level is essential for characterizing present and future extremes, along with their potential impacts at the coast (Vousdoukas, et al., 2018).

In the following subsections 1.1 to 1.2, the WL components and the knowledge about their variability at different time scales are introduced. Tides are discussed in subsection 1.1., including a summary of trends observed in tidal levels over the last century (subsection 1.1.1). Subsection 1.2 provides an introduction of the surge component, with special focus on the analysis of storm surge events for flood assessments, and its temporal and spatial variability. Finally, the objectives and research questions of this thesis are presented and discussed in Section 1.3.

## **1.1. Tides**

As stated before, tides can be defined as the periodic movement of the sea surface caused by the gravitational forces of the moon and the sun and the inertia of the rotation of the Earth (e.g. Pugh, 2004). This periodic movement of the sea-level on a daily time scale affects all coastal processes and activities worldwide, albeit to different extents as the amplitude and period of the tidal cycle vary from place to place. Although most of the tidal variability can be explained by the astronomical forces that generate

them (i.e. Equilibrium tide), hydrodynamics determine the propagation of the tides and thus the resulting tidal oscillation (Dynamic Theory; e.g. Parker, 2007; Pugh and Woodworth, 2014)

Using only the Equilibrium tide we cannot fully explain the tidal variation observed at the coast. Nevertheless it is used as a reference system for estimating the astronomical tidal constituents of sea-level records because the frequencies of the observed tide are equal as in the Equilibrium tide. The most common method used for discerning the tidal variation is harmonic analysis, which is based on decomposing the tidal signal in a number of harmonics, which are known as tidal constituents. These harmonics are represented by a frequency, which can be related to astronomic motions and is therefore known; an amplitude; and a phase lag with respect to the Equilibrium tide. A long list of harmonics is required for a full description of the tide generation forces due to the complex relative motions of the Earth-Moon-Sun system, with elliptical orbits which are not in line with the equator. In addition, the tidal amplitude and the characteristics of the tidal curve such as the timing of the high (low) tidal peaks (hereafter HW and LW) are determined by shallow-water processes in coastal regions, which transfer tidal energy to new frequencies (higher harmonic constituents called overtones) or generate new tidal constituents from the interaction of astronomical constituents (compound tides, which can have the same frequency as astronomical constituents). However, most of the tidal energy is found in the semidiurnal and diurnal frequencies, corresponding to the rotation of the Earth and the declination of the Moon respectively. Therefore, most of the tidal variability can be represented by few tidal constituents. The main semidiurnal harmonics are the M2 and S2 which represent the gravitational effects of the Moon (M2) and Sun (S2), with frequencies being half of the solar and lunar days. During a lunar month, the relative position of the Sun and the Moon changes and produces a modulation of the tide due to the balance of their gravitational forces. When both are aligned their forces sum up creating larger tidal amplitudes (spring tides), but when they are right-angled their forces counteract and thus produce lower tidal amplitudes (neap tides). Most of this modulation is represented by the synchronization of the M2 and S2 constituents. The effect of the lunar declination is represented by two diurnal constituents, O1 and K1, with maximum combined effect when the Moon is at the largest angle with the equator (i.e. maximum declination) and minimum when it is in line with the equator. The K1 also has a part that comes from the declination of the Sun i.e. the angle between the Earth's orbit around the Sun and the Earth's equator. The amplitude of these main diurnal constituents is enhanced in some coastal areas due to hydrodynamics (or the

semidiurnal constituents reduced), which can be of similar magnitude or even larger than the semidiurnal M2 and S2, and can cause a daily tide (i.e. one HW and LW peaks per day). Therefore, the relative magnitude of these main semidiurnal and diurnal constituents lead to different tidal regimes. When the amplitude of the diurnal constituents is small, the tide shows a half-day cycle with two HWs and LWs of similar magnitude, known as the semidiurnal tidal regime. However, when the relative contribution of the diurnal tides increases to 25% of the semidiurnal tides, a diurnal inequality on the half-day cycle is observed (mixed semidiurnal regime), characterized by two HWs and LWs tidal peaks per day but of different magnitude (Figure 1.2 case of Buenos Aires).

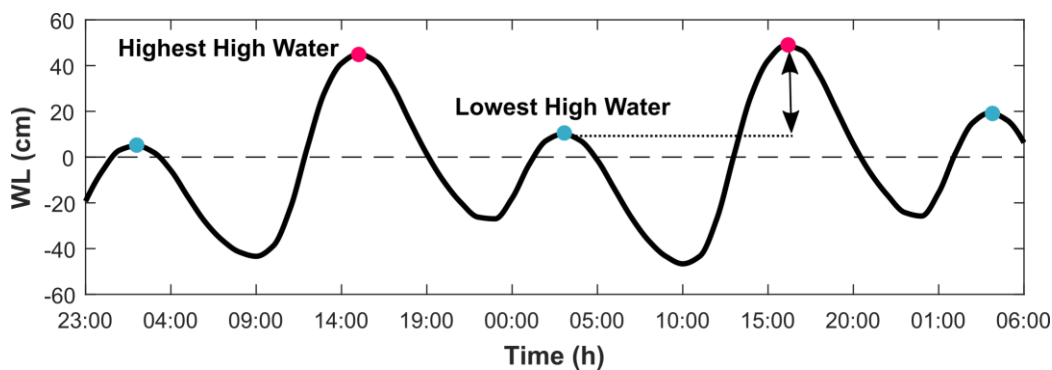


Figure 1.2 Tidal curve and high water levels of the mixed semidiurnal regime of Buenos Aires

The elliptical orbits of the Earth-Moon-Sun system cause tidal modulations at longer time scales such as fortnightly, monthly and annual, that are represented by long-term tidal constituents (e.g. Mf, Mm, Sa). However, the astronomic amplitude of these constituents is small compared to the modulation induced by meteorological effects at these frequencies. The modulations caused by the 8.85y perigean cycle and the nodal cycle (18.6y) produce variations in the lunar constituents that are not represented as additional tidal constituents, but by correction factors of the amplitude and phase of the lunar constituents affected.

In shallow coastal areas, the propagation of the tide is affected by non-linear shallow water processes, which cause distortions of the tidal curve such as asymmetry between the ebb and flood phases. The changes in the tide induced by shallow-water effects are also represented by harmonic constituents with frequencies related to the astronomic constituents (multiples, sums or differences; e.g. M4).

### 1.1.1. Non-astronomical tidal changes

Tidal characteristics have always been assumed stationary due to the astronomic nature of the tidal generation forces. However, recent studies have shown a tidal variability at different time scales (e.g. seasonal, inter-annual and secular) which is not related to astronomic motions and which forcing factors remain unknown (see Haigh et al., 2020 for a review). These non-astronomical changes in the tides have been observed in most regions of the world, but positive and negative trends have been detected and the rate of change is not globally homogeneous, which points to different driving mechanisms or to more than one process driving the changes.

Large-scale and quasi-global studies of tide-gauge records showed that regionally coherent trends occurred over the 19<sup>th</sup> and 20<sup>th</sup> centuries. These studies are mostly focused on the northern hemisphere where a higher density of tide gauges and longer records exists (Woodworth et al., 2017). In this context, a large decrease of the S2 amplitude and small increase of the M2 along the Eastern North American coast over the 20<sup>th</sup> century was reported by Ray (2009), Müller (2011) and Woodworth (2010). The latter also analyzed trends in the main diurnal constituents K1 and O1, finding increases of the amplitude of both constituents at the majority of the tide gauges. However, this general pattern is not homogeneous along the entire East coast of North America, and trends of an opposite sign can be found at some tide gauges (see e.g. Figure 4 of Woodworth, 2010). From archive records, Ray and Talke (2019) found that the M2 amplitude was stable along the Gulf of Maine during the 19<sup>th</sup> century, and the increasing trend started in the 20<sup>th</sup> century, suggesting the changes in stratification due to long-term warming as a potential driver. At the Pacific coast of North America, Jay (2009) found an average increase of 0.56mm/y of the amplitude of both M2 and K1, but although the rate of change was not spatially homogeneous, the regional coherence of the tidal changes pointed to large-scale drivers such as changes in stratification or wind-driven motions. Woodworth (2010) also reported an increase of the amplitude of M2 and K1, but also found an increase of the amplitude of S2 and O1 at the western coast of North America. These increases of the amplitudes of the main tidal constituents probably led to the increase of the tidal range reported by Mawdsley et al., (2015) for this region. Regionally coherent trends were also found at the western Pacific along the coast of Japan, China and Australia. Woodworth (2010) found a general decrease of the M2, K1 and O1 amplitudes and an increase of the S2 amplitude along Japan. These findings are in line with the later study of Rasheed and Chua (2014), who also reported a consistent decrease of the M2 amplitude along the

Japanese tide gauges. However, Rasheed and Chua (2014) reported an increase of the tidal range along Japan, while the opposite was found by Mawdsley et al., (2015). More consistent trends were reported for the Australian tide-gauge records, where a general increase of the amplitude of the main constituents (i.e. M2, S2, O1 and K1) was reported by Woodworth (2010) and an increase of the tidal range was found by Mawdsley et al., (2015). At the Chinese coasts and adjacent seas, Feng et al., (2015) reported significant increases in the amplitude of the main semidiurnal constituents (i.e. M2, S2 and N2) while the main diurnal constituents (O1 and K1) remained stable throughout the second half of the 20<sup>th</sup> century. In Europe, consistent trends were reported for the German Bight, where an increase of the main tidal constituents and a subsequent increase of the tidal range was found (Woodworth, 2010; Mawdsley et al., 2015). On the other hand, trends in tidal levels and constituents are not spatially coherent around the UK, and both significant increases and decreases were observed (Woodworth, 2010; Mawdsley et al., 2015). However, Haigh et al., (2010) reported a small significant increase (0.2-0.6 mm/y) of the tidal range along the English Channel throughout the 20<sup>th</sup> century, caused by a small increase of the M2 amplitude.

Despite the number of studies performed, the exact drivers of the observed tidal changes over the last century remain unknown. The regionally coherent trends observed in some areas suggest large-scale processes are responsible for the tidal changes. In this context, the rise of the MSL is one of the main candidates for driving the tidal changes because it has also experienced a rapid change over the 20<sup>th</sup> century. It is well established that changes in water depth alter the tidal characteristics by modifying the tidal wave propagation and changing the natural period of resonance of the ocean basin (see e.g. Haigh et al., 2020). However, no previous studies have found a strong link between the tidal and MSL changes. Devlin et al., (2017) investigated the links between the tidal and MSL anomalies at monthly to interannual time scales from the tide gauges along the Pacific Ocean. They found that the MSL variability seems to be correlated to the anomalies of the main tidal constituents at these time scales, with rates between  $\pm 10$  to  $\pm 500$ mm per meter of MSL change. However, Mawdsley et al. (2015) did not find a significant correlation between the MSL rise and the changes in the tidal levels from a quasi-global tide-gauge records network. The links between the MSL rise and the tidal changes have also been investigated by numerical modelling simulations, but although an increase of the MSL can alter the tidal characteristics (see e.g. Arns et al., 2015; Pickering et al., 2017), results suggest that larger MSL increases are required for producing the tidal changes observed in tide-gauge records (e.g. Müller et al., 2011). Therefore, the rise of the MSL is not the

only driver of the changes in the tides over the 20<sup>th</sup> century. Changes in stratification have also been suggested as a driving mechanism of tidal changes by a number of studies (e.g. Colosi and Munk, 2006; Jay, 2009; Müller et al., 2011). Variations in stratification of the ocean and the depth of the thermocline can alter the coupling of the barotropic and internal tides at seasonal time scales (Müller et al., 2011), thus being a potential large-scale mechanism at longer time scales.

In addition to the large-scale driving mechanism, local-scale processes seem to also play an important role in changing the tides because trends of different rates and sign were observed at neighboring tide gauges. In this context, morphological changes in the coast such as land reclamation, dredging of harbors or estuaries have been shown to alter the tides by modifying the tidal dynamics (e.g. Feng et al., 2015). Changes in river discharge can be an important factor altering the tidal characteristics in estuaries by dampening the tidal propagation when the river discharge is large (e.g. Pugh and Woodworth, 2014).

Changes in the tides that occurred along the southern Atlantic coasts remain unexplored because the density of tide gauges in this region is low or the long-term tide-gauge records such as the one of Buenos Aires are not included in global datasets. Therefore, the changes in the tides in Buenos Aires and Mar del Plata (Argentina) are explored in detail in Chapter 2.

Knowledge about the past changes in the tides and their drivers from local to large scales is important to also predict potential future changes. Future changes in the tides might alter coastal processes, and in the case of coastal flooding, they can exacerbate/alleviate future flooding. However, future changes in the tides are not included in coastal flood assessments (see e.g. Vousdoukas et al., 2017) even though their trends over the last century were of similar magnitude to that of the MSL increase (e.g. Mawdsley et al., 2015). In addition, flood adaptation measurements that alter the shorelines can induce extra changes in the tides and thus tidal effects need to be considered.

## **1.2. Storm surges**

The term surge refers to variations of the water level (i.e. deviating from the predicted astronomical tide) that last from several hours to days. The surge is produced by meteorological forcing, namely a combination of mean sea level pressure and winds. These two forcings can produce both positive and negative variations of the water level

from the reference astronomical tidal level. The isostatic response of the water level to changes in the sea-level pressure can be explained by the inverse barometer effect (Eq. 1), resulting in a water level increase (decrease) of approximately 1cm for every a decrease (increase) of 1mbar of air pressure (Pugh and Woodworth, 2014).

$$\Delta WL = -\frac{\Delta P_{sl}}{\rho g} \quad \text{Eq.1}$$

Where  $\Delta WL$  is the variation of the water level,  $\Delta P_{sl}$  is the variation of the sea-level pressure,  $\rho$  is the ocean water density and  $g$  is acceleration due to gravity.

In shallow coastal waters, the rise of the WL caused by wind stress can be large, with resulting WL gradients according to:

$$\frac{\partial WL}{\partial x} = \frac{\rho_{air} C_d W^2}{\rho g D} \quad \text{Eq.2}$$

Where  $\rho_{air}$  is the density of the air,  $C_d$  is the drag coefficient,  $W$  is the wind velocity,  $\rho$  is the ocean water density,  $g$  is the acceleration due to gravity and  $D$  is the water depth (Pugh and Woodworth, 2014).

The contribution of each surge driver (i.e. mean sea level pressure and wind) cannot be separated as these two drivers usually occur simultaneously. In addition, due to the stochastic nature of the drivers, the surge cannot be defined using characteristics of a periodic wave such as the tides. Therefore, the surge component is defined as a difference between the observed WLs (i.e. still WLs) and the tidal WLs, but two different definitions exist, namely the non-tidal residual (NTR) and the skew surge.

### 1.2.1. Non-tidal residual, skew surge and tide-surge interaction

Historically, the surge has been defined as the NTR by subtracting the tidal levels from observed tide-gauge records at each time step (e.g. Pugh, 2004). However, in shallow-waters, non-linear interactions between the tide and the surge occur mainly due to two processes: 1) the rise of the WL due to wind stress is inversely proportional to the water depth (Eq. 2) and thus the wind stress is more effective generating larger surge levels when the tide is low; 2) the speed of the tidal wave (Eq. 3) depends on the water depth, which increases with the surge generation, resulting in a high water peak occurring earlier than the predicted tidal HW peak.

$$c = \sqrt{gD}$$

Eq.3

The definition of the surge as the NTR includes therefore the contribution of the tide-surge interaction, which causes a dependency between both components as larger NTRs tend to occur more often around LWs (e.g. Horsburgh and Wilson, 2007). When assessing extreme WLs, the contribution of the tide-surge interaction included in the NTR produce an overestimation of up to 30% (or 70 cm) if independence is assumed between the tide and the NTR (i.e. any level of the NTR can occur at any tidal level; Arns et al. 2020). However, the magnitude of the tide-surge interaction not only depends on the water depth but also on other factors such as the local bathymetry and the evolution of the meteorological forcing, making the quantification of the tide-surge interaction difficult (see e.g. Olbert et al., 2013). In order to overcome these complications, another parameter, namely the skew surge, has been introduced and defined as the difference between maximum observed and predicted WLs during a tidal cycle, irrespective of timing differences (e.g. Batstone et al., 2013). Extreme skew surges have been shown to be independent from the associated HW level along the UK, Ireland and eastern coast of US (e.g. Batstone et al., 2013; Williams et al., 2016), resulting in an increasing utilization of the skew surge parameter for extreme WL assessments worldwide (e.g. Haigh et al., 2014; Mawdsley et al., 2016; Stephens et al., 2020). However, previous studies that analyzed the dependency of extreme skew surges to their associated HW levels were performed for places with a semidiurnal tidal regime and thus with a likely smaller variability of HW levels than e.g. places with mixed semidiurnal regimes. The dependency between extreme skew surges and HW levels at mixed semidiurnal regimes is explored in Chapter 4.

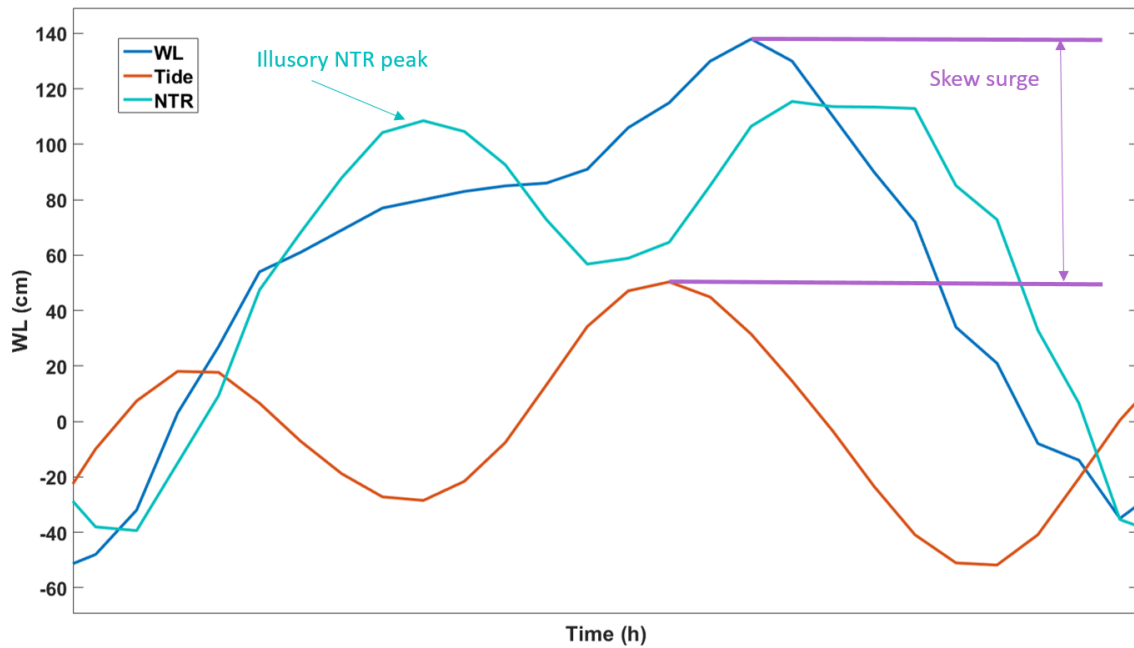


Figure 1.3 Diagram showing the skew surge and the NTR.

Another limitation of the skew surge is the lack of information about the temporal evolution of the surge (i.e. hydrograph) because the skew surge is an integrated measure per tidal cycle. The majority of extreme WL assessments only estimate the occurrence probability of the WL or surge peaks and do not account for the WL curve or hydrograph because the extreme sample is assumed to be independent in extreme statistical models (e.g. Coles, 2001). However, the evolution of the storm surge is important from the perspective of flood risk modelling as differences in total overflow volumes result in different inundation extent and depths (e.g. Quinn et al., 2014). In addition, current velocities also depend on the duration of the flood phase of the storm surge event, and are therefore important for assessing erosion and failure of coastal structures. Hydrodynamic flood models require the WL curve as boundary conditions for simulating flooding and the lack of information of the storm surge WL curve from extreme WL analysis is commonly overcome by using a “design curve”. This approach consists of: 1) defining a design curve based on the WL curve of one historical storm surge event (e.g. the largest WL event recorded) or by superimposing the time series of the highest levels recorded from each component; and 2) Scaling the design curve to the desired return WL (e.g. Bruss et al., 2010a; Gönner and Gerkenmeier, 2015; Wadey et al., 2015; Vousdoukas et al., 2016). As this approach has been extensively used in the past, little is known about the uncertainties introduced when assessing coastal flooding due to the temporal variability of storm surge curves. In this context,

Quinn et al., (2014) showed that even a small variability of the WLs near to the peak can produce large changes in the total overflow volumes in a UK site. In addition, the variability of the storm surge curve changes significantly along the coast of UK, which introduces more uncertainties when using a single design curve along large coastal segments. A later study of Höffken et al., (2020) also showed that the variability of the storm surge curve can produce variations of up to 5% in the simulated flood extent, which results in a 20% increase of exposed properties, in a micro-tidal site at the German Baltic coast. They additionally assessed the effects of SLR by linearly adding 1m to the storm surge curves under investigation. Therefore, the potential non-linear effects of SLR on the temporal variability of storm surge curves remain unexplored. In Chapter 3, the uncertainties introduced when assessing flooding due to the temporal evolution of storm surge curves and their spatial variability are investigated for a coastal stretch of the German Bight. In addition, the potential effects of SLR on both the temporal and spatial variability of storm surge curves are also assessed.

### **1.2.2. Long-term variability of storm surges**

As previously mentioned, knowledge about the temporal variability and secular trends of storm surges is important for assessing their potential impacts on the coast. Due to their stochastic nature, predicting the occurrence of storm surges is difficult over long periods of time (i.e. longer than few days. Storm surge forecasting is not discussed in this thesis). Although the natural variability of storm surges is large, the frequency and intensity of storm surges show variability at seasonal and inter-annual scales related to the variability of large-scale meteorological patterns. Knowledge of this variability and its drivers can reduce uncertainties when modelling the likelihood of future storm surges (e.g. Cid et al., 2015; Wahl and Chambers, 2015, 2016). Besides the natural variability, climate change can induce changes in the magnitude and frequency of storm surges due to an intensification of storminess and non-linear changes in shallow-waters caused by SLR (e.g. Arns et al., 2015a; Vousedoukas et al., 2017; Wahl, 2017; Wahl et al., 2017b).

Throughout the last century, trends and variability of observed storm surges have extensively been investigated at quasi-global scale (e.g. Woodworth and Blackman, 2004; Menéndez and Woodworth, 2010; Mawdsley and Haigh, 2016), and especially, at those regions with a high density of long tide-gauge records such as the US and Europe (e.g. Cid et al., 2015; Marcos et al., 2015; Haigh et al., 2016; Wahl and Chambers, 2016). For the majority of the sites, these studies found that the secular

trends of the storm surges over the last century were similar to the trend of the MSL. However, the latest study at a quasi-global scale of Mawdsley and Haigh, (2016) found small but significant positive and negative secular trends (within the range of  $\pm 2 \text{ mm y}^{-1}$ ) at some tide-gauge sites after removing the MSL contribution. The differences in the resulted secular trends between studies can be caused by differences in the periods of data analyzed (Mawdsley and Haigh, 2016). Because of these differences, only the results of the study of Mawdsley and Haigh, (2016) will be discussed, as this study is the most recent, and thus covers a longer time period, at a quasi-global scale. Their findings show little spatial coherence of the significant trends in both magnitude and sign. In Australia, negative trends were found in the northern tide gauges, while positive in the southern sites. Positive trends were also found along the Gulf of Mexico and Florida's' coasts. A spatially coherent decrease was found along the southern European tide gauges, while no coherent trend was observed along the east coast of North America and both positive and negative significant trends were found at neighboring tide gauges.

The study of Mawdsley and Haigh, (2016) also investigated the links between the inter-annual and decadal variability of storm surges with climate indices finding no significant correlation at the 90% significance level. However, many other previous studies have found significant connections between climate indices, which are used as a proxy of large-scale climate patterns, and decadal changes in storminess (Marcos et al., 2015) or inter-annual variability (e.g. Menéndez and Woodworth, 2010). Again, some regions such as the southern Atlantic coasts remain unexplored because the observed WLs are not included in the quasi-global tide-gauge network. Therefore, the long-term trends and inter-annual variability of extreme WLs for the longest tide-gauge records of the southern Atlantic, namely Buenos Aires and Mar del Plata (Argentina), are explored in Chapter 2.

### **1.3. Objectives and outline of the thesis**

As pointed out in the previous sections, knowledge of the variability at different time scales of WLs and its components separately, as well as the phenomena driving the variability, is required and essential for reducing uncertainties when assessing future flood risk. Variability and trend analyses have been extensively performed for the northern hemisphere tide-gauge records, but very little for the southern hemisphere due to the lack of observational data. For the first research question, two of the longest

tide-gauge records from the Southern Hemisphere have been selected. These two tide-gauge series are not included in the global databases and thus not analyzed in the studies mentioned before.

**1. Have the WLs and WL components at Buenos Aires and Mar del Plata (Argentina) shown any secular trend or inter-annual variability over the last century? Can these trends and variability be linked to large-scale climate patterns?**

The tide gauges selected for these variability and trend analyses are located in Buenos Aires and Mar del Plata (Argentina). Both tide-gauge records span more than 50 years, unlike most of the tide-gauge records of the southern hemisphere. In addition, these tide-gauge records are not included in global databases such as GESLA (Woodworth et al., 2017) and have therefore not been included in the previous variability studies.

The presence of significant trends and variability of the WL records of Buenos Aires (1905-2013) and Mar del Plata (1956-2013) is investigated using a percentile analysis, a method previously used in the literature and thus producing results comparable to other sites (see e.g. Marcos & Woodworth, 2017; Menéndez & Woodworth, 2010). In order to assess whether the inter-annual variability is linked to climate systems, a correlation analysis is carried out. In addition, significant secular trends in the tidal component (tidal levels and main tidal constituents) are analyzed by a moving harmonic analysis and the potential drivers of these trends, such as the rise of the MSL and the river discharge, are investigated.

The rate of rise of the MSL over the last century ( $1-3 \text{ mm y}^{-1}$ ; e.g. Dangendorf et al., 2017) is one order of magnitude smaller than the rates of SLR projected under future scenarios (Garner et al., 2018). This larger increase of the MSL can, in turn, induce larger non-linear changes in the tides and surges than those observed in the past. These potential induced changes by the rise of the sea-level were only investigated for the storm surge peaks (Arns et al., 2017), but the effects of SLR to the temporal evolution of storm surges and its implications for coastal flooding are still unknown. In addition, the temporal (i.e. time evolution of the storm) and spatial variability of storm surge levels are not accounted for at local scales, where the levels of a single site and event are commonly used for areas of several kilometers. Therefore, the second research question formulated is:

**2. How large are the uncertainties associated with not considering the spatial and temporal variability of storm surges at local scales? How would the rise of the sea-level affect the temporal and spatial variability of storm surges and what are the implications for coastal flooding?**

Both the temporal and spatial variability of the hydrographs or WL curves of 75 historical storm surge events are analyzed for 13 sites along 15 km of the coastline of St. Peter Ording, in the German North Sea coast. In addition, the effects of three SLR scenarios, namely RCP 4.5, RCP 8.5 and high-end RCP 8.5, on the hydrographs of these storm surge events are also analyzed comparing them to the historical conditions. Finally, the implications and uncertainties related to the temporal and spatial variability of the WL curves for coastal flooding are investigated by means of two parameters: fullness and overflow volumes.

Following the previous research question, the temporal evolution of storm surge events is commonly not included when assessing coastal flooding due to the tide-surge interaction. As a result of this interaction, larger surge levels tend to coincide with lower levels of the tide due to differences in water depth. Because of that, the “skew surge” parameter was defined and proven to be statistically independent on the HWP (Williams et al., 2016). The dependence analysis was only performed at locations with a semidiurnal tidal regime, which is characterized by having two tidal cycles per lunar day of similar magnitude. However, water depth changes between consecutive HWPs in mixed semidiurnal regimes, where diurnal and semidiurnal tides are of similar magnitude, maybe larger. These water depth changes can produce a similar effect as the so-called “tide-surge interaction”, and thus result in larger skew surges occurring at the LHWs. For this reason, the third research question is:

**3. Are extreme skew surges independent of high water levels in a mixed semidiurnal tidal regime?**

Following previous studies performed to measure the dependency between extreme skew surges and their associated HWPs, I statistically analyze whether extreme skew surges show a dependency to associated HWPs at 15 sites around the world with a mixed semidiurnal tidal regime. The statistical analysis consists of assessing whether the probability distribution function (PDF) of HWPs associated with extreme skew surges is statistically different to the PDF of all HWPs. For that, the tidal time series are first generated from the harmonic analysis of the tide gauge records of the 15 sites, and the HWPs are extracted and divided into HHWs and LHWs. In a second step, the

skew surges are calculated for the recorded periods and two extreme skew surge samples are selected 1) the largest 1% and 2) the largest 1% but with an independent time of 2 days between consecutive events.



## Chapter 2.

# **Long-term trends and variability of water levels and tides in Buenos Aires and Mar del Plata, Argentina**

*Sara Santamaria-Aguilar, Mark Schuerch, Athanasios T. Vafeidis  
and Silvina C. Carretero*

*Frontiers in Marine Science (2017), doi: 10.3389/fmars.2017.00380*

*Received: 13 September 2017, Accepted: 13 November 2017*



## Abstract

We present an analysis of the long-term trends and variability of extreme water and tidal levels and the main tidal constituents using long-term records from two tide gauges in the wider region of the Rio de la Plata estuary: Buenos Aires (1905–2013) and Mar del Plata (1956–2013). We find significant long-term trends in both tidal levels and the main tidal constituents (M2, S2, K1, O1, and the overtideM4) from a running harmonic analysis in both locations. The tidal range decreased on average 0.63mm y<sup>-1</sup>, as a result of an increase of the low water levels and a decrease of the high water levels. We also find a secular decrease in the amplitude of the semi-diurnal constituents and an increase of the diurnal ones, but of different magnitudes at each location, which suggests that different processes are producing these changes. In Buenos Aires, an increase of river discharge into the estuary seems to reduce the tidal range by hampering the propagation of the tidal wave into the estuary, whereas no influence of river discharge on water and tidal levels can be detected in Mar del Plata. We believe that other factors such as thermohaline changes or the rise of mean sea-level may be responsible for the observed tidal range decrease. Despite the tidal long-term trends, we find no significant trends in the meteorological component of the tide-gauge records other than an increase in the mean sea-level. In addition, we explore teleconnections between the variability of the meteorological component of the tide-gauge records and climate drivers.

## Keywords

Tide, sea-level, water level, secular trends, variability, Buenos Aires, Mar del Plata, Argentina

## 2.1. Introduction

Determination of trends and variability of extreme water levels (WLs) is complex due to their high natural variability arising from the nature of extreme WLs components: mean sea level (MSL), tide and surge. Climate change can alter the natural variability of extreme WLs, for example by raising MSL (see e.g., Rhein et al., 2013). Knowledge of past long-term trends and inter-annual variability of extreme WLs as well as the drivers of these changes is required in order to reduce uncertainty when modeling the frequency and magnitude of future extreme WLs (Wahl and Chambers, 2015), because the uncertainties related to future trends and variability of WLs caused by

climate change (e.g., sea-level rise, changes in storminess) are high (Wahl et al., 2017). In most areas of the world, secular changes in extreme WLs over the last century have been found to be of similar magnitude as the rise in MSL (see e.g., Woodworth and Blackman, 2004; Menéndez and Woodworth, 2010). In recent years some studies have additionally identified significant secular trends in both tide and surge components in many regions of the world (Marcos et al., 2015; Mawdsley et al., 2015, for global analyses). However, a better understanding of the links between atmospheric dynamics and extreme WLs variability is needed in order to better model their occurrence probability (see e.g., Cid et al., 2015).

Trends and variability of extreme WLs have been extensively analyzed in some areas of the world such as along the U.S. coast (e.g., Wahl and Chambers, 2016) and Europe (e.g., Cid et al., 2015; Haigh et al., 2016); but not for most of the Southern Hemisphere, where only few studies have been performed due to a lack of observational data (Woodworth and Blackman, 2004; Menéndez and Woodworth, 2010). Nevertheless, long time series of observed WLs are available in some locations, as for example in Buenos Aires and Mar del Plata (Argentina), where more than 100 and 58 years of hourly WLs, respectively, have been recorded by the Naval Hydrographic Service of Argentina (SHN). These time series are not included in any of the previously mentioned global datasets or analyses, and only few studies related to long term changes of extreme WLs in these two locations are available (D'Onofrio et al., 1999, 2008; Fiore et al., 2009).

Both cities are densely populated, Buenos Aires being the capital of Argentina and Mar del Plata the largest tourist resort of the country with more than 7 million of tourists per year. Buenos Aires is located in the inner part of the Río de la Plata (RdIP) estuary, which is characterized by a shallow coastal bathymetry; Mar del Plata is located at the open Atlantic coast, south of the Río de la Plata. Both extreme positive and negative extreme WLs have caused high impacts in Buenos Aires: positive extreme WLs produced flooding due to the low elevation of the city, extreme negative WLs caused significant impacts on navigation safety and drinking water supply (D'Onofrio et al., 1999, 2008). On the other hand, the coastline of Mar del Plata is highly threatened by erosion, which is intensified by the occurrence of extreme WLs (Fiore et al., 2009).

Fiore et al., (2009) analyzed decadal changes in the frequency, magnitude and duration of positive surges in Mar del Plata for the period between 1956 and 2005. They concluded that there was an increase in these three variables corresponding to the rise of the MSL over the studied period. However, they obtained the non-tidal

residual component of WLs by subtracting the astronomic WLs produced by a harmonic analysis over 19 years of observed records, hence assuming no changes in the tidal component over time. Therefore, any changes in the tidal component would have been accounted for within the surge and the MSL components. Similarly, D'Onofrio et al., (2008) studied decadal changes in both positive and negative surges in Buenos Aires, but not in the tide. They performed harmonic analyses over four consecutive periods of 19 years in order to subtract the tidal signal, thus subtracting any tidal variation between these periods. MSL changes were included within the surge component. They concluded that the decadal averages of surge frequency and duration were rising as a consequence of the rise in MSL over the studied period (1905–2003), while the height of both positive and negative surges decreased in the last one and two decades, respectively.

As previously mentioned, accounting for the connections between variations in climate systems and the inter-annual variability of extreme WLs when modeling extreme WLs can reduce the uncertainty of the estimates (Wahl and Chambers, 2015). However, the connections between climate systems of the Southern Hemisphere and the inter-annual variability of extreme WLs in Buenos Aires and Mar del Plata have not yet been assessed. In this context, the El Niño Southern Oscillation (ENSO) has been shown to be linked to wind anomalies as well as extreme river discharge in this region (Jaime, 2002; Meccia et al., 2009), thus potentially influencing extreme WLs. The inter-annual variability of extreme WLs at these locations could also be linked to other climate phenomena such as the South Atlantic Ocean Dipole, which is characterized by a warming (cooling) of the surface waters off West Africa associated with concurrent cooling (warming) off the Argentina-Uruguay-Brazil coast (Nnamchi et al., 2011). In addition, the Southern Annular Mode (SAM), also termed Southern Hemisphere Circulation or Antarctic Oscillation, has been shown as a significant forcing of the variability of some climate variables such as precipitation and temperature in the Southern Hemisphere (e.g., Gillett et al., 2006). However, contradictory results were reported over the east of South America (Gillett et al., 2006; Silvestri and Vera, 2009), where the teleconnections of these climate variables with SAM seem to be driven by a shift of the circulation anomaly associated to SAM (Silvestri and Vera, 2009).

While trying to assess changes in extreme WLs tides have been assumed to remain constant, although some recent studies have reported significant positive and negative trends in tidal levels and tidal constituents in most regions of the world (Woodworth and Blackman, 2004; Jay, 2009; Ray, 2009; Haigh et al., 2010b; Woodworth, 2010;

Müller, 2011; Feng et al., 2015; Mawdsley et al., 2015; Hill, 2016). However, secular tidal changes in Buenos Aires and Mar del Plata have not yet been analyzed and have therefore not been considered in previous studies on the trends and variability of storm surges (D'Onofrio et al., 2008; Fiore et al., 2009). In this context, Luz Clara et al., (2014) showed that the inter-annual variability of the river discharge into the RdIP estuary between 1965 and 2011 produced changes in the amplitude and phase of the M2 constituent in Buenos Aires. In addition, changes in the phase of the tidal constituents can produce increases or decreases of the tidal range by constructive or destructive interference between constituents.

In this study, we aim to extend the knowledge of secular trends and variability of extreme WLs and tides in two locations that are not included in global tide-gauge datasets. We explore the presence of significant secular trends in the hourly tide-gauge datasets of Buenos Aires and Mar del Plata over the last 109 years and 58 years, respectively, by performing an annual percentile analysis. In addition, we assess if the residual component (after subtracting the MSL and tidal signals) is linked to the regional climate system by assessing its correlation with different climate indices such as El Niño 3, SOI, SAODI, and SAM. Finally, we examine whether the tide shows any significant long-term trend over the study period by a 19 years running harmonic analysis, assessing both changes in the tidal levels and main tidal constituents: M2, S2, K1, O1, and M4.

## **2.2. Data**

Hourly WLs recorded from 1905 to 1961 in Buenos Aires were obtained from the Permanent Service for Mean Sea Level (PSMSL), and from 1959 to 2013 from the SHN of Argentina. Both WL series are referenced to Riachuelo Tidal Datum, which is 79 cm below MSL. Although the WL series were measured at two different tide-gauge stations (Buenos Aires and Palermo, respectively) separated by 9 km, we find no significant differences in the WLs of the 3 years overlapping period ( $p = 0$ ). We therefore combine the PSMSL WL series with the WL series of the SHN, referencing them to MSL. The final WL series of Buenos Aires comprises 109 years with a two-year gap between 1963 and 1964.

Similar to Buenos Aires, we use two WL series recorded at two separate tide-gauge stations for Mar del Plata both from the SHN. The first one, covering the period from 1956 to 1998, was recorded at the Club de Pescadores station, for which the tide-gauge zero is 112 cm below MSL. The second WL series includes data from 1999 to

2013 from the Base Naval station, and is referenced to a tidal datum 91 cm below MSL. In this case, there is no overlapping period between both WL series and there is an approximate 5-min phase lag between the two series. Similarly to previous studies (Fiore et al., 2008), we neglect the phase lag and combine both WL series, which we reference to MSL. From 1980 onward, the WL series of Mar del Plata is 91% complete, but has temporary gaps of up to 4 months. Both WL series were visually checked for datum shifts and outliers.

In order to represent the decadal variations in the climate system governing our study area, we collected time series of the climate indices El Niño 3.4, Southern Oscillation Index (SOI), South Atlantic Ocean Dipole Index (SAODI) and Southern Annular Mode (SAM) (Table 2.1). Due to the fact that ENSO is a multifaceted phenomenon that involves different aspects of the atmosphere and the ocean, we use two indices, namely El Niño 3.4 and SOI, which are based on two different variables (Sea Surface Temperature and Sea Level Pressure), as a proxy of this phenomenon. We use monthly time series in order to analyze potential links between ENSO and the inter-annual variability of WLs in Buenos Aires and Mar del Plata and to analyze whether one of these indices shows a greater teleconnection to the WLs variability. Similarly to ENSO, there are several climate indices that represent the atmospheric pattern of the SAM and that differ on several factors such as the data source or the method used to estimate it (Ho et al., 2012). We use annual time series of SAM from Visbeck, (2009) because it covers most of the study period. In addition, we use a monthly time series of the SAODI (Nnamchi et al., 2011) as a proxy of the climate variability in the Southern Atlantic Ocean. The runoff entering the RdIP estuary comes mainly from the Paraná and Uruguay rivers. Therefore, we use daily discharge time series of both rivers, measured at two upstream stations, Túnel Subfluvial for the Paraná river and Paso de los Libres for the Uruguay river. The employed data are freely available from Base de Datos Hidrológica Integrada (BDHI) of the Sistema Nacional de Información Hídrica of Argentina.

Table 2.1 Description, period, and source of the Climate Indices.

Climate Index	Period	Description	Source
El Niño 3.4	1905-2013	Area averaged SST from 5S to 5N and 170 to 120W.	National Oceanic and Atmospheric Administration (NOAA)
SAODI	1905-2012	Difference of area averaged SST between 10E and 20W and 0-15S and 10-40W and 25-40S.	Nnamchi et al., 2011
SAM	1905-2005	Difference of averaged pressure anomaly between regionalized subtropical and subpolar stations.	Visbeck, 2009
SOI	1905-2013	Difference of sea surface pressure between Tahiti and Darwin.	National Oceanic and Atmospheric Administration (NOAA)

## 2.3. Methods

### 2.3.1. Percentile Analysis

In order to analyze long-term changes in the frequency distribution of extreme high and low WLs, we examine the presence of linear trends in the series of annual WL percentiles. This method is widely used to assess changes in extreme WLs because it is less sensitive to outliers than the analysis of annual maxima (Woodworth and Blackman, 2004; Marcos et al., 2009; Haigh et al., 2010b; Letetrel et al., 2010; Mudersbach et al., 2013; Wahl and Chambers, 2015). In addition, percentile analysis allows assessing whether changes in extreme WLs are similar to the ones in MSL or whether other factors affect the distribution of extreme WLs.

In a first step, we produce annual series of percentiles, including the 0.05<sup>th</sup>, 0.5<sup>th</sup>, 2<sup>th</sup>, 5<sup>th</sup>, 10<sup>th</sup>, 20<sup>th</sup>, 50<sup>th</sup>, 80<sup>th</sup>, 90<sup>th</sup>, 95<sup>th</sup>, 98<sup>th</sup>, 99.5<sup>th</sup>, and 99.95<sup>th</sup> percentiles of both WL records for each calendar year (hereafter WL percentile series) with <25% missing values (Haigh et al., 2010b; Wahl and Chambers, 2015). The median (50<sup>th</sup> percentile) can be assumed as a good approximation of MSL, because this percentile is less affected by outliers than the mean. To remove the signal of the MSL we subtract the values of the 50<sup>th</sup> percentile series from each of the other percentile series, creating another set of annual percentiles series reduced to the medians (hereafter RedM percentile series). In addition, any signal related to vertical land movement is included within the value of the 50<sup>th</sup> percentile and thus removed by this reduction (Woodworth and Blackman, 2004). However, the contribution of the tide is still present. In order to remove the tidal contribution, we create series of annual tidal percentiles from the predicted WLs. For this purpose, we perform a harmonic analysis for each year

separately using the UTide Matlab package (Codiga, 2011), which gives a standard set of 63 tidal constituents with a value of signal-to-noise-ratio of at least two. Based on these tidal constituents, we produce the astronomical WLs of each calendar year of records, and calculate the tidal annual percentiles (0.05<sup>th</sup>–99.95<sup>th</sup>) of each calendar year (hereafter Tide percentile series). From each RedM percentile series, we subtract the corresponding Tide percentile series, creating another set of annual percentile series reduced to the median and to the tide (hereafter Residual percentile series). However, the Residual percentiles series still contain the tidal variability related to the perigean (4.4 years) and the nodal cycle (18.6 years) components, which cannot be estimated from annual harmonic analysis. Most of the remaining variability and trends of the Residual percentile series can be attributed to forcings different than MSL and tides, or to non-linear effects caused by the changes in the MSL and tides (Woodworth and Blackman, 2004). We calculate the standard deviation (std) of the Residual percentile series as a measure of the inter-annual variability.

In a next step, we analyze the presence of secular trends in the WL, Tide, and Residual percentile series and the link of the variability of the Residual percentile series to the decadal variability in the regional climate system. Long-term trends are assessed by fitting linear regressions to each annual percentile series of all sets and calculating the significance of the fitted linear model at the 5% significance level. In order to analyze whether extreme WLs are linked to the climate systems of this region, we calculate Spearman's rank correlations, at the 95% confidence level, between the Residual percentiles series and the climate indices El Niño 3.4, SAODI, SOI, and SAM. Spearman is a non-parametric test that measures the strength between two variables using a monotonic function and it does not make any assumption regarding the distribution of the two variables. We produce annual time series of each of these indices by averaging their monthly values per calendar year in order to synchronize them with the Residual percentiles series. We also assess the influence of extreme river runoff by correlating the annual 99.95<sup>th</sup> percentile series of river discharge from each river tide-gauges (i.e., Túnel subfluvial and Paso de los Libres) with the Residual annual percentile series of Buenos Aires and Mar del Plata.

### **2.3.2. Tidal Analysis**

In order to assess secular changes in tidal levels and the main tidal constituents in Buenos Aires and Mar del Plata, we perform a second harmonic analysis over

consecutive periods of 19 years, in order to account for both the perigean and nodal cycle components and reducing the errors of the constituents estimates.

Prior to the harmonic analysis, we de-trend both WL series in order to remove the seasonal variability and long-term trend of the MSL, as well as the vertical land movement signal (Mawdsley et al., 2015). The detrending of the WL series is performed by subtracting the centered 30-days moving average of each hourly WL from both time-series.

Again, we use the UTide Matlab package (Codiga, 2011) to perform a centered 19 years moving harmonic analysis with a lag of 1 year over the detrended time-series. By using the moving harmonic analysis, we shorten our records but we still obtain estimates of the tidal constituents over 90 and 40 years for Buenos Aires and Mar del Plata, respectively. We predict hourly astronomical WLs for each calendar year using the tidal constituents estimated from the harmonic analysis centered on the corresponding year. We calculate the annual mean of different tidal levels of the astronomical WL series of both locations and fit linear regressions to them in order to assess whether the tidal levels show a significant linear trend over the study period.

Buenos Aires and Mar del Plata have a mixed semidiurnal tide, with one of the daily high (low) water peaks being higher (lower) than the other peak (Figure 2.1). Therefore, the tidal levels selected for the analysis are: higher high water (HHW), lower low water (LLW) and greater diurnal tidal range (GDTR; i.e., difference between the HHW and LLW); lower high water (LHW), higher low water (HLW) and lesser diurnal tidal range (LDTR; i.e., difference between LHW and HLW); mean high water (MHW; mean of HHW and LHW), mean low water (MLW; mean of LLW and HLW) and mean tidal range (MTR; difference between MHW and MLW).

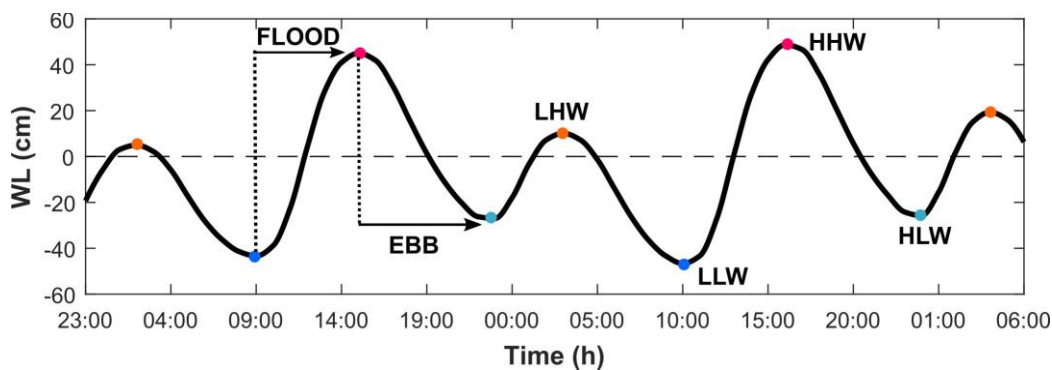


Figure 2.1 Diagram of the tidal levels and phases of the tidal curve analyzed

Changes in water depth, e.g., triggered by sea level rise, alter shallow water processes such as tidal wave velocity and energy dissipation by bottom friction, which may change the tidal curve. To assess secular changes in the tidal curve, we analyze the presence of significant long-term linear trends in the annual duration of the ebb and flow phases over the predicted period. We therefore calculate the duration of each flood phase of the astronomical WL series as the time between a low water peak and the following high water peak, as well as the duration of each ebb phase as the time between a high water peak and the successive low water peak. Then, we average both flood and ebb series per each calendar year and fit a linear regression through the flood and ebb annual series as well as to the annual flood/ebb ratio, which is a measure of tidal asymmetry.

Similarly, we assess secular trends in the amplitudes and phases of the main tidal constituents M2, S2, K1, and O1, and the overtide M4 at Buenos Aires and Mar del Plata by fitting linear regressions and analyzing their significance level.

## **2.4. Results**

### **2.4.1. Percentile Analysis**

In Buenos Aires, most WL percentile series show significant positive trends ranging between 1.17 to 2.32mm  $y^{-1}$  (Table 2.2). Assuming the 50<sup>th</sup> percentile series to be a good approximation of MSL, we obtain a linear MSL rise of 1.35mm  $y^{-1}$  over the last century in Buenos Aires. The WL percentile series lower than the median show larger increases than the upper percentiles series, with a difference higher than 1mmy<sup>-1</sup> in some cases (e.g., 0.5<sup>th</sup> percentile and 99.5<sup>th</sup> percentile). In Buenos Aires, most of the lower RedM percentile series show a significant positive trend, but none of the upper RedM percentile series. In Mar del Plata, half of the RedM percentile series also show a significant positive trend and we do not find any significant trend in the upper RedM percentile series. Therefore, the lower WL percentile series appears to have risen faster than MSL over the last century, while the upper percentiles series followed a trend similar to MSL. The lower Tide percentile series (i.e., lower than the 50<sup>th</sup> percentile) also show significant positive trends between 0.27 and 0.51mm  $y^{-1}$ . However, only the Residual 2nd percentile series show a significant positive trend of 0.32mm  $y^{-1}$ .

The WL percentile series of Mar del Plata show generally smaller trends than the trends of the WL percentile series of Buenos Aires. We obtain a MSL rise of 1.02mm  $y^{-1}$  in Mar del Plata over the studied period (1956–2013), which is approximately half of the studied period of Buenos Aires (1905– 2013). In Mar del Plata, we also obtain a difference around 1mm  $y^{-1}$  between the trends of the lower and upper WL percentile series (i.e., below and above the 50<sup>th</sup> percentile). Only the Tide 0.05<sup>th</sup> percentile series shows a significant positive trend of 1.04mm  $y^{-1}$  in Mar del Plata, and none of the Residual percentile series shows a significant trend.

Table 2.2 Trends (mm  $y^{-1}$ ) of the WL, RedM, Tide (reduced to their median) and Residual annual percentile series of Buenos Aires and Mar del Plata.

Station	Dataset	Percentiles' Trends (mm $y^{-1}$ )												
		0.05	0.5	2	5	10	20	50	80	90	95	98	99.5	99.95
Buenos Aires	WL	3.00*	2.32	2.10	1.86	1.68	1.58	1.35	1.34	1.27	1.29	1.35	1.17	1.29*
	RedM	1.65*	0.97	0.75	0.51	0.33	0.23	-	0.01*	0.08*	0.06*	*	0.18*	1.29*
	Tide	0.51	0.42	0.42	0.40	0.35	0.27	-	0.03*	0.03*	0.05*	*	0.10*	0.10*
	Residual	1.14*	0.55*	0.32	0.11*	0.02*	0.04*	-	0.02*	0.11*	0.11*	*	0.09*	1.39*
Mar del Plata	WL	2.20	1.43	1.61	1.46	1.26	1.14	1.02	1.02	1.02	1.14	1.24	0.70*	0.85*
	RedM	1.18*	0.41*	0.59	0.44	0.25	0.12*	-	0.00*	0.00*	0.12*	*	0.32*	0.85*
	Tide	1.04	0.62*	0.28*	0.09*	0.06*	0.15*	-	0.04*	0.22*	0.30*	*	0.03*	0.07*
	Residual	0.14*	0.20*	0.31*	0.35*	0.20*	0.03*	-	0.04*	0.22*	0.18*	*	0.35*	0.91*

\*Not significant with a 5% of significance level

In Figure 2.2, we can observe that the WL percentile series of Buenos Aires (Figure 2.2A) also show a greater inter-annual variability than the WL percentile series of Mar del Plata (Figure 2.2C). Specifically, the Residual 99.95<sup>th</sup> and 0.05<sup>th</sup> percentiles series of both locations (Figures 2.2B,D) show the greatest inter-annual variability, which can be two to three times greater in Buenos Aires ( $std_{0.05} = 62.96$  cm and  $std_{99.95} = 31.12$  cm) compared to Mar del Plata ( $std_{0.05} = 12.90$  cm and  $std_{99.95} = 16.92$  cm). In Buenos Aires, we observe that the lowest percentile series has a larger inter-annual variability than the 99.95<sup>th</sup> percentile. Meanwhile, the inter-annual variability of these percentile series in Mar del Plata is of similar magnitude.

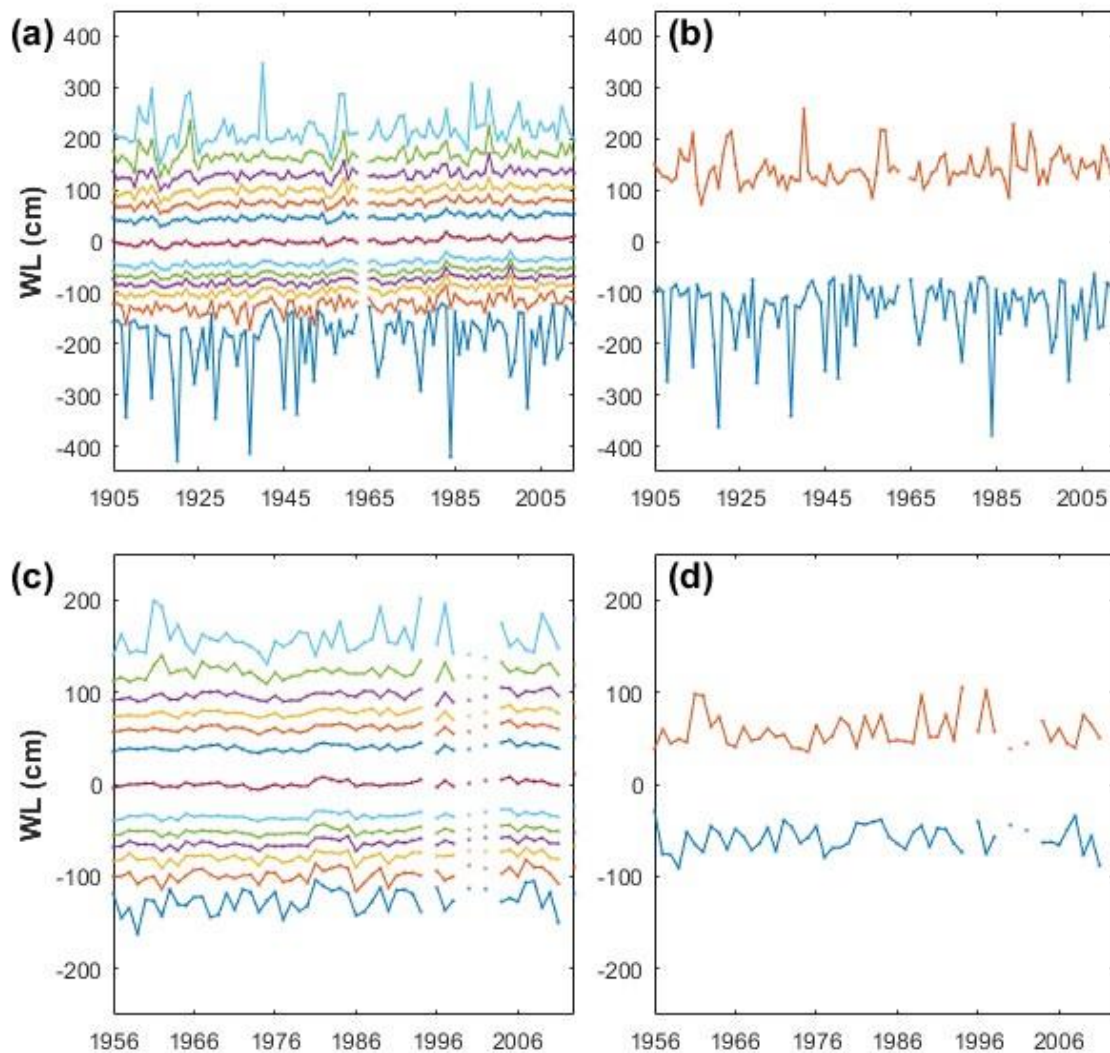


Figure 2.2 Series of (A) WL percentile series at Buenos Aires (top: 99.5<sup>th</sup>; bottom: 0.05<sup>th</sup>), (B) Residual 99.5<sup>th</sup> (orange) and 0.05<sup>th</sup> (blue) percentile series at Buenos Aires, (C) WL percentile series at Mar del Plata (top: 99.5<sup>th</sup>; bottom: 0.05<sup>th</sup>), and (D) Residual 99.5<sup>th</sup> (orange) and 0.05<sup>th</sup> (blue) percentile series at Mar del Plata.

From the correlation analysis (Figure 2.3), the Residual 98<sup>th</sup> and 99.5<sup>th</sup> percentile series of Buenos Aires show significant correlation with the ENSO indices, positive with El Niño 3.4 and negative with SOI. Meanwhile, in Mar del Plata we observe a negative correlation between the Residual 5<sup>th</sup>, 10<sup>th</sup>, and 80<sup>th</sup> percentile series and El Niño 3.4, and only the 80<sup>th</sup> percentile series shows a positive correlation with SOI. Regarding the SAODI, we observe a negative correlation with one percentile series in each location, the 98<sup>th</sup> percentile series in Buenos Aires and the 90<sup>th</sup> percentile series in Mar del Plata. Similarly, only one Residual percentile series of each location shows a significant correlation to SAM, namely a positive correlation with the 90<sup>th</sup> percentile series of Buenos Aires and a negative correlation with the 80<sup>th</sup> percentile series of Mar

del Plata. Regarding the correlation with river discharge, we obtain a significant positive correlation between all percentile series above the median, with exception of the 99.95<sup>th</sup> percentile, in Buenos Aires and the Paraná river discharge (Subfluvial station). However, we only find significant positive correlation between two percentile series (80<sup>th</sup> and 99.5<sup>th</sup> percentiles) and the discharge of the Uruguay river (Libres). On the contrary, only the 80<sup>th</sup> percentile series of Mar del Plata shows a significant negative correlation to the discharge of the Uruguay river.

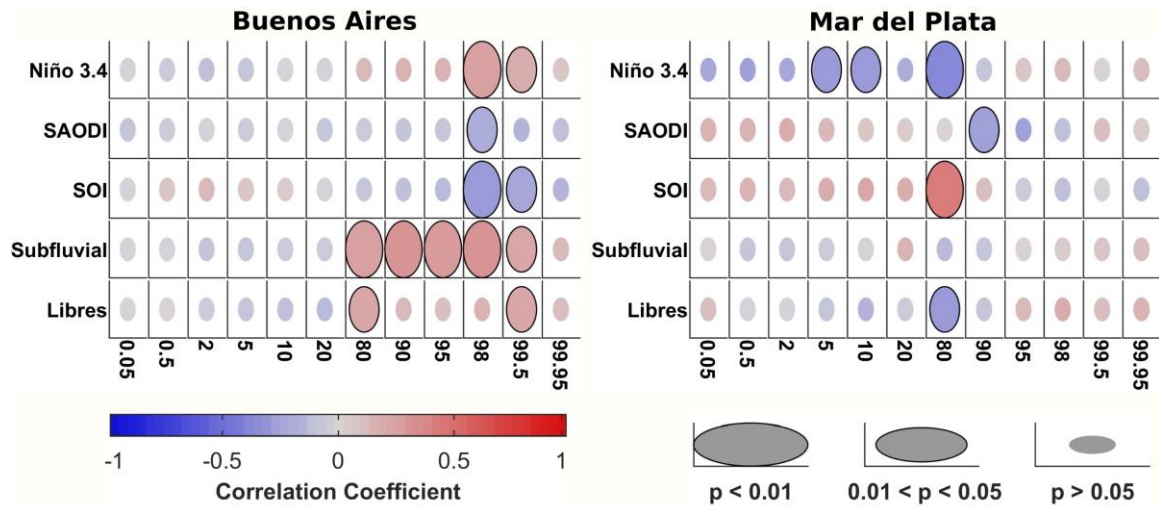


Figure 2.3 Correlation between climate indices, river runoff and the reduced (to median and tide) annual percentiles of Buenos Aires and Mar del Plata.

## 2.4.2. Tidal Analysis

In places with a mixed semidiurnal tide, changes in HHW, LLW and thus GDTR may cause greater impacts on flooding, erosion and navigation safety than changes in the other tidal levels, as these levels account for the highest and lowest astronomical WLs. In Figure 2.4, we present the annual HHW, LLW, and GDTR of Buenos Aires and Mar del Plata over the corresponding study periods. We observe that all tidal levels show an inter-annual variability of several centimeters, but a linear secular trend can also be distinguished in all tidal levels in both locations. As a general pattern, we observe an overall decrease of the annual GDTR driven by an increase of the LLW and a decrease of the HHW. In Buenos Aires, the decrease of the GDTR is more pronounced ( $0.62\text{mm y}^{-1}$ ) than in Mar del Plata ( $0.43\text{mm y}^{-1}$ ), and it arises from a large increase of the LLW ( $0.55\text{mm y}^{-1}$ ) and a low decrease of the HHW ( $0.08\text{mm y}^{-1}$ ). However, in Buenos Aires we can observe the opposite pattern over some periods e.g., during the first 50 years of records, we observe an increase of the HHW and a decrease of LLW, resulting in an increase of the GDTR of more than 5 cm (Figure 2.4). In Mar del Plata, these tidal

levels show a periodic inter-annual variability of around 2 cm and cycles of 5 years in the HHW and 3 years in the LLW. Besides the inter-annual variability, LLW raised with a rate of  $0.15\text{mm y}^{-1}$  during the second half of the century, and the HHW decreased  $0.28\text{mm y}^{-1}$  during the same period (Figure 2.4).

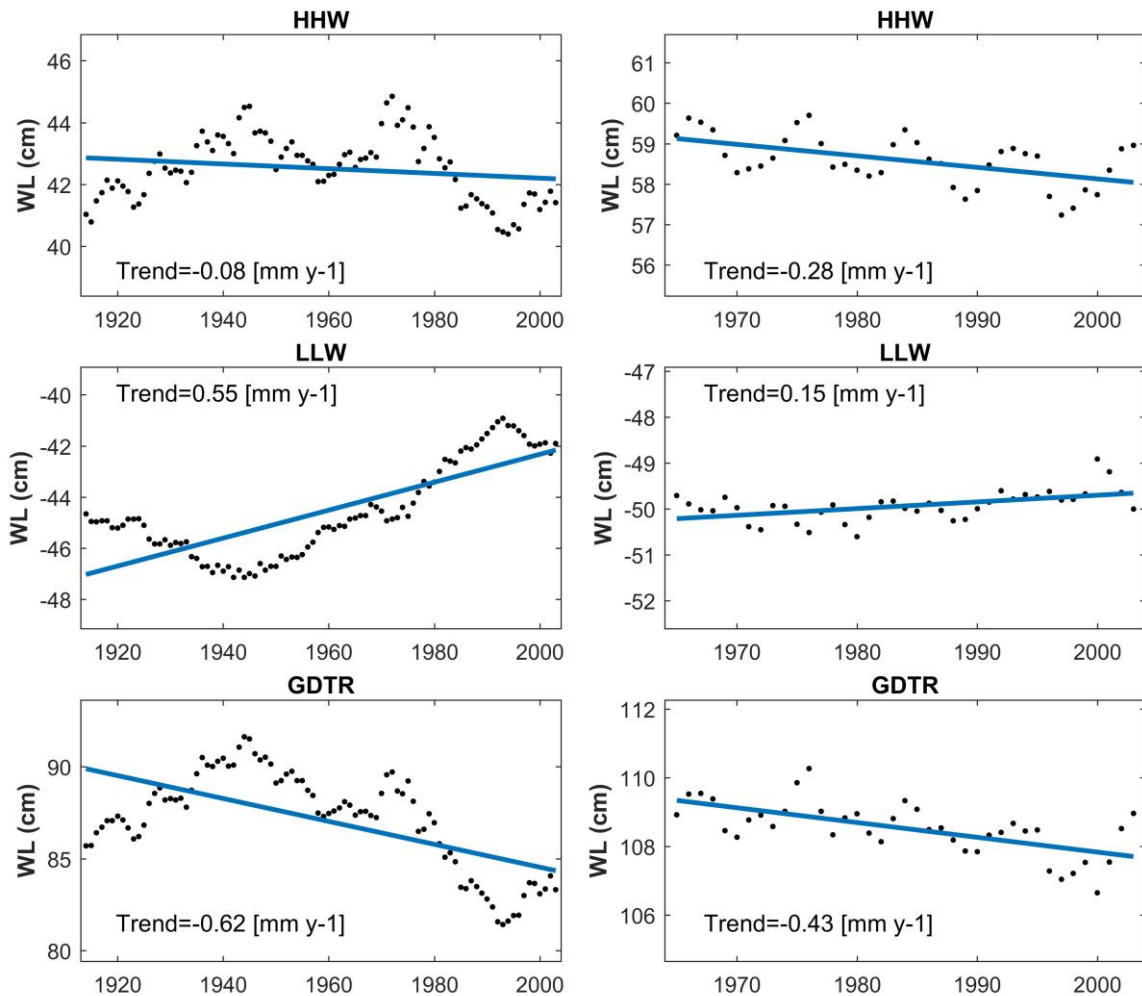


Figure 2.4 Linear trends of Annual HHW, LLW, and GDTR of Buenos Aires (Left) and Mar del Plata (Right).

The general pattern described for the HHW, LLW and GDTR is also observed in the other tidal levels analyzed (i.e., LHW, HLW, LDTR, HW, LW, and MTR), although they show trends of different magnitude. The results of the other tidal levels can be found in Appendix A (Figures A.1, A.2).

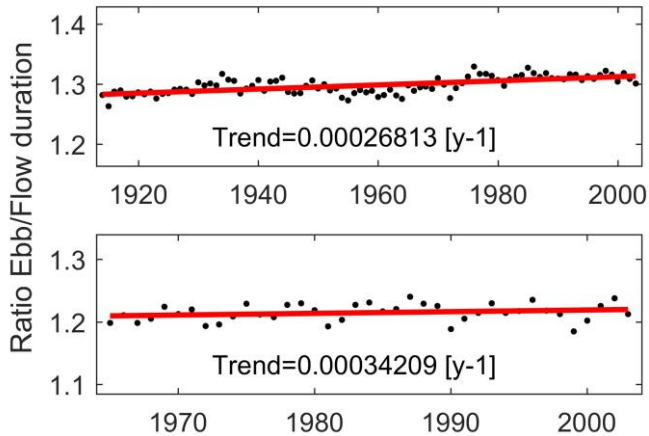


Figure 2.5 Ratio of the annual mean ebb and flood duration of Buenos Aires (Upper) and Mar del Plata (Lower).

The differences obtained in the secular trends of the HHW and LLW may produce a change in the tidal curve, thus altering the ebb and flood phases. In shallow water, the asymmetry of the tidal curve is generally characterized by a shorter flood phase with stronger currents and a longer ebb phase with weaker currents (Pugh and

Woodworth, 2014). We use the ratio between the annual mean duration of the ebb and flood phases as a measure of the asymmetry of the tidal curve (Figure 2.5). We observe that both places are flood dominated, as the duration of the flood phase is shorter than the ebb phase, and the asymmetry is greater in Buenos Aires than in Mar del Plata. We find that the asymmetry of the tidal curve shows a small significant increase over the study periods at both locations and also shows an inter-annual variability with a 4 year cyclicity and a magnitude larger than the long-term trend.

The changes observed in the tidal levels and the asymmetry of the tidal curve have to arise from secular changes in any of the main tidal constituents. Figures 2.6, 2.7 show the amplitude and phases of the M2, M4, S2, K1, and O1 constituents obtained from the harmonic analysis over consecutive periods of 19 years for Buenos Aires and Mar del Plata and their secular trends. Almost all tidal constituents show significant trends in both amplitude and phase, with the exception of the O1 amplitude in Buenos Aires. In both locations, the semidiurnal constituents (M2 and S2) show a decrease in the amplitude, while an increase is found in the amplitude of the diurnal constituents (K1 and O1). However, we observe an increase in the phase of both diurnal and semidiurnal tidal constituents, with the exception of the K1 phase in Mar del Plata. In addition, the amplitude and phase of all constituents show an inter-annual variability, which is generally greater in Buenos Aires than in Mar del Plata. For most of the constituents, the inter-annual variability of the amplitude and phase are not showing the same temporal patterns (see e.g., variability of the amplitude and phase of the M2 in Buenos Aires).

M2 is the tidal constituent with the largest amplitude in both places and the constituent that shows the greatest change in amplitude over the study period. The amplitude of

M2 decreased with a similar rate during the last century in Buenos Aires ( $0.29\text{mm y}^{-1}$ ; Figure 2.6) as during the last 30 years in Mar del Plata ( $0.27\text{mm y}^{-1}$ ; Figure 2.7). However, the M2 amplitude shows some periods of increase in Buenos Aires, but an almost constant decrease in Mar del Plata. The variability observed in the annual GDTR in Buenos Aires (Figure 2.3) shows a correlation of 0.96 ( $p = 0$ ) with the pattern of the M2 amplitude, and can thus be explained by the changes in the M2 constituent. In Mar del Plata, the M2 amplitude shows a smaller correlation (0.64 and  $p = 2.16 \cdot 10^{-5}$ ) with the GDTR that may be due to the different inter-annual variability observed in both variables (Figure 2.4).

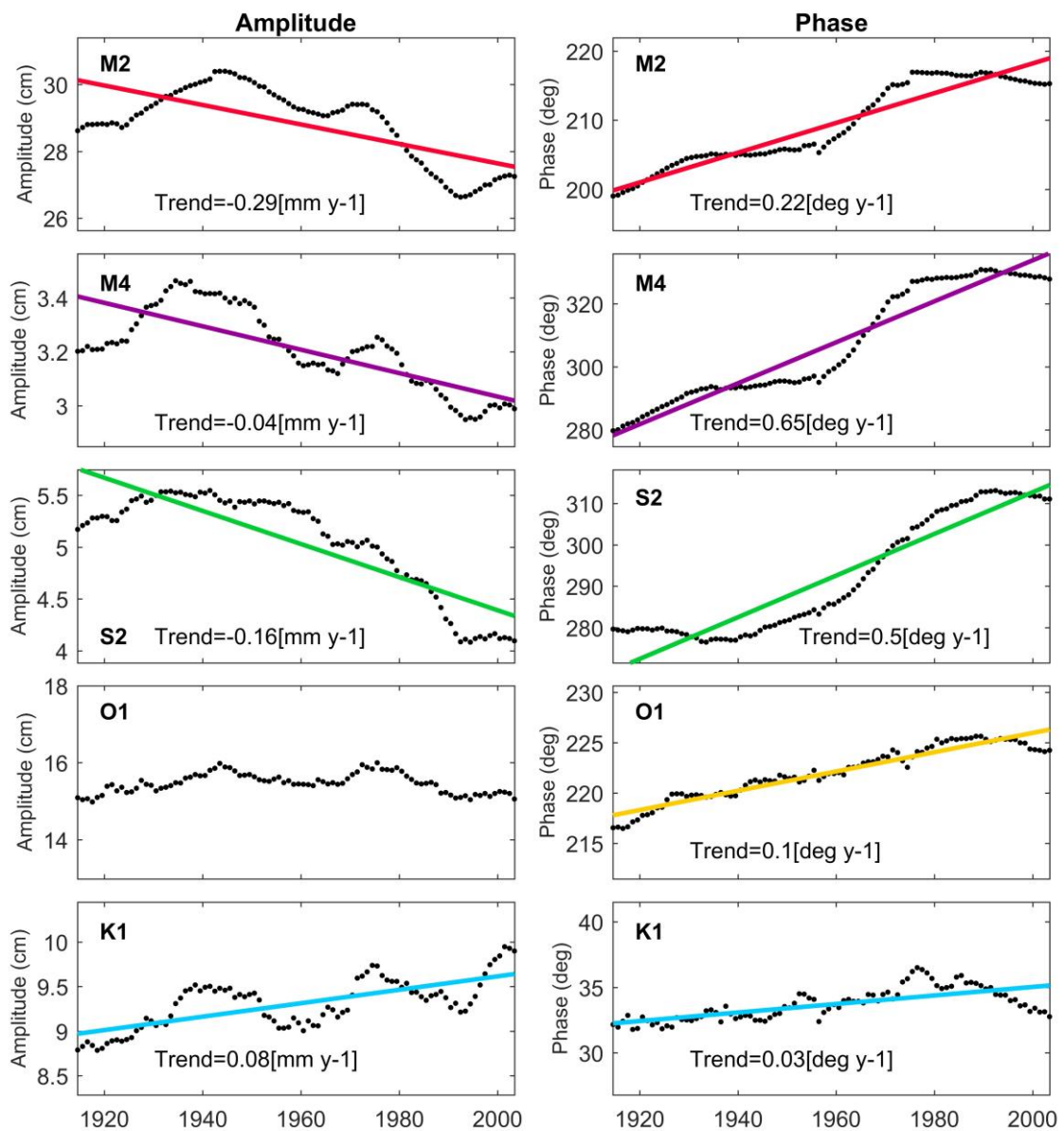


Figure 2.6 Variability and linear trends of the amplitude and phase of the main tidal constituents of Buenos Aires (only significant trends are shown)

The S2 constituent, which has a radiational forcing in addition to the gravitational, shows the second more pronounced negative trend in both Buenos Aires ( $0.16\text{mm y}^{-1}$ ; Figure 2.6) and Mar del Plata ( $0.21\text{mm y}^{-1}$ ). We observe that the changes in the amplitude and phase of S2 are simultaneous in both locations, i.e. in periods when the amplitude shows greater decreasing trends, the phase shows a greater increasing trend.

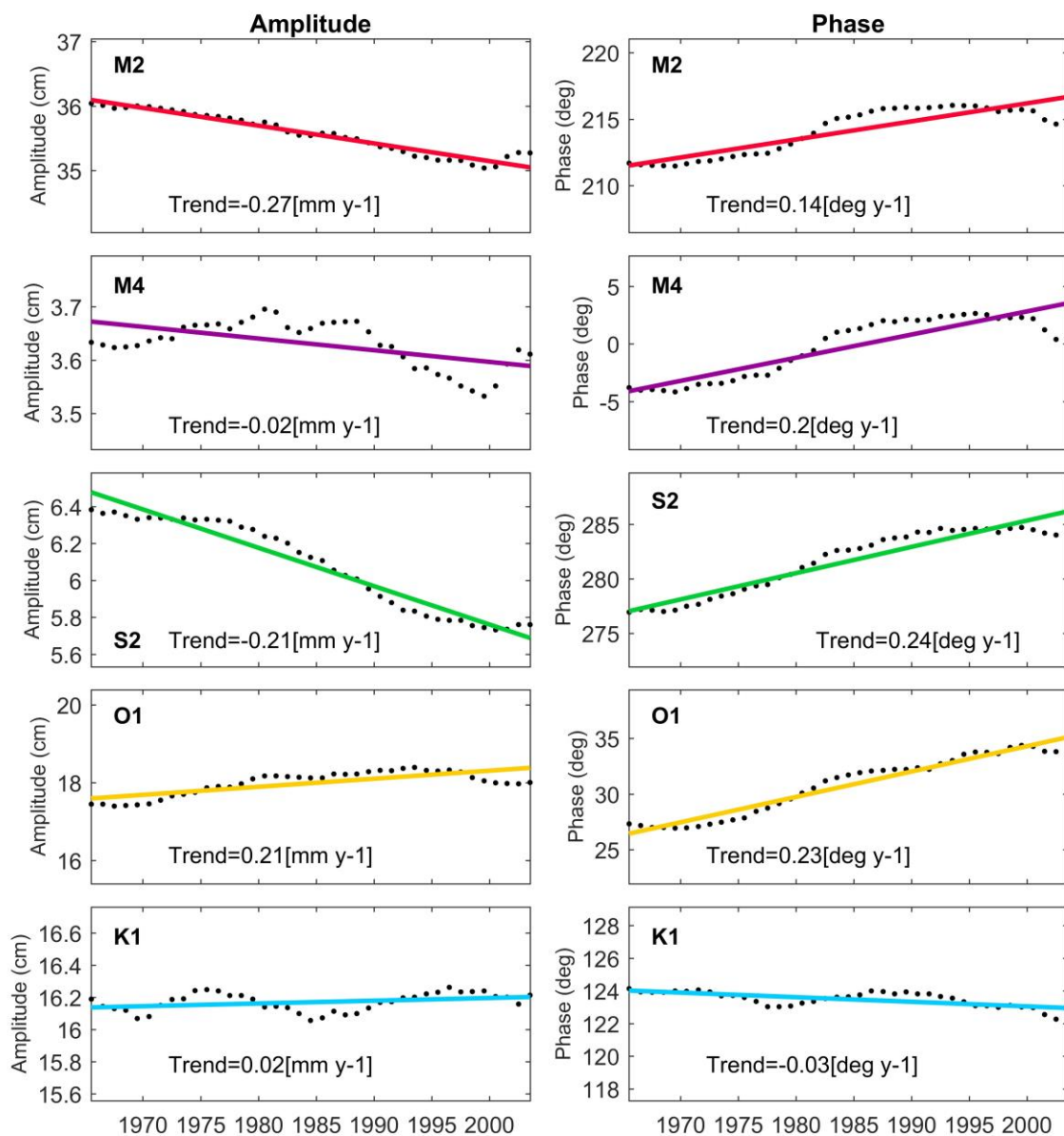


Figure 2.7 Variability and linear trends of the amplitude and phase of the main tidal constituents of Mar del Plata

The two diurnal constituents O1 and K1 are the second and third highest constituents in terms of amplitude, at Buenos Aires and Mar del Plata. Opposite to the long-term trends observed in the main semidiurnal constituents, we observe a secular increase in the amplitude of the diurnal constituents at both locations.

The asymmetry of the tidal curve depends on the phase difference between the M2 and M4 constituents (see e.g., Pugh and Woodworth, 2014). In both locations, we find that the phases of both constituents show a positive trend, which is more pronounced for the M4 phase. The difference between the rising rates of the M2 and M4 phases is greater in Buenos Aires (0.22 and 0.65 deg  $y^{-1}$ , respectively; Figure 2.6) than in Mar del Plata (0.14 and 0.2 deg  $y^{-1}$ ; Figure 2.7). These results are in line with the greater increase in the tidal asymmetry in Buenos Aires than in Mar del Plata.

## **2.5. Discussion**

Long-term trends in WLs can arise from changes in their different components: MSL, tides and non-tidal residuals. Our analysis shows that the WLs of both Buenos Aires and Mar del Plata show significant long-term trends, which originate from MSL rise but also from long-term trends occurring in the tide component. The detailed analysis of the tides corroborates the significant trends observed in the percentile analysis, and shows a long-term decrease of the tidal range in both locations. On the other hand, the residual component shows no significant long-term trends in both locations.

### **2.5.1. Percentile Analysis**

The lower WL percentile series (i.e., lower than the median) of both Buenos Aires and Mar del Plata show larger trends than the upper WL percentile series indicating that the low WLs rose faster than the high WLs and MSL over the study period. Trends in Buenos Aires were higher than those in Mar del Plata. This difference seems to be caused by changes in the tide as we find significant positive trends in the lower RedM and Tide percentile series in Buenos Aires. In Mar del Plata, only three percentile series (2<sup>th</sup>, 5<sup>th</sup>, and 10<sup>th</sup>) show significant trends after their reduction to the median (RedM) and none of the Residual percentile series show a significant trend. However, the Tide 0.05<sup>th</sup> percentile series presents a significant positive trend, which is 1.04mm  $y^{-1}$  after subtracting the MSL trend. Therefore, changes in the WLs of Buenos Aires and Mar del Plata are not only caused by an increase in MSL, but also by changes in the tidal component. Although, such changes can affect the generation and

propagation of the surge component we do not obtain significant trends in the Residual percentiles series over the study period in both locations. However, Fiore et al., (2009) and D'Onofrio et al., (2008) reported an increase in the magnitude and frequency of the non-tidal residual component of a similar magnitude as MSL rise in Mar del Plata and Buenos Aires, respectively. These two studies assumed the tidal component to be constant over the studied period, thus the changes in the tidal levels that we observe were accounted for as changes in the non-tidal residual component.

We observe that the inter-annual variability of extreme WLs is greater in Buenos Aires compared to Mar del Plata (Figures 2.2B,D). The location of Buenos Aires, in the inner part of the RdIP estuary results in WLs also being affected by river discharge in addition to the wind-induced set-up. In previous studies on WLs in Buenos Aires, the effect of river runoff on WLs was denied (e.g., D'Onofrio et al., 1999). However, we find a significant correlation between most of the upper WL percentile series and the annual 99.5<sup>th</sup> percentile series of the Paraná river discharge, and between two WL percentile series and the annual 99.5<sup>th</sup> percentile series of the Uruguay river discharge. This indicates that at least extreme river discharge events have a significant effect on the WLs in Buenos Aires.

Extreme river discharge seems to have no effect on the WLs in Mar del Plata as no significant correlation is found between the WL and the river percentile series. An exception is the 80<sup>th</sup> percentile series, which shows a significant negative correlation to extreme river discharge of the Uruguay river (Paso de los Libres station). It is likely that this significant correlation is due to the meteorological conditions that produce extreme precipitation and alter the WLs in Mar del Plata, and not due to extreme river discharge itself, because the annual mean discharge of this river is lower than the Parana river. Further we also find a significant correlation between this percentile series and the two indices related to ENSO. The opposite can be true for Buenos Aires; we find a significant correlation between two of the upper percentile series and El Niño 3.4 index and SOI that do not necessarily mean a direct effect of the meteorological conditions associated to ENSO on the WLs, but to the higher river runoff associated to this phenomenon (Jaime, 2002). The conditions associated to the SAODI and SAM seem not to be linked to the inter-annual variability of WLs in both locations, because we only find significant correlation of one Residual percentile series of each location to these indices.

## 2.5.2. Tidal Analysis

We find a long-term trend and inter-annual variability in all tidal levels caused by the changes observed in the amplitude and phase of the main tidal constituents in Buenos Aires and Mar del Plata. The observed secular trends are of similar magnitude as the long-term trends reported in tidal levels of some locations along the northeastern coast of the US and Japan (Mawdsley et al., 2015). However, the magnitude of the trends that we find for the main tidal constituents differs from the ones reported at those locations (Ray, 2009; Rasheed and Chua, 2014).

As a general pattern, we observe a long-term decrease in the tidal range mainly caused by a decrease found in the amplitude of the main semidiurnal constituents M2 and S2. However, it seems that different processes are responsible for the changes observed in Buenos Aires compared to Mar del Plata, as we find substantial differences between the secular trends and inter-annual variability obtained for the tidal levels and constituents between them (e.g., a difference of  $0.4\text{mm y}^{-1}$  in the trend of LLW; Figure 2.4). We cannot exclude though that the same factors can have an effect of different magnitude on the tidal levels in Buenos Aires and Mar del Plata.

Changes in the tides have been reported globally with largescale ocean processes appearing to be the cause (Mawdsley et al., 2015). Nevertheless, different trends in both tidal levels and constituents have been observed in different regions, suggesting that regional and local factors can play an important role (Mawdsley et al., 2015). Several factors have been discussed as responsible for changes in the tidal characteristics observed in other regions. At global scale, these factors are the rise of MSL and changes in ocean stratification, while at local scale morphological changes (i.e., dredging, land reclamation) can also modify tide characteristics (see e.g., Woodworth, 2010; Müller, 2011; Devlin et al., 2014; Hill, 2016).

The rise of the MSL is one of the factors that can produce changes in tidal levels. An increase of the water depth can produce changes in the resonance characteristics of shelves, in the location of amphidromes and in shallow areas, a reduction of frictional effects that in turn affect overtides such as the M4 as we observe in the RdIP (Pugh and Woodworth, 2014). In Figure 2.8, we present the 19 years running average of the WLs in Buenos Aires and Mar del Plata and their respective GDTR series showing the co-evolution of the two variables (time series and scatter plot). In Buenos Aires, we observe that MSL and GDTR trends are inversely related in some periods, such as from 1975 to beginning of the 90's, when we see a rapid increase of MSL and

simultaneously a rapid decrease of the GDTR occurs. However, we observe a positive correlation of the trends from the beginning of the study period to the mid 40's and since the beginning of the 90's. In Mar del Plata, we can also observe a predominantly negative correlation between the MSL and GDTR, although it is less clear.

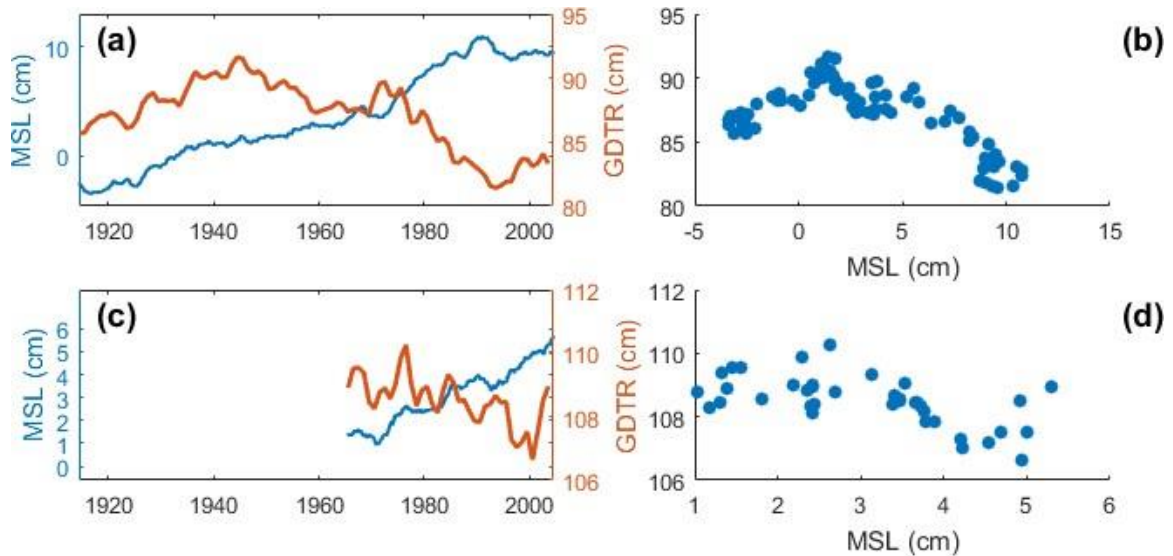


Figure 2.8 Comparison of the MSL (19-y running average) and the GDTR of (A) Buenos Aires and (C) Mar del Plata; scatter MSL and GDTR of (B) Buenos Aires and (D) Mar del Plata.

None of the above studies comprising the analysis of long-term trends in the tides was able to detect a correlation between the changes observed in the MSL and tides. In addition, studies comprising model simulations of tidal evolution under different SLR scenarios reported that greater rises of water depth are needed in order to produce significant changes in the tides (see e.g., Müller et al., 2011; Pickering et al., 2012, 2017; Carless et al., 2016). Tidal changes obtained from simulations under SLR scenarios depend not only on the SLR scenario and its spatial variability, but also on the stratification scheme and on whether land is allowed to flood (Pickering et al., 2012; Carless et al., 2016). Simulations of high end SLR scenarios (i.e., above 1m) over the Patagonian shelf performed by Carless et al., (2016) and Luz Clara et al., (2015) showed an increase of the M2 amplitude in the coastal region of Mar del Plata and a decrease of its phase. We observe the opposite pattern during the last 40 years at this location. For Buenos Aires, the global study of Pickering et al., (2017) showed a decrease of the MHW in all SLR scenarios and flooding schemes simulated. According to these contradictory results, the rise of the MSL does not appear to be the only factor producing the changes observed in the tidal levels in Buenos Aires and Mar del Plata.

Changes in stratification and in the thermocline have also been discussed as potential factors causing tidal changes by modifying the coupling of barotropic and internal tides

(Colosi and Munk, 2006; Jay, 2009; Müller, 2011; Devlin et al., 2014). The ocean circulation off the study area is characterized by the confluence of the Brazil and Malvinas currents (Palma et al., 2008). The Brazil current brings tropical water of high temperature and salinity, while the Malvinas current transports cold and fresh water from the Antarctic Circumpolar current (Piola et al., 2000; Artana et al., 2016). The different characteristics of these two currents produce a strong thermohaline front with a complex structure (Palma et al., 2008). Besides the seasonal variability of the Brazil/Malvinas confluence region, Combes and Matano (2014) reported a southward trend of this confluence region over the last decade of the twentieth century due to a weakening of the Malvinas current. In addition, the simulations performed by Carless et al., (2016) under an increased stratification scenario over the Patagonian shelf showed a decrease of 15 cm on average of the M2 amplitude along the Argentinian coasts. Therefore, changes in stratification could be responsible for the observed trends in both tidal levels and constituents.

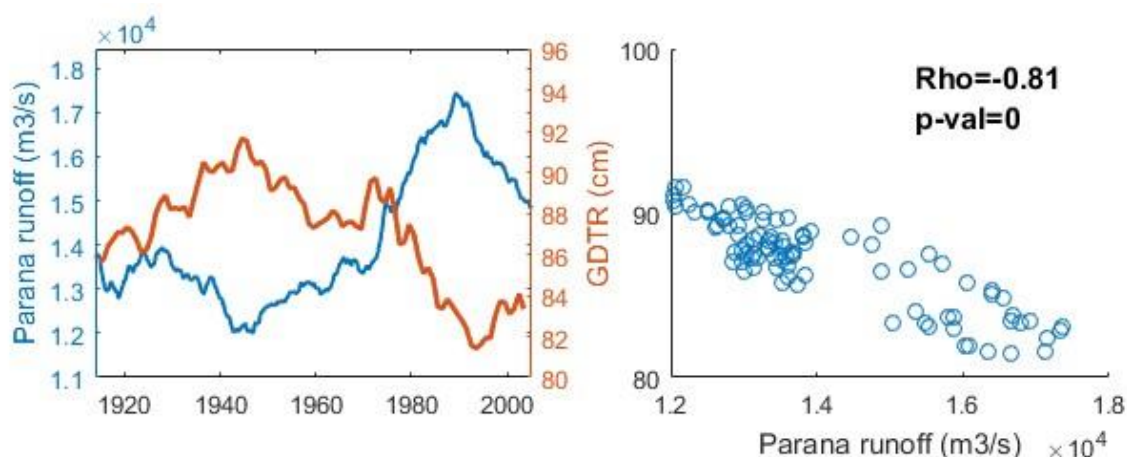


Figure 2.9 Comparison of the Paraná runoff (19-y running average) and the GDTR of Buenos Aires.

In Buenos Aires, the river discharge into the RdIP is the main factor affecting mixing and tidal propagation into the estuary (Nagy et al., 2008). Luz Clara et al., (2014) reported that the amplitude and phase of the M2 constituent in Buenos Aires show cycles of inter-annual variability that are negatively correlated with the cycles of river runoff, which are positively related to El Niño over the second half of the century. During El Niño, river discharge largely increases and thus increases the downstream currents affecting the upstream progression of the tidal wave (Luz Clara et al., 2014). Therefore, it is likely that the secular trends of both tidal levels and constituents are linked to the increasing river discharge into the RdIP estuary over the last century

(Jaime, 2002; Pasquini and Depetris, 2007, 2010), caused by an increase in precipitation and land use changes (Doyle and Barros, 2011). In Figure 2.9, we present the GDTR of Buenos Aires and the 19-years running average of the Paraná river discharge, which is double the discharge of the Uruguay river and can have a greater impact in the tidal levels in Buenos Aires. We can observe that both series are inversely correlated and the trends of the different periods show a strong negative. The M4 constituent shows a similar inter-annual variability and a negative correlation with the river discharge. The increased bottom friction with higher river discharge modulates the phase and amplitude of the M4 constituent. The secular increase of the river discharge into the RdIP might also be responsible of the observed increase of the asymmetry of the tidal curve, increasing the time of the ebb phase compared to the flood phase.

In addition, changes in the atmospheric dynamics and wind-driven circulation may produce changes in the MSL, depth of the mixed layer and sea surface temperature that may affect the tide (Jay, 2009; Müller, 2011; Müller et al., 2014). However, no significant correlation is found between the tidal anomalies in Mar del Plata and any Climate Index. In Buenos Aires, we find significant correlation to ENSO, but it is likely due to the increase of the river discharge in ENSO years (Jaime, 2002).

Local morphological changes caused by e.g., dredging can also produce changes in the tidal characteristics. The tide-gauge of Mar del Plata is located inside the port, which is periodically dredged. In addition, three beaches of Mar del Plata were nourished in 1998, using sand from a sand bank located near the port dikes (Marcomini and Lopez, 2006). Some navigation channels of the RdIP estuary are also periodically dredged and may affect the tidal characteristics of Buenos Aires. In addition, parts of the city of Buenos Aires have been settled on areas gained from the sea, and the vast majority of the land gain (~50 ha) occurred between 1836 to 1998 (Perez Garcia, 2012). These factors can be responsible for periodical or isolated changes of the tidal levels and constituents, but not for the constant trends observed in both tidal levels and constituents at these locations.

Tides control and influence all coastal and biological processes such as sediment transport and coastal ecosystems, and thus secular changes in the tidal characteristics alter those processes. The observed increase of the MLWs in and decrease of MHWs in Buenos Aires may produce a decrease of the intertidal region, thus reducing the area available for intertidal ecosystems. In addition, the vertical growth of the marshes of the RdIP estuary are also affected by changes in tidal range and river discharge

(Schuerch et al., 2016). Tide characteristics of Buenos Aires are likely modulated by the river discharge into the RdIP estuary and therefore their effects on marsh development should jointly be taken into account. The observed changes in the tidal levels and constituents as well as the increase in the asymmetry of the tidal curve indicate that also changes in the tidal currents have occurred, which in turn affect sediment transport within the estuary. In the context of flood risk, the observed decrease of the HWs would imply a decrease of the intensity of extreme WLs, in the case that there is no increase of the intensity of storm surges. However, the increase of MLWs leads to an increase of intensity and frequency of storm surge levels coincident with MLWs. Therefore, the observed changes in the tide should be taken into account in trend and extreme analysis of storm surges.

## 2.6. Conclusions

Our analysis shows that low WLs have risen faster than MSL over the last century in Buenos Aires and the last 40 years in Mar del Plata. However, we find no significantly different trend than the MSL trend in those WLs higher than the median. The percentile analysis suggests that the greater trends in the low WLs are mainly caused by trends in the tide component, as we obtain significant trends in the Tide percentiles that can double the trends of the MSL (i.e., 50<sup>th</sup> percentile). This is confirmed with the results of the running harmonic analysis, which show secular trends in all tidal levels caused by changes in the main tidal constituents (M2, S2, O1, and K1). In both locations, we observe a decrease of the tidal ranges (MTR, GDTR, and LDTR) of  $0.5\text{mm y}^{-1}$  on average that arises from a decrease of the amplitude of the semidiurnal constituents and an increase of the diurnal constituents, as well as changes in the phases.

Despite trends of the tidal range and tidal constituents being similar in both locations, the drivers do not seem to be the same for Buenos Aires and Mar del Plata. In Buenos Aires, we find a larger positive trend in the LLW than the decrease of the HHW and the changes of these tidal levels show a coherent variability with the variability of the river discharge into the RdIP. Large river discharge reduces the tidal wave propagation into the estuary. Therefore, the large increase of the river discharge over the second half of the twentieth century is likely the reason for the negative trend observed in the tidal range of Buenos Aires. Although, high river discharge may reduce the tidal range and MHWs at Buenos Aires, we also find significant correlation between extreme river discharge and the upper Residual percentiles series. In Mar del Plata, we find a lower increase of the MLWs and a greater decrease of the MHWs than in Buenos Aires, and

there is no correlation between the changes in the tides and the river runoff as well as between the Residual percentiles series and extreme river discharge into the RdIP. Therefore, the observed tidal changes are produced by a different factor than in Buenos Aires such as changes in the thermohaline structure of the Brazil/Malvinas confluence region or the rise of the MSL, although for the latter studies have shown that greater increases of the MSL are required to produce significant changes in the tides (Luz Clara et al., 2015; Carless et al., 2016).

## **Acknowledgments**

SS-A and AV were supported by the EU FP7 project RISESAM (grant agreement 603396). MS was financially supported by the “Deutsche Forschungsgemeinschaft” (DFG) through the Cluster of Excellence 80 “The Future Ocean,” funded within the framework of the Excellence Initiative on behalf of the German federal and state governments, the personal research fellowship of MS (Project Number 272052902) and by the Cambridge Coastal Research Unit (Visiting Scholar Programme). SC work was developed under the research project “Bases para un manejo sustentable de los recursos hídricos en la franja costera arenosa oriental de la Provincia de Buenos Aires” [“Guidelines for the sustainable management of water resources in the eastern coastal sand-dune barrier of the Province of Buenos Aires”] (PICT 2013-2117, ANPCyT, Argentina). We acknowledge the support of the Servicio de Hidrografía Naval (SHN) of Argentina for providing the tide-gauge series. We acknowledge financial support by Land Schleswig-Holstein within the funding programme Open Access Publikationsfonds. We would also like to acknowledge the two reviewers for providing constructive and valuable comments that helped improving the paper.

## Chapter 3.

# **Sea-level rise impacts on the temporal and spatial variability of extreme water levels: A case study for St. Peter-Ording, Germany**

*Sara Santamaria-Aguilar, Arne Arns and Athanasios T. Vafeidis*

*Journal of Geophysical Research: Oceans (2017)*

*doi: 10.1002/2016JC012579*

*Received: 23 November 2016, Accepted: 7 March 2017*



## Abstract

Both the temporal and spatial variability of storm surge water level (WL) curves are usually not taken into account in flood risk assessments as observational data are often scarce. In addition, sea-level rise (SLR) can further affect the variability of WLs. We analyze the temporal and spatial variability of the WL curve of 75 historical storm surge events that have been numerically simulated for St. Peter-Ording at the German North Sea coast, considering the effects induced by three SLR scenarios (RCP 4.5, RCP 8.5, and a RCP 8.5 high end scenario). We assess potential impacts of these scenarios on two parameters related to flooding: overflow volumes and fullness. Our results indicate that due to both the temporal and spatial variability of those events the resulting overflow volume can be two or even three times greater. We observe a steepening of the WL curve with an increase of the tidal range under the three SLR scenarios, although SLR induced effects are relatively higher for the RCP 4.5. The steepening of the WL curve with SLR produces a reduction of the fullness, but the changes in overflow volumes also depend on the magnitude of the storm surge event.

## Key Points

- Sea-level rise (SLR) results in a steeper storm water level curve that is proportionally greater for a moderate SLR scenario
- When accounting for temporal variability of the water level curve estimated overflow volume can be up to three times higher
- Overflow volume differences due to spatial variability can be similar to the difference between the T=200 and T=10,000 year event in one site

## 3.1. Introduction

Coastal flooding from extreme water levels (WL) is considered a major risk for coastal low-lying areas worldwide (Wong et al., 2014). These regions are densely populated and often exhibit higher rates of growth and urbanization than the hinterland, which further exacerbates their exposure to flood hazard (e.g., Hinkel et al., 2014; Neumann et al., 2015). In addition, the likelihood and intensity of current extreme WLs is expected to increase as a consequence of sea-level rise (SLR) (e.g., Seneviratne et al., 2012; Church et al., 2013). For the development of effective coastal management strategies, it is therefore essential that flood risk assessments account for these factors.

For coastal management and protection, flood risk assessments at high temporal and spatial resolution are needed in order to account for local effects. At such resolutions, hydrodynamic models are able to simulate physical processes (i.e., atmospheric-ocean-land interactions) accounting for local geometries such as bathymetries and dike heights. However, these models are computationally expensive, which constrains their application to regional-to-local scales at high spatial resolution and limits the potential number of hazard scenarios that can be simulated (Ramirez et al., 2016).

Nevertheless, flood risk assessments need to cover a wide range of hazard scenarios, from high-probability of occurrence and low-consequences to low-probability and high-consequences, in order to account for uncertainties and sensitivity within the assessment (Nicholls et al., 2014; Hinkel et al., 2015). The definition of low-probability hazard scenarios is complex because extreme WLs can arise from several combinations of mean sea level, tide, and surge conditions due to their different origin and high level of natural variability (e.g., Dangendorf et al., 2013, 2014). In addition, most observed WL series are limited to 100 years or less, making it likely that observational records do not contain the worst physically possible conditions (e.g., Dangendorf et al., 2016).

Therefore, low-probability WLs are often estimated using extreme value statistics that are used to extrapolate beyond the range of observations. Although significant efforts have been directed toward reducing the uncertainties in extreme WLs (see e.g., Haigh et al., 2010a; Arns et al., 2013b; Batstone et al., 2013), classical assessments usually only focus on peak WLs and thus do not include information about their duration and temporal evolution (Quinn et al., 2014), whereas reliable flood risk assessments require the entire WL curve to describe the temporal development of inundation. To overcome the lack of information related to the WL curve, simplified hazard scenarios are defined selecting the peak WL at certain return period (e.g., the 100 year return WL) and a WL curve is approximated using so-called “design curves.” The “design curves” are normally defined based on time series of historical events (e.g., the one at the highest ever recorded peak WL) (e.g., Dawson et al., 2005) or by superimposing the time series around the highest levels of each component (e.g., spring tide levels and the time series of the highest observed surge peak) and scaling to the return WL under investigation (e.g., Bruss et al., 2010; Gönner and Gerkenmeier, 2015; Wadey et al., 2015). Due to the scarcity of observed data (especially at extremes events), such synthetic extreme WL curves are often calculated at a single tide-gauge location and assumed representative for an entire area (e.g., McMillan et al., 2011). As a result,

uncertainties regarding both the temporal and spatial behavior extreme WLs are introduced.

An alternative method to produce extreme WL curves is shown in Wahl et al., (2011), who introduced an approach to stochastically simulate a large number of physically possible extreme WL curves using observational data as input. They parameterized WL curves of observed storm surge events and fitted distribution functions to the parameters. The distributions were then used to produce 10 million values of each of the WL parameters by a Monte Carlo simulation; these values were then interpolated to reconstruct WL curves. In a companion paper Wahl et al., (2012) present a bivariate statistical approach to estimate joint probabilities of storm-peak heights and their ‘intensity’ (also termed “fullness,” which is defined as the area between the WL and the reference datum). A feature of this approach is that an event of equal joint probability can be generated by several different combinations (i.e., storm-peak heights and intensities), which results in different flooding extents and depths (e.g., Prime et al., 2016). Although the WL curve of an extreme event which has not been observed but is physically plausible can be approximated using the above-mentioned methods of Wahl et al., (2011, 2012), the range of potential extreme WL curves is still too wide to be simulated using dynamic models. An assessment of potential implications of the variability of extreme WL curves on coastal flooding can be found in Quinn et al., (2014). They analyzed the variability of WLs within the 6 h anterior and posterior to the storm peak of observed extreme WLs at several tide-gauged sites along UK. They showed that even if the variability of the WLs at times close to storm peak is low, they can have large effects upon overflow volumes. In addition, significant differences in WL variability between tide-gauged locations were found, showing the spatial variability of storm surge WL curves.

However, in some regions such as the German North Sea coast extreme WLs often last for more than 12 h, consisting of several high tides connected by very high low tides (Wahl et al., 2011). This may increase the uncertainties related to the effects of the WL curve variability upon flooding because flooding is more likely at the times of the high tide. In addition, the German North Sea region is strongly affected by nonlinear shallow water effects, producing significant differences between WLs at neighboring tide-gauged locations (see e.g., Arns et al., 2015b).

The above factors refer to the historical variability of extreme WLs. However, in order to assess future risk of flooding it is essential to also account for SLR and its impact on extreme WLs (see e.g., Arns et al., 2015a). To date, the most commonly used

approach to include SLR effects in flood risk assessments is by linearly adjusting current extreme WL estimates upward by an amount equivalent to the projected SLR (see e.g., Wadey et al., 2015). Although this approach is justified in several regions of the world where changes in extreme WLs are driven by SLR alone (see e.g., Menéndez and Woodworth, 2010), in the German North Sea a significant higher trend in extreme WLs has been reported (Mudersbach et al., 2013). Furthermore, the study of Arns et al. (2015a) showed that a moderate SLR scenario can also produce nonlinear increases in extreme WL peaks in this region. These changes differ spatially along the coastline and are mainly due to variations in the tidal component. Therefore, it is possible that not only the extreme WL peaks are affected by SLR but also the entire WL curve, altering the storm surge intensity and inundation areas.

In this study, we explore the consequences of the temporal and spatial variability of extreme WLs time series on flood hazard assessments compared to assuming a temporally and spatially constant “design WL curve.” For this purpose, we analyze both factors along 13 locations of the German North Sea coastline. In addition, we evaluate potential changes in the WL curve of storm surge WLs and their variability predicted for three SLR scenarios: RCP 4.5, RCP 8.5, and RCP 8.5 HE (see Slangen et al., (2014) and Grinsted et al., (2015) for a detailed description). Furthermore, we quantify the effects of SLR induced changes on two parameters directly related to flooding: overflow discharge rates and fullness; in order to assess the potential consequences of the changes in the WL curve caused by SLR in flooding.

The paper is organized as follows: we first describe the characteristics of the study area as well as the WL data sets used (section 2). In section 3, we detail the methods used to correct the simulated WLs (section 3.1); to assess the impact of SLR on the WL curve of storm surge events and their temporal and spatial variability (section 3.2), and to analyze the effects of these factors on overflow rates and fullness (section 3.3). We present and discuss the results of the SLR induced changes on the WL curve variability and their consequences on overflow and fullness in section 4. Finally, we summarize the most important findings in section 5.

## **3.2. Study area and Data**

### **3.2.1. Study area**

The German North Sea coastline is a low-lying region, with some parts even below sea level, frequently threatened by extreme WLs. One of its largest communities

directly bordering the North Sea is St. Peter-Ording, which is located on the west coast of the Eiderstedt peninsula (Figure 3.1). St. Peter-Ording is not surrounded by the barrier islands of the Wadden Sea (Figure 3.1) and is therefore highly exposed to extreme WLs. In the last century, the highest WLs have reached nearly 5 m above mean sea level (Kaiser and Kortenhaus, 2008).

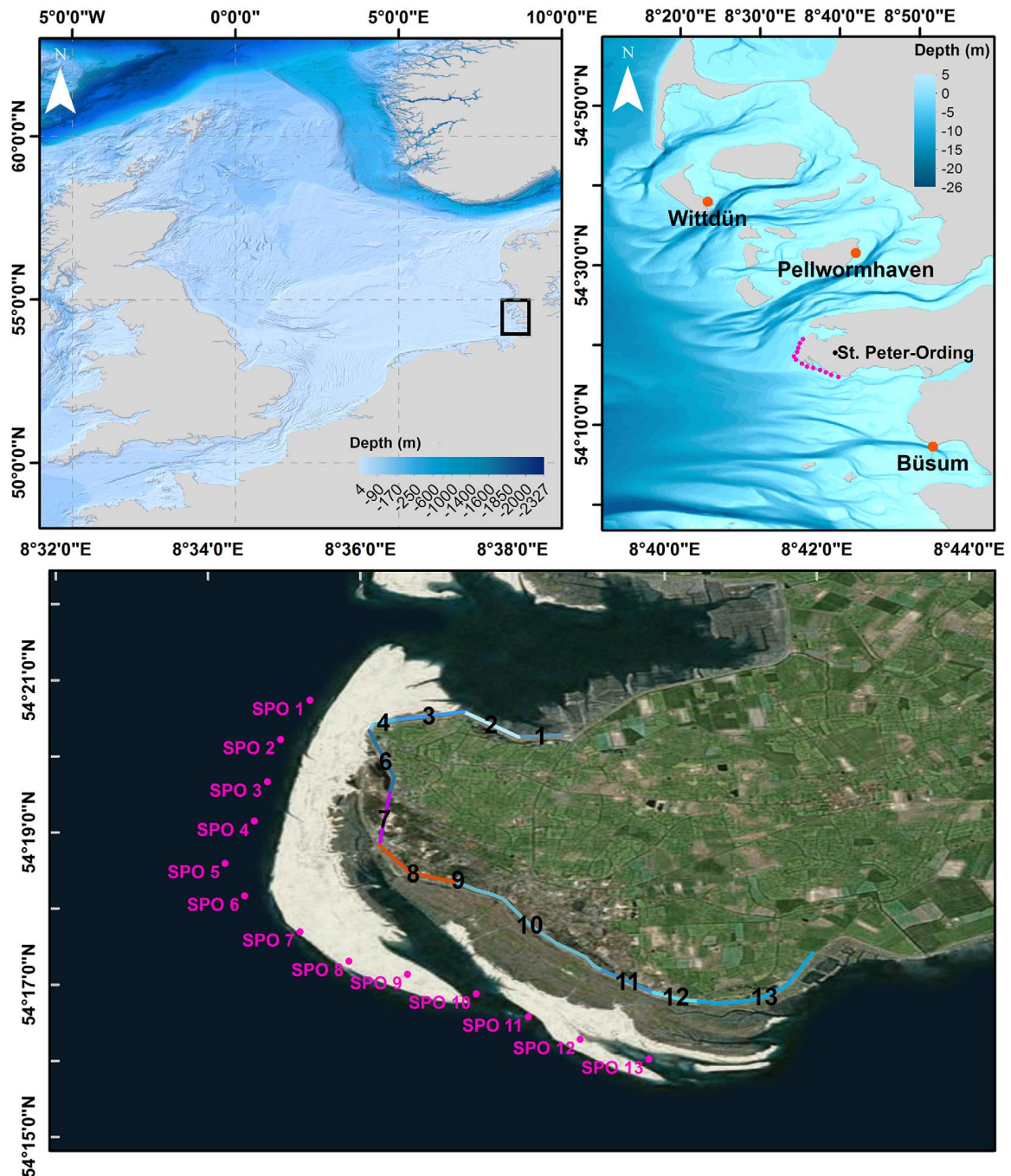


Figure 3.1 Location of the study area (upper left map) in the North Sea; bathymetry of the study area showing tide-gauge stations (as orange dots) and St. Peter-Ording locations (as pink dots) are shown in the upper right map. Sections of the dike-ring of St. Peter-Ording (modified from [www.FLOODsite.net](http://www.FLOODsite.net)) and locations of numerically simulated WLs (lower map).

St. Peter-Ording has a population of 6300 permanent inhabitants and is the largest seaside resort in the state of Schleswig-Holstein with around 100,000 guests each year. A great part of the tourism sector is related to natural health treatments due to its sulfur spring and therefore, several hospitals, elderly and children's homes are located in this community. Part of the municipality also belongs to the Schleswig-Holstein Wadden Sea National Park, which has been part of the UNESCO World Heritage Site since 2009. The entire Eiderstedt peninsula is considered flood-prone as its elevation does not exceed 5 m NHN (local datum). Hence, if flooding occurs in St. Peter-Ording, the water can potentially spread far into the hinterland causing damages to assets of the Eiderstedt peninsula, as well as to agricultural fields, pastures, and flora of the park area due to salt water intrusion (Kaiser and Kortenhaus, 2008).

St. Peter-Ording is protected by a defense structure covering ~15 km of coastline. This defense mainly consists of a dike ring with a length of more than 12 km, comprising several dike sections of different heights and lengths being covered by grass and asphalt, a natural dune belt and an overtopping dike with a retention reservoir behind the dike (Kortenhaus et al., 2006). The location of the different dike sections is shown in the lower map of Figure 3.1 and their characteristics in Table 3.1.

### **3.2.2. Data**

For this study, there are no observational WL records available in the direct surroundings of St. Peter-Ording and the nearest available stations are located in enclosed areas at both sides of the Eiderstedt peninsula, in Büsum and Hüsüm. WL records at those stations have been used in previous flood hazards assessments for St. Peter-Ording (Kortenhaus et al., 2006; Kaiser and Kortenhaus, 2008). However, analyses of observational records over the last decades indicate strong tidal dynamics in that region (see e.g., Mudersbach et al., 2013; Arns et al., 2015a) and this is why WLs even at neighboring stations can differ significantly. We therefore use numerically simulated storm WLs (hereafter simulated WLs) presented in Arns et al., (2015a, 2015b) for 13 locations along the St. Peter-Ording coastline (equidistant spacing of ~1 km, Figure 3.1) at a temporal resolution of 10 min. The WLs were simulated with a two-dimensional, depth-averaged barotropic tide-surge model of the entire North Sea using the MIKE21 FM (flexible mesh) modelling suite of the Danish Hydraulic Institute (DHI). The coastline resolution was resampled from 30 km along the open boundaries to 1 km at the German Bight coastline and a high resolution bathymetry (~15 m) of the

Wadden Sea areas was interpolated onto the flexible mesh. Hindcast WLs from 1970 to 2009 were simulated forcing model's open boundaries with astronomical tidal levels from the MIKE21 internal global tide model. Over the entire model domain, mean sea level pressure fields and 10 m wind fields from the CIRES 20th century reanalysis project (Compo et al., 2011) were used as atmospheric forcing. The same model was used to simulate WL changes under three different SLR scenarios, but keeping the atmospheric forcing identical to the hindcast run. In order to account for uncertainties related to future SLR projections, the scenarios considered are based on the RCP 4.5 (0.54 m), RCP 8.5 (0.71 m), and the RCP 8.5 high end (hereafter HE, of 1.74 m) scenarios. In each hindcast and scenario run, a total number of 75 storm surge events were simulated. Further details of model configuration can be found in Arns et al., (2015a, 2017).

Additionally, we use observed WLs from three gauged locations, provided by the Schleswig-Holstein Agency for Coastal Protection, National Parks and Ocean Protection (LKN-SH), in order to validate and correct the simulated WLs at St. Peter-Ording (for more information see section 3.3.1). The locations of the three stations (Büsum, Pellwormhaven, and Wittdün) are shown in Figure 3.1. The observed WLs are composed of hourly values covering the periods from 1997 to 2007 in Büsum, from 1995 to 2007 in Pellwormhaven, and from 1999 to 2009 in Wittdün. However, only the simultaneous data of the three tide-gauges (i.e., 1999–2007) are used for correction purposes.

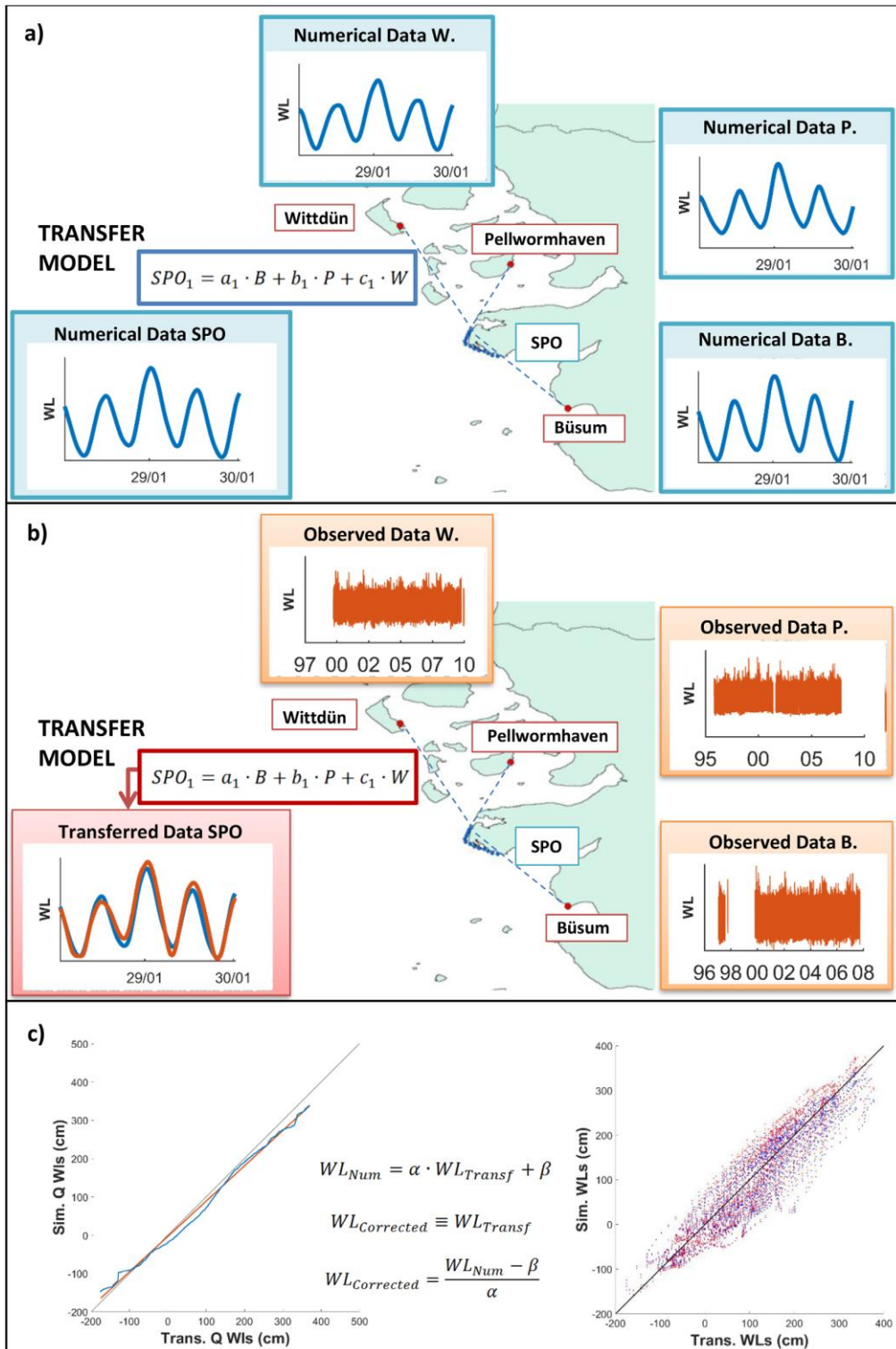


Figure 3.2 Conceptual diagram of WLs transfer and correction methodology: (a) Fitting the transfer models (multiple-linear regression) using the simulated WLs of the three gauged sites to each of the 13 St. Peter-Ording locations. (b) Transferring the observed WLs from the gauged sites to each of the 13 St. Peter-Ording locations using the transfer models. (c) Correction of the simulated WLs of each St. Peter-Ording location: the linear regression fitted to simulated (y axis) and transferred (x axis) WLs of one location is shown in the left graph; scatter of uncorrected simulated WLs versus transferred WLs (blue) and corrected simulated WLs versus transferred WLs (red) are shown in the right plot.

Table 3.1 Characteristics of the Different Sections of the Dike-Ring Protecting St. Peter-Ording and Design WLs for 2020<sup>a</sup>

Dike Sections	Defense type	Year of construction	Height (m)	Width (m)	Inner slope	Outer slope	Length (m)	Reference WL <sub>200</sub> 2020 (NHN+m)
1	Dike with grass cover	1996	8.28	1	3	6	670	5.3
2	Dike with grass cover	1996	8.35	1.5	3	6.4	996	5.3
3	Dike with grass cover	1996	8.19	1.5	3	6.5	1123	5.3
4	Dike with asphalt cover	1964	8.43	0.9	2.8	4.5	187	5.2
5	Dike with asphalt cover	1964	8.30	0	3.2	4.3	286	5.2
6	Dike with asphalt cover	1964	7	1.5	3	4.1	1381	5.2
7	Dunes	-	15	2.2	4	10	1010	-
8	Overtopping asphalt dike	-	6.22	1.7	4	3	1655	5.05
9	Dike with asphalt cover	1965	5.99	2.0	8	10	199	5.2
10	Dike with asphalt cover	1965	7.18	2.2	4.5	5.5	2986	5.2
11	Dike with grass cover	1965	6.98	3.5	4.8	8	1295	5.2
12	Dike with grass cover	1965	7.05	1.8	4.5	7	452	5.2
13	Dike with grass cover	1965	8	1	2.9	5.2	1042	5.2

<sup>a</sup>Modified from *Kortenhaus and Lambrecht, [2006]* and *MELUR [2013]*

### 3.3. Methods

#### 3.3.1. Correction of numerically simulated water levels

Comparing observed and simulated WLs at the gauged sites shows good agreement, with a coefficient of determination of at least  $r^2=0.8[-]$  at all three locations (Büsum, Pellwormhaven, and Wittdün). However, in order to further reduce systematic inaccuracies, a parametric bias correction is applied to the numerical model outputs of both the hindcast and the three SLR scenarios. Arns et al., (2015a, 2015b) performed a nonparametric bias correction aiming at a correction of hindcast WLs that have also been recorded at some locations, adjusting each individual simulated and discrete WL value to the simultaneously observed WLs. However, this methodology is limited to the

observational period and cannot be applied to scenario runs. For this reason, we focus on a parametric bias correction, which provides a transfer function that can be applied beyond the range of observations. The method essentially consists of fitting a parametric regression to the observed and simulated WLs of the hindcast and the three SLR scenarios (see e.g., Ulm et al., 2016).

As there are no observed WLs available at the study area to validate and correct the simulated WLs, we use a multiple-linear regression model to transfer the observed data from the gauged stations to each ungauged St. Peter-Ording location. The model is constructed using the simulated WLs at the gauged sites as predictor variables and the simulated WLs of each St. Peter-Ording location as response variable. Assuming that the intramodel correlation is accurate, consistent, and constant, we can transfer the observed WLs from the gauged stations to each of the 13 ungauged Sankt Peter-Ording locations using the regression model and consider the transferred WLs as being representative. As mentioned in the previous section, WLs can significantly differ between tide-gauged sites and study locations due to local effects. However, Arns et al. (2015b) showed that there is a systematic bias between observed and simulated WLs, i.e., the model tends to overestimate low WLs and underestimate high WLs at all tide-gauged sites despite local effects, probably due to a coarse atmospheric forcing (spatial resolution of 28 and temporal resolution of 3 h). Therefore, the systematic bias can be reduced at the study sites using the transferred WLs, despite differences between the dynamics of the tide-gauged sites and the study locations.

Although there is high multicollinearity between the predictor variables, the predictions made with the multiple regression model are not affected as the predictor variables maintain the same multicollinearity pattern along the observed period of data (Studenmund, 1997). On average, predictor correlation coefficients vary by approximately 0.02 between the observed and hindcast data set, indicating a constant pattern. Figure 3.2 shows a conceptual diagram of the transfer and correction approach.

In order to transfer the WLs, we test the sensitivity of the multiple-linear regression model to different data sampling methods using the simulated and observed WLs of the tide-gauged sites (further details can be found in Appendix B). The multiple-linear regression model constructed with the quantiles equally spaced in double logarithmic scale is chosen as transfer model due to its better performance. Therefore, multiple-linear regression models are fitted for each St. Peter-Ording location (equation (5)) and are used to transfer the observed WLs to ungauged locations

$$SPO_1 = a_1 \cdot B + b_1 \cdot P + c_1 \cdot W$$

Eq.5

where  $SPO_1$  denotes the WLs of one St. Peter-Ording location,  $a_1$ ,  $b_1$ , and  $c_1$  are the regression coefficients and B, P, and W denoting the WLs of the gauged locations Büsum, Pellwormhaven, and Wittdün.

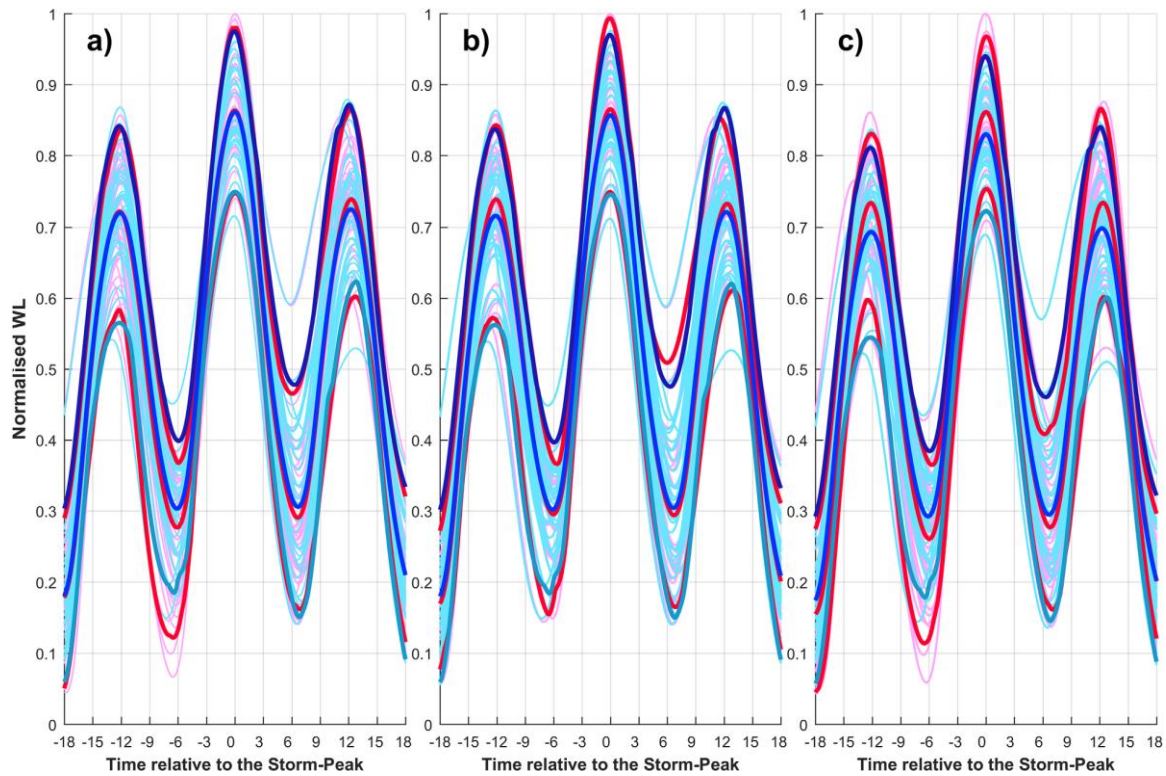


Figure 3.3 Normalized set of hindcast events (light blue lines) and SLR scenarios (pink lines): (a) RCP 4.5 scenario, (b) RCP 8.5 scenario, and (c) RCP 8.5 HE scenario; and upper, mean and lower envelopes (dark blue lines for the Hindcast scenario and red lines for the SLR scenarios) at location 6.

On average, the constructed multiple-linear regression models have a coefficient of determination of  $r^2 \sim 1[-]$ . Based on this value and on the low variation of predictor correlation coefficients, we can assume that the transferred WLs are representative as observed WLs at the study area. Once the observed WLs are transferred to each location, we perform the parametric bias correction by fitting linear regressions to the WLs in double logarithmic scale (Figure 3.2c). Although only systematic inaccuracies can be corrected by this procedure (see right graph of Figure 3.2c), the coefficient of determination increases from  $r^2=0.87[-]$  to  $r^2=0.98[-]$  on average.

### 3.3.2. Analysis of temporal and spatial variability of storm WLs

We implement a modified version of the approach presented in Quinn et al., (2014) to assess the temporal variability of all storm surge events at each of the 13 locations of the study area, as well as for the hindcast and SLR scenarios. This approach is adopted because the WLs temporal variability is quantified relative to the storm peak, which is the parameter commonly used and recommended to perform extreme value analysis in this area, and consequently for flooding assessments (Kaiser and Kortenhaus, 2008; Wahl et al., 2011; Arns et al., 2013b). However, we modify the normalization approach in order not to alter the shape of the WL curves of the different scenarios, hence allowing comparisons between the individual scenarios. In addition, we modify the time window length and threshold level aiming to equalize these parameters to the ones used in the analysis of extreme events in our study area.

In a first step, we identify the storm water peaks at each location along the St. Peter-Ording coastline. Following the recommendations of Arns et al., (2013b) on creating samples for extreme value analyses along the German North Sea coast, we select the storm peaks exceeding the 99.7th percentile at each location and scenario. According to the study of Wahl et al., (2011), the majority of storm surge event in the German North Sea region do not last longer than three tidal cycles. Therefore, in a second step we select the WLs within the 18 h before and after the storm peak (tidal high water), thus comprising three high tides.

In order to remove negative values prior to normalization, we refer all WLs to the lowest WL of the entire set of events (i.e., we add an offset of 180 cm to all WLs and scenarios). In addition, the SLR of all scenarios is removed before the events selection and normalization in order to analyze nonlinear changes in the WL curve driven by the SLR.

Next, we normalize the WL curves of the hindcast scenario relative to each of the three SLR scenarios, producing one normalized hindcast set of events per SLR scenario (Figure 3.3). The normalization of the WL curves is carried out by dividing each value (i.e., every 10 min) of every WL curve by the maximum storm peak of the corresponding SLR scenario.

Finally, we calculate the mean, standard deviation, 95th and 5th percentiles at each time step (i.e., each time point of the WL curve relative to the peak time) of the set of normalized events. The process is repeated for each scenario and location of the study

area. The variability of the WLs at each time step is measured as the standard deviation obtained at this time step, and the 95th and 5th percentiles are the upper and lower envelope of the set of storm surge events.

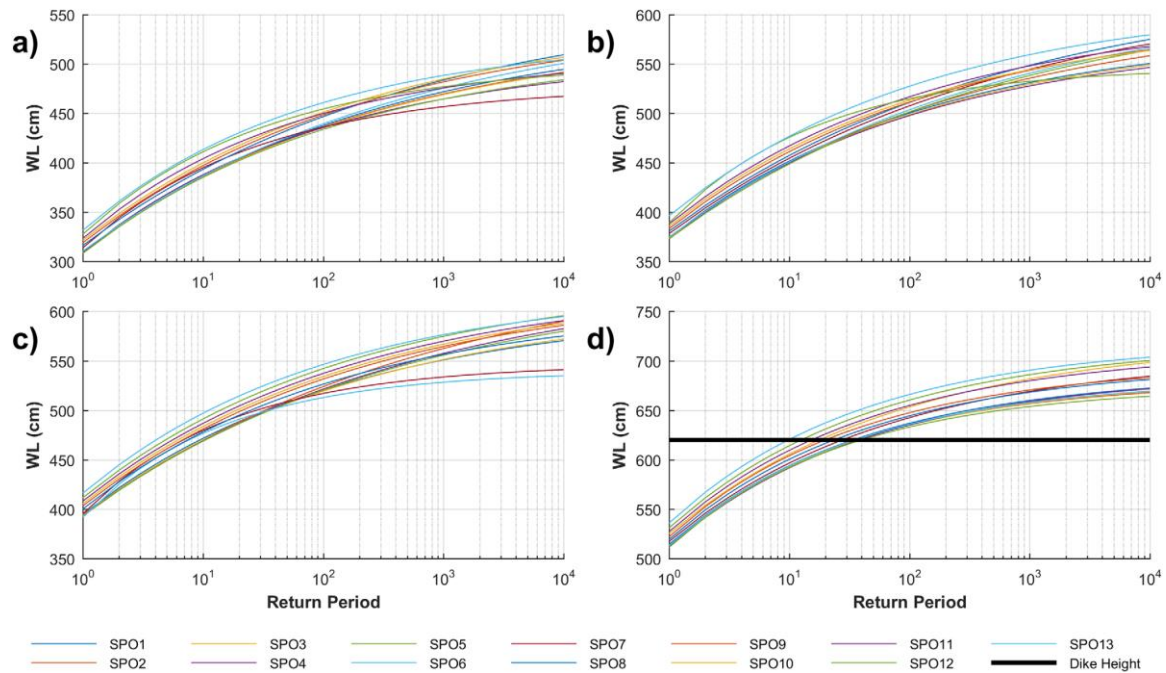


Figure 3.4 GPDs fitted for the different locations and scenarios: (a) hindcast, (b) RCP 4.5, (c) RCP 8.5, and (d) RCP 8.5 HE.

### 3.3.3. Accounting for effects of storm WL Variability

Both the temporal and spatial WL variability can affect different processes contributing to inundations, such as overtopping and overflow discharge as well as erosion and breaching of defense structures. Therefore, we assess (1) the effects of storm WLs variability and (2) changes in the WL curve due to SLR, on two parameters related to the above-mentioned processes, namely overflow discharge rates and fullness. The first parameter is directly related to the volume of water flowing inland in a flooding event, while the fullness (parameter also named “intensity”) is a parameter used as a proxy of the energy input into defense structures during a storm event (Salecker et al., 2011; Wahl et al., 2011, 2012).

To analyze the effects of the WL curve variability, we produce three WL curves for each scenario with the same storm-peak value but different temporal behavior. For this purpose, we adjust the mean, 5<sup>th</sup> and 95<sup>th</sup> percentiles normalized WL curves to four storm-peak values corresponding to the  $T = \{200, 500, 1000, 10,000\}$  year events. The

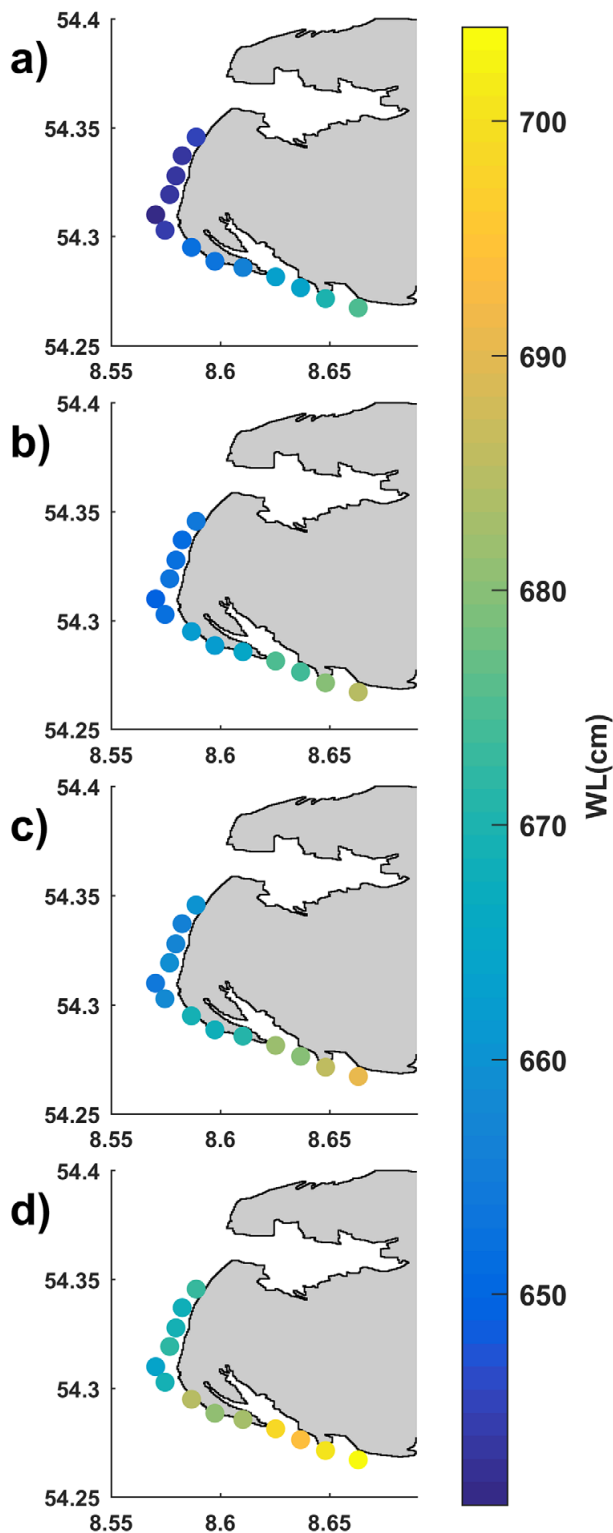


Figure 3.5 Return WLs of the four events: (a)  $T = 200$  year; (b)  $T = 500$  year, (c)  $T = 1000$  year, and (d)  $T = 10,000$  year, at each St. Peter-Ording location.

latter have been calculated following the recommendations of Arns et al., (2013b) to perform extreme value analysis in the study area. In Figure 3.5, we show the Generalized Pareto Distributions (GPD) of the storm-peak values for all locations and scenarios, and the crest level of the lowest dike section (620 cm) of the study area (see section 2 for the characteristics of the dike ring). As shown in Figure 3.4, the only case in which a section of the dike can be exceeded is in the RCP 8.5 HE scenario. Therefore, we select the  $T = \{200, 500, 1000, \text{ and } 10,000\}$  year storm peak heights of the RCP 8.5 HE scenario (Figure 3.5).

In order to analyze the effects of the changes in the WL curve caused by SLR on overflow and fullness, we also estimate the WL curve for those storm-peak heights using the normalized WL curves of the hindcast, RCP 4.5 and RCP 8.5 scenarios. We must note that these are theoretical WL curves as the dike height cannot be exceeded in these scenarios. To generate the WL curve for those storm-peak heights, we first rescale the WL curves of each scenario in order to set the normalized storm-peak height to 1. We then interpolate the WL curve from a temporal resolution of 10 to 1 min to improve the precision in the

overflow rates and fullness estimations. For this purpose, we use the piecewise cubic hermite interpolation method based on the results of Wahl et al., (2011), who performed a sensitivity analysis of interpolation methods applied to the WL curve,

finding the lowest errors for this method. We remove the offset of 180 cm added within the normalization stage, and thus the absolute values are referred to the NHN (i.e., the German ordnance datum).

We calculate theoretical overflow discharge rates using the general formula for a broad-crested weir (Kay, 2007):

$$q_{overflow} = \sum C \cdot L \cdot H^{1.5} \quad \text{Eq.6}$$

where  $q_{overflow}$  is the overflow discharge rate ( $m^3/s \cdot m$ ),  $H$  is the head of water over the crest (m),  $L$  is the crest width (m), and  $C$  is the weir coefficient (which in the case of broad-crested weirs takes the value of 1.6). The crest width of the dike section that can be exceeded by those events is 1.7 m.

The second parameter assessed is the fullness, which is defined as the area between the storm WL and the ordnance datum NHN:

$$fullness = \int_{t_1}^{t_2} WL(t) dt \quad \text{Eq.7}$$

where the unit of fullness is  $cm^2$  and  $WL(t)$  is the WL curve over the entire duration of the event (36 h). We calculate the fullness of the events estimated by the  $T = \{200, 500, 1000, 10,000\}$  year WLs of the RCP 8.5 HE scenario and the WL curves of all scenarios.

## 3.4. Results and Discussion

### 3.4.1. Temporal and spatial variability of extreme WLs

Figures 3.6, 3.7 and 3.8 present the spatial WL changes at each time step of the lower (5%), mean (50%), and upper envelopes (95%) between the hindcast and the three SLR scenarios. In these graphs, it can be observed that SLR caused WL changes at all three envelopes and in most of the time steps, with a magnitude ranging between  $\pm 15\%$  (see, e.g., time steps -14 to -4 of Figure 3.6c). In the three scenarios, the lower envelope shows the highest WL changes (Figure 3.6), while the WL changes of the mean and upper envelope are of comparable magnitude (Figures 3.7 and 3.8).

Although the WL changes of the three envelopes are not uniform, we observe a general pattern consisting of SLR induced increases of high-water peaks (hereinafter

HWP) and decreases of low-water peaks (hereinafter LWP). This is consistent with the findings of Arns et al., (2015a), who reported an increase of HWP under the RCP 4.5 scenario produced by nonlinear changes in the tidal component. Their analysis pointed to an increase in the amplitude of the M2 tidal constituent and a decrease of the nonlinear constituents, resulting in an increase of the tidal range. However, in the RCP 4.5 scenario (Figures 3.6a, 3.7a, and 3.8a) we find that the increase of the HWP is spatially not uniform in magnitude and a decrease of the lower envelope HWP can also be observed in some locations (Figure 3.6a). The latter is true for the anterior HWP at locations 3 and 4, for the main storm peak of location 1, and for the posterior HWP at locations 6 and 7. We find that these spatial differences remain in the RCP 8.5 scenario (Figure 3.6b), while in the RCP 8.5 HE scenario, we observe a more regular pattern in the three envelopes (Figures 3.6c, 3.7c, and 3.8c). These spatially non-uniform WL changes with SLR show that the changes in the tidal component are highly influenced by local effects. This highlights the uncertainties which are introduced when using WLs from too distant locations as input for flood risk assessments.

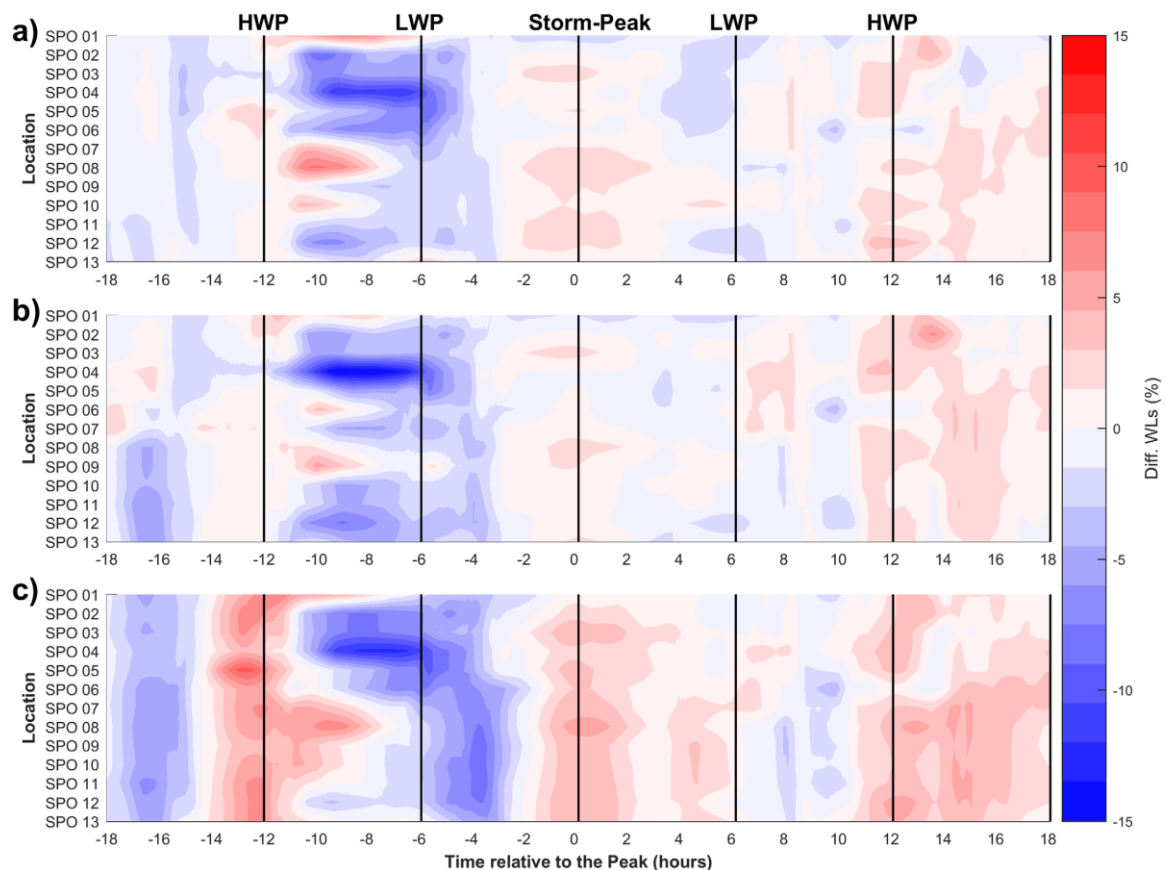


Figure 3.6 Spatial-temporal differences of the 5th percentile envelope (relative WLs in %) between (a) the RCP 4.5 scenario and the hindcast, (b) the RCP 8.5 scenario and the hindcast, and (c) the RCP 8.5 HE scenario and the hindcast. Positive values (red) represent an increase of the relative WL in the SLR scenarios (blue a decrease).

Nevertheless, the WL changes caused by SLR are not only limited to the times of the HWP and LWP as we can observe WL changes at most of the time steps. In the three envelopes of all SLR scenarios, we observe that WL increases are mostly constrained to the time of the HWP (time steps -12, 0, and +12) plus 1 or 2 h. However, the decrease surrounding the LWP (time steps -6 and +6) generally comprises more time steps. Thus, the extreme WL curve becomes steeper with SLR, regardless of uncertainties related to future SLR projections.

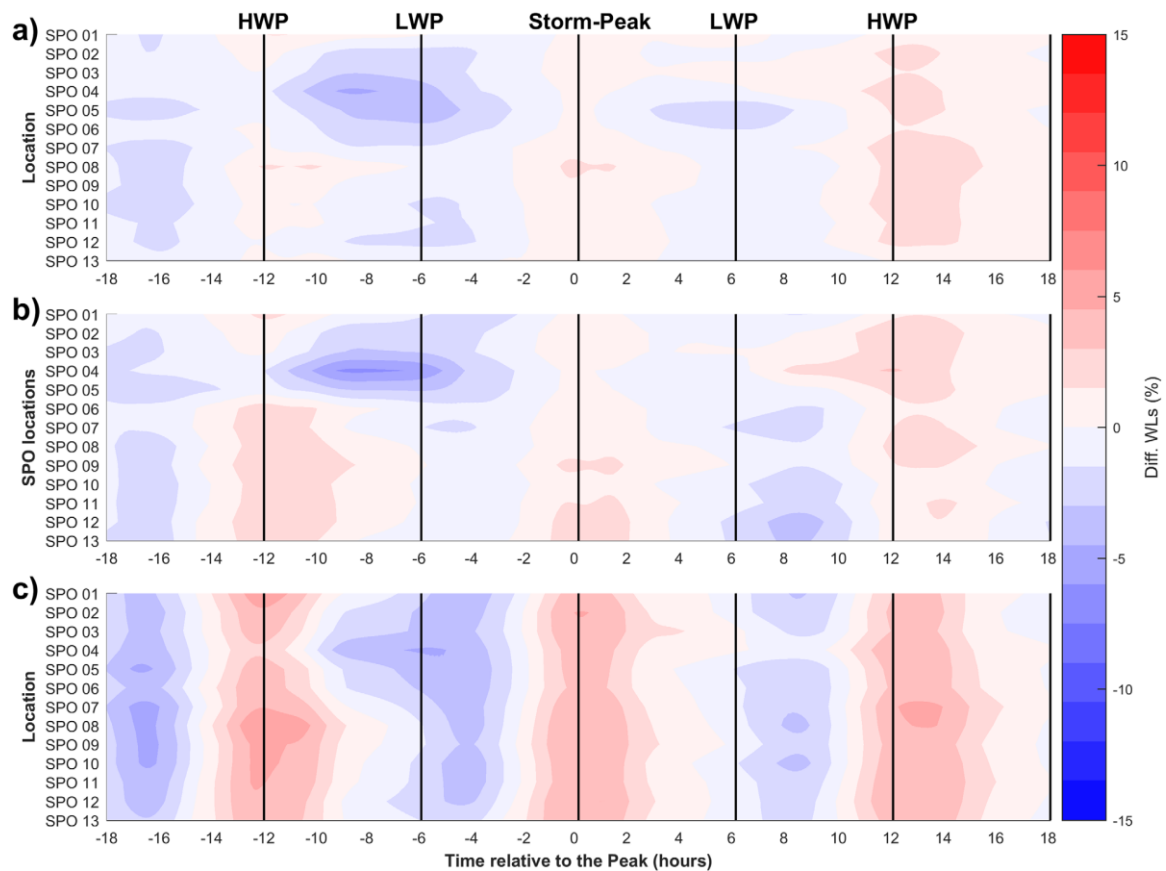


Figure 3.7 Spatial-temporal difference of the mean envelope (relative WLs in %) between (a) the RCP 4.5 scenario and the hindcast, (b) the RCP 8.5 scenario and the hindcast, and (c) the RCP 8.5 HE scenario and the hindcast. Positive values (red) represent an increase of the relative WL in the SLR scenarios (blue a decrease).

Moreover, in several locations, we find nonlinear WL changes with SLR. In some cases, we observe higher WL changes for the RCP 4.5 scenario than for the RCP 8.5 (e.g., storm peak of the lower envelope at the southern locations, Figures 3.6a and 3.6b), or a different pattern between these two scenarios and the RCP 8.5 HE scenario. For example, in the flow phase (between time step +6 and +12) in the posterior HWP

of the upper envelope (Figure 3.8), a moderate increase is found in the RCP 4.5 and RCP 8.5 scenarios and a decrease in the RCP 8.5 HE scenario. The different pattern of the WL changes in the RCP 8.5 HE scenario compared to the RCP 4.5 and RCP 8.5 is probably caused by the stronger reduction of shallow water effects related to the larger water depth of that scenario. Due to the shallowness of this area, a moderate rise of sea level may cause higher WL changes than an HE scenario.

We observe that the maximum variability values (between 10% and 12%) in the hindcast scenario (Figure 3.9) are reached at the flow phase of the posterior HWP (time steps from 6 to 12) and the ebb-phase of the anterior HWP (time steps from 212 to 26), whereas the lowest variability is obtained at the times of the main storm peak. We also find a high variability at the HWP times, which is higher for the anterior and posterior HWP (8–9%) than for the main storm peak (6–7%). One factor that may cause this high variability, besides the intensity of the different events, is the different duration of the storm events included in the analysis. As a consequence of the approach we use for selecting events, we also include storm events (i.e., the 99.7<sup>th</sup> percentile threshold exceedances) that last for less than 36 h, thus potentially resulting in a higher variability of WLs for the time further away from the storm-peak time. Due to the fact that flooding (overflow/overtopping) occurrence is more probable at the HWP times, the high values of variability obtained at these time steps highlight the uncertainties related to the use of a single WL curve (“design WL curve”) in flooding assessments.

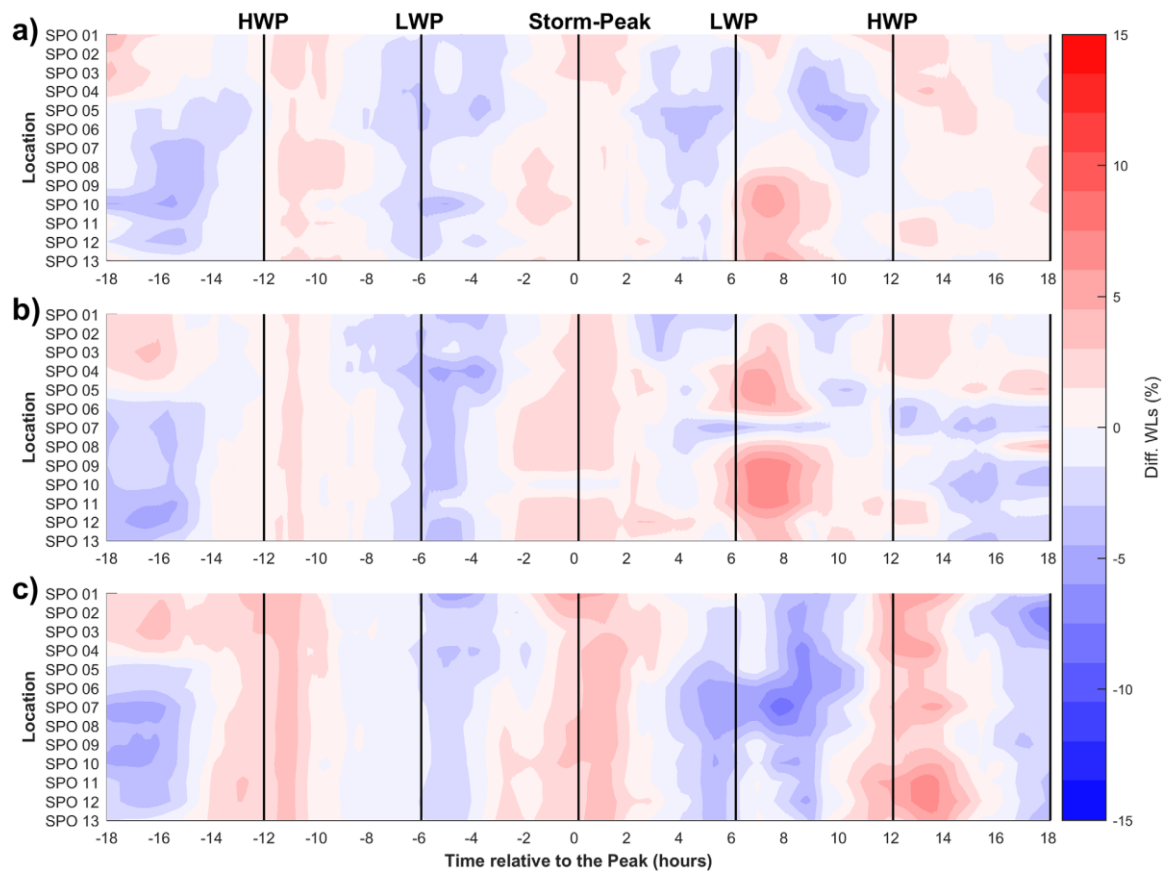


Figure 3.8 Spatial-temporal differences of the 95th percentile envelope (relative WLs in %) between (a) the RCP 4.5 scenario and the hindcast, (b) the RCP 8.5 scenario and the hindcast, and (c) the RCP 8.5 HE scenario and the hindcast. Positive values (red) represent an increase of the relative WL in the SLR scenarios (blue a decrease).

Regarding the spatial distribution of the WL variability, we find a generally higher variability at each time step for the southern locations than for the northern ones. As shown by Arns et al., (2015a, 2015b), small local changes in water depth can produce differences in frictional and shallow water effects due to the shallowness of the German North Sea coast and the strong tidal dynamics of this region. Therefore, differences in WL variability between northern (from 1 to 7) and southern locations may be due to differences in the bathymetric features between the northern and southern locations. Specifically, as the southern locations are situated closer to a tidal channel than the northern locations, WLs can be stronger affected by tidal currents, thus leading to increased WL variability. However, we cannot confirm these hypothesis based on the analysis performed and further research is needed in order to better describe the hydrodynamics of this area.

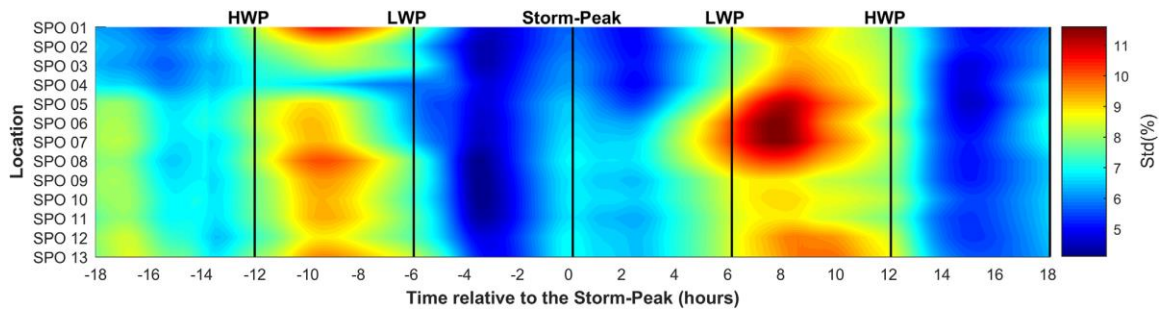


Figure 3.9 Spatial and temporal variability (standard deviation) of the normalized set of events from the hindcast scenario.

The WL changes caused by SLR have their subsequent impact on the variability. We can observe that the changes in the variability are of similar magnitude for the three SLR scenarios, with values ranging between 66% (Figure 3.10). We do again find that the changes in the variability are spatially not homogeneous, as for some time steps we find an increase of the variability at some locations and a decrease at others. Nevertheless, we observe an increase of the LWP variability at most locations of the three SLR scenarios, excluding the second LWP of the RCP 8.5 HE scenario (Figure 3.10c). However, there is no clear pattern of the changes in the variability of the HWP as we find an increase in some cases and a decrease in others. For example, we observe an increase of the anterior HWP variability in the RCP 4.5 and RCP 8.5 scenarios (Figures 3.10a and 3.10b), whereas a decrease is found at this time step in the RCP 8.5 HE (Figure 3.10c). These non-uniform changes in the variability are in line with the observed WL changes due to SLR, and highlight the importance of accounting for local dynamics in this region.

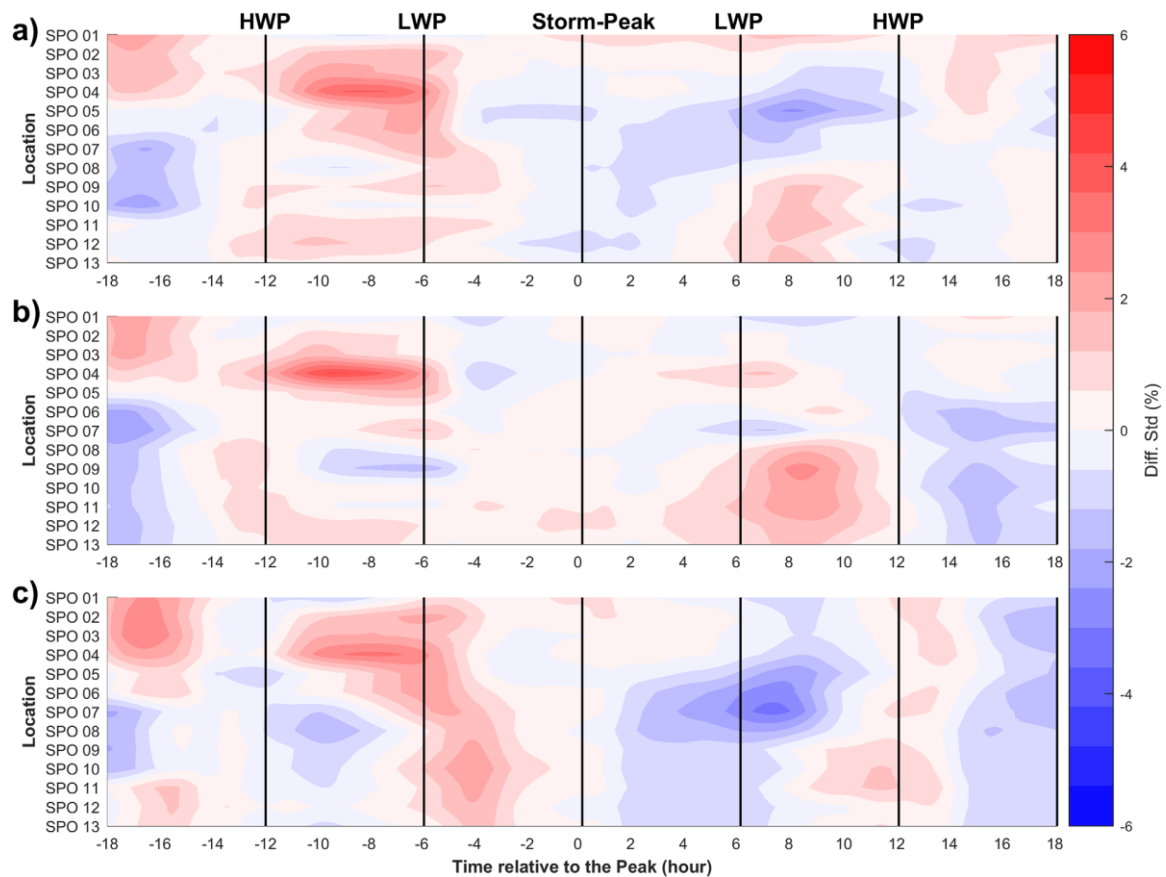


Figure 3.10 Differences of variability between (a) the RCP 4.5 scenarios and the hindcast, (b) the RCP 8.5 scenario and the hindcast, and (c) the RCP 8.5 HE scenario and the hindcast. Positive values (red) represent an increase of the variability in the SLR scenarios (blue a decrease).

### 3.4.2. Implications of storm WL variability on overflow rates and fullness

Figure 3.12 shows the overtopping rates obtained for the events estimated by the  $T = \{200, 500, 1000, 10,000\}$  year WLs of the RCP 8.5 HE scenario and the WL curves of all scenarios. At each location, we show the overflow rates corresponding to one return WL of the RCP 8.5 HE scenario and each WL curve (lower, mean, and upper envelope) of the four scenarios (hindcast, RCP 4.5, RCP 8.5, and RCP 8.5 HE).

We observe higher overflow rates at the southern locations (from 7 to 13) compared to the northern ones (Figure 3.11). These spatial differences are mainly due to the storm-peak heights obtained for each location (Figure 3.5) because we have

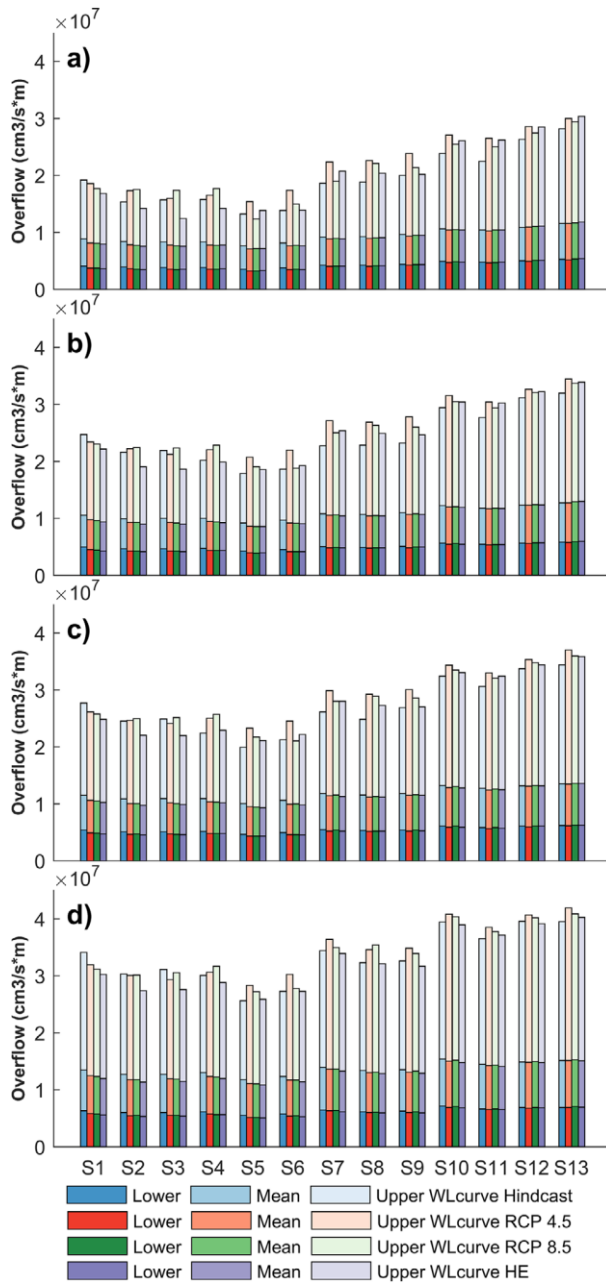


Figure 3.11 Overflow rates obtained for the (a)  $T = 200$  year, (b)  $T = 500$  year, (c)  $T = 1000$  year, and (d)  $T = 10,000$  year storm-peak heights of the RCP 8.5 HE scenario and the normalized WL curves of all scenarios

calculated overflow assuming an equal crest height at all locations. Although the dike-ring of St. Peter-Ording comprises dike sections of different heights, the estimated design WLs of the  $T=200$  year by 2020 (Table 3.1) are nearly identical for all dike sections, with the northern sections having the highest values (MELUR, 2012). Importantly, we obtain a different pattern of the  $T=200$  year WLs for the RCP 8.5 HE scenario, namely: a greater spatial variability and higher values at the southern locations than at the northern locations (absolute values cannot be compared as they correspond to different scenarios). The discrepancies between the design values and the patterns that we obtained are probably due to the different approaches used to derive the return WLs at ungauged sites and the SLR induced changes. The local authority responsible for coastal protection in the study area uses an approach based on the Regional Frequency Analysis, which does not account for local hydrodynamics (Arns et al., 2015b)

The  $T=200$  year storm-peak heights differs between the northern and southern locations by approximately 30 cm, resulting in differences of overflow rates of around  $1 \times 10^7$  and  $1.5 \times 10^7 \text{ cm}^3 \cdot \text{s}^{-1} \cdot \text{m}^{-1}$ . These differences between locations are of similar magnitude to the difference between the overflow rates obtained from the  $T=200$  year (Figure 3.11a) and  $T=10,000$  year event (Figure 3.11d) at the same location. This high difference of overflow rates between locations for the same event highlights the importance of accounting for the spatial variability of extreme WLs. For example, if we

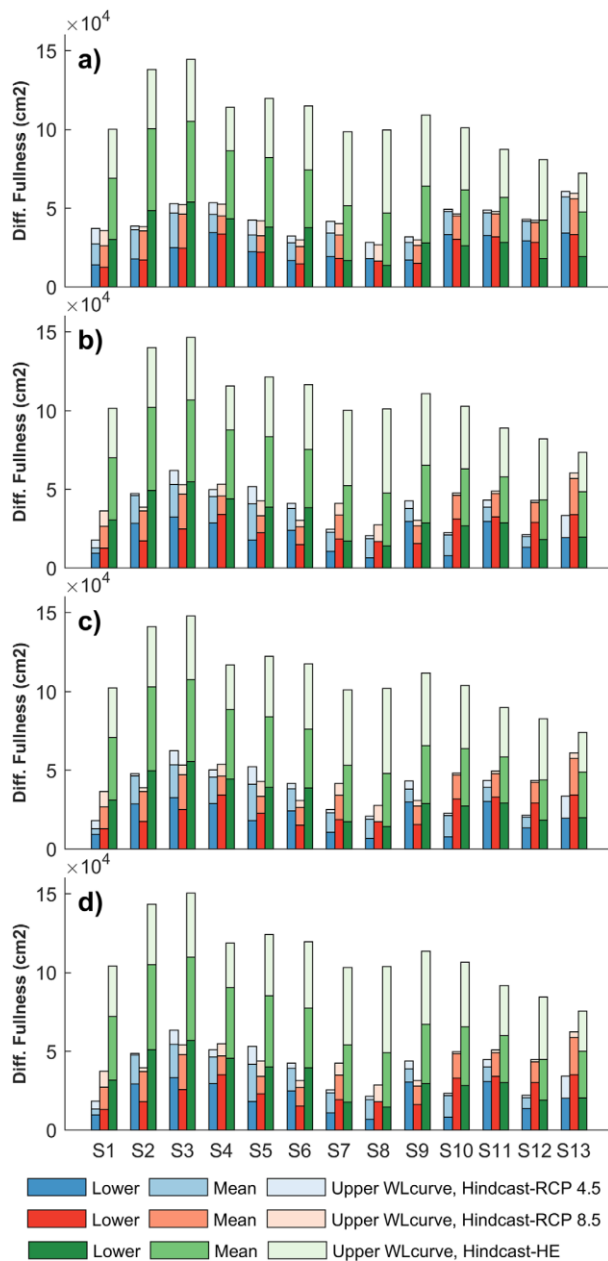


Figure 3.12 Differences in fullness obtained between the WL curves of the hindcast and the three SLR scenarios of the (a)  $T = 200$  year, (b)  $T = 500$  year, (c)  $T = 1000$  year, and (d)  $T = 10,000$  year events of the RCP 8.5 HE scenario.

assess flooding of the  $T=200$  year event only using information of extreme WLs of location 5, we are underestimating by 50% the overtopping rate at location 13, which corresponds to the overtopping resulting in location 5 for the  $T=10,000$  year event.

We also find differences in the overflow rates resulting from the upper, mean, and lower envelopes of all scenarios. Although the differences between the overflow rates of the lower and mean envelope are almost negligible at most of the locations, the overflow rates resulting from the upper envelope of all the events are up to three times higher. This confirms that the use of a single “design WL curve” is subject to high uncertainties when assessing flood risk in this region. To evaluate the effects of WL changes due to SLR on overflow rates, we compare the hypothetical overflow rates obtained for the  $T = \{200, 500, 1000, 10,000\}$  storm-peak heights of the RCP 8.5 HE scenario and the WL curves of all

scenarios at each location. The differences between the overflow rates resulting from the lower and mean envelope are almost negligible, although we can observe higher overflow rates for the WL curves of the hindcast scenario (blue bars) than for the SLR scenarios at some locations (see, e.g., locations 1–6). However, the differences of the overflow rates belonging to the upper WL curve (darker shades) of the different scenarios are higher, reaching up to  $5 \times 10^6 \text{ cm}^3 \cdot \text{m}^{-1} \cdot \text{m}^{-1}$ . For this WL curve, there is no clear spatial pattern for the different scenarios. From locations 5 to 13, we find the highest overflow rates in all events for the WL curve of the RCP 4.5 scenario (red bars),

whereas it corresponds to the WL curve of the RCP 8.5 at location 4 (green bars) and the hindcast scenario at location 1 (blue bars). In addition, we observe the relevance of the WL changes for the time steps beyond the storm peak comparing the overflow resulting for the different events at the same location. For example, we find a significant higher overflow for the T=200 year event for the upper WL curve of the RCP 8.5 scenario compared to the hindcast scenario at location 3 (Figure 3.11a). However, the difference between the overflow of the T=10,000 year event for these two scenarios is almost negligible (Figure 3.11b).

By contrast, we obtain the highest fullness values for the WL curves of the hindcast scenario at all locations and events. We must emphasize that the storm peak values of all events correspond to the RCP 8.5 HE scenario, and the WL curves have been constructed using the normalized WL curves (mean, 5<sup>th</sup> and 95<sup>th</sup> percentiles curves) of all scenarios (hindcast and SLR scenarios) in order to assess potential consequences of not accounting for changes in the WL curve. Therefore, the differences of fullness between the SLR scenarios and the hindcast scenario shown in Figure 3.12 are not absolute as the absolute values of the SLR scenarios would always be larger than the hindcast. In most cases, we observe that the differences from all WL curves of the RCP 8.5 HE scenario (green bars) are approximately two times higher than the ones of the other two scenarios (blue and red bars). However, comparing the values obtained for the other two scenarios we find different patterns depending on the event and location, with higher differences in some cases obtained for the RCP 4.5. For example, for the T=200 year event we obtain higher fullness differences for the WL curve of the RCP 4.5 (Figure 3.12a, blue bars) than for the WL curve of the RCP 8.5 (red bars), whereas for the other three events we obtain higher differences for the WL curve of the RCP 8.5 in more than half of the locations (see, e.g., locations 10–13). Regarding the differences obtained for each WL curve (i.e., mean, 5<sup>th</sup> and 95<sup>th</sup> percentiles WL curves), we observe in general lower differences for the upper WL curve of all scenarios (lighter shades), which are nearly negligible at some locations for the RCP 4.5 and RCP 8.5 scenarios.

These results are in line with the WL changes discussed in the previous section and specifically with the increase of the tidal range with SLR that results in a steeper WL curve. The reduction of the fullness related to the WL curves of the SLR scenarios is due to the fact that the WL increase close to the HWP (i.e., around the 2 h before and after the HWP) is relatively lower than the decrease of the WLs at the remaining time steps of the WL curve. This is more noticeable for the lower and mean WL curves,

where we obtain greater decreases of the fullness. In addition, we find a greater reduction in fullness at those locations where we obtained a lower relative increase of the HWP (e.g., locations 2 and 3). This suggests that if SLR induced changes in the WL curve are not accounted for when estimating fullness, this parameter will be overestimated and so will the energy input upon the defense structures.

### **3.5. Conclusions**

In this study, we have assessed the temporal and spatial variability of historic extreme WLs at St. Peter-Ording in the German Bight, and potential changes in the WL variability as consequence from SLR. In addition, we have quantified the effects of WL variability on overflow volumes and fullness in order to assess potential consequences on flooding.

We found a high degree of WL variability highlighting the uncertainties related to the assumption of defining a “design” WL curve as representative for a region in flooding assessments. The high WL variability obtained at the times around the anterior and posterior HWPs is of particular importance as the WL height of those peaks is usually excluded in extreme value analysis, where only the storm-peak height is commonly analyzed, and the overflow/overtopping occurrence is more probable at those time steps. This study shows that the anterior and/or posterior HWP height of some historical events nearly reached the level of the storm-peak height, showing that is possible that an extreme event of two or even three HWPs in a row of similar height can occurs in the future. The temporal variability of the WL curve produces high differences in overflow volumes, with the upper WL curve resulting in rates that are double or even triple than those computed with the lower WL curve.

In general, SLR produces an increase of the WLs around the times of the HWPs and a decrease of the WLs around the times of the LWPs. This generally results in higher overflow volumes for the WL curves of SLR scenarios compared with the hindcast WL curves. However, this general pattern is not linear with SLR, resulting in a higher increase in the overflow volume for the WL curves of the RCP 4.5 and RCP 8.5 scenarios compared to the WL curve of the RCP 8.5 HE scenario. Therefore, a low to moderate SLR may have greater relative effects over the WL curve than an HE scenario in the study area. In addition, we found both spatial WL variability and WL changes caused by SLR along the study area, which highlights the role of the local (~1 km) shallow water processes on WLs. These spatial variations also have significant impacts on overflow volumes and return WLs, which can be of the same order as the

different overflow volume obtained for the T=200 year and T=10,000 year events at the same location. Therefore, the assumption of a constant WL curve along a flooding model domain in this spatial scale at the study area may entail high uncertainties with respect to overflow volumes.

The changes caused by SLR over the WL curve of the analyzed storm surge events from the RCP 8.5 HE scenario produce a decrease in fullness compared to the values estimated for the hindcast WL curves. Therefore, if SLR induced changes in the WL curve are not taken into account (i.e., if only the changes induced by SLR in the storm peak values are considered), fullness will be overestimated.

This study has focused on a small region of the German North Sea coast where SLR is predicted to induce high impacts on the WL curve of storm surge events. The results of this study cannot be directly extrapolated to other areas of the world because SLR induced effects are highly spatially variable and strongly depend on local features (i.e., bathymetry, coastal morphology, etc.). However, the methodology presented here can be used to locally assess SLR impacts on the WL curve of storm surge events in those regions where SLR induced changes in the tidal levels have also been reported and predicted (see e.g., Mawdsley et al., 2015; Idier et al., 2017).

Further research should include potential changes on the bathymetry induced by SLR such as changes in tidal channels and sand bar locations, which may affect the hydrodynamics of the region by altering propagation processes (e.g., dissipation by bottom friction) (e.g., Bilskie et al., 2016) and thus affecting the variability of extreme WLs.

## **Acknowledgments**

S. Santamaria-Aguilar and A.T. Vafeidis were supported by the EU FP7 project RISES-AM (grant agreement 603396). A. Arns was funded by the University of Siegen. All data used in this paper is properly cited and referred to in the reference list. We acknowledge the support of the Agency for Coastal Protection, National Parks and Ocean Protection of Schleswig-Holstein for providing the tide-gauge series, which are available for scientific purposes under request ([http://www.schleswig-holstein.de/DE/Landesregierung/LKN/lkn\\_node.html](http://www.schleswig-holstein.de/DE/Landesregierung/LKN/lkn_node.html)). We would also like to acknowledge the two anonymous reviewers for providing constructive and valuable comments that helped improving the paper.

## Chapter 4.

# **Are extreme skew surges independent of high waters in mixed tidal regimes?**

*Sara Santamaria-Aguilar and Athanasios T. Vafeidis*

*Journal of Geophysical Research: Oceans (2018),*

*doi:10.1029/2018JC014282*

*Received: 18 June 2018, Accepted: 27 November 2018*



## **Abstract**

Based on previous studies of tide-gauge records from locations with semidiurnal tidal regimes, extreme skew surges are always assumed independent of the high water (HW). However, differences in water depth between HW peaks of semidiurnal tidal regimes can be much lower than those in mixed semidiurnal regimes, where one daily HW is higher than the other. We statistically analyze tide-gauge records of 15 sites worldwide with a mixed semidiurnal regime and find that for approximately half of these sites extreme skew surges occur more often during smaller HWs. This dependence is not caused by seasonality effects, and the places that show dependence are all located in areas with a shallow continental shelf, thus indicating possible tide-skew surge interactions. In those cases where dependence exists, using the skew surge does not seem to offer any advantages over the non-tidal residual.

## **Plain Language Summary**

The water level during storms (i.e., storm surges) in coastal areas largely depends on the level of the tide. This effect can be more noticeable in places with a mixed semidiurnal regime, which is characterized by two high water peaks per day, with one high water peak being larger than the other. Knowledge of this effect can help forecasting and prevention of flooding events in these regions. We statistically analyze water level records of 15 sites worldwide with a mixed semidiurnal regime and find that in around half of these sites storm surges occur more often at lower high water levels. These places are all located in areas with a shallow continental shelf, such as estuaries or closed seas.

## **Key Points**

- Extreme skew surges are not independent of the high water level in some sites with mixed tidal regime
- Extreme skew surges occur more often during lower high tidal waters in the sites that show dependence
- The dependence observed between extreme skew surges and high waters does not arise from seasonality effects

## 4.1. Introduction

Storm surge commonly designates the meteorological component of observed water levels and can be defined as the extreme rise of water caused by strong winds and low pressure systems. However, defining the surge component from the tide-gauge records is not an easy task due to the interactions with the other water level components, namely, astronomical tide and mean sea level (hereafter MSL). MSL variations are generally removed by subtracting the water level average over a certain period, from a month to years, and tidal levels can be predicted from the harmonic analysis of the tide-gauge records. After subtracting MSL fluctuations and the astronomical tide, the remaining water level or non-tidal residual also contains the interaction between the tide and the surge component. This interaction occurs mainly in shallow water areas and is caused by two processes: (1) wind stress ( $\tau_s$ ) being more effective in generating storm surges in low water (hereafter LW) levels due to the fact that the surface stress ( $F_s$ ) is inversely proportional to water depth (equation (4) and (3)) the rise of water caused by the wind stress increases the speed ( $c$ ) of the tidal wave propagation, which in shallow waters depends on the water depth (equation (3); Pugh and Woodworth, 2014).

$$c = \sqrt{gD} \quad \text{Eq.3}$$

$$F_s = \frac{\tau_s}{D\rho} \quad \text{Eq.4}$$

where  $D$  is the water depth and  $\rho$  is the water density.

As a result of the tide-surge interaction the large non-tidal residual peaks tend to occur more often during LWs and before high waters (hereafter HW) than at HWs (Horsburgh and Wilson, 2007). Therefore, assuming that any non-tidal residual peak can occur at any HW level could lead to an overestimation of the total water levels due to the tide-surge interaction (Batstone et al., 2013). In order to avoid the complication of accounting for the tide-surge interaction, the “skew surge” term was defined as the difference between maximum observed and predicted water levels during a tidal cycle, irrespective of timing differences (Batstone et al., 2013; Haigh et al., 2014; Wahl and Chambers, 2015; Mawdsley and Haigh, 2016). In recent years, the skew surge has become a more popular term than the non-tidal residual for defining the surge component because it has been shown to be independent from the tidal level (Batstone et al., 2013; Williams et al., 2016). However, these dependence analyses have been

performed in regions with a semidiurnal tidal regime, where water depth differences between HWs usually do not largely differ. Since there are places that experience a mixed semidiurnal tidal regime, where larger water depth differences between consecutive HWs can occur, it is possible that extreme skew surges could occur more often during lower HWs (LHWs) peaks than at higher HWs (HHWs) peaks. If this were the case, extreme skew surges would not be independent from the HW level, and therefore, using the concept of skew surge could lead to an overestimation of the total water levels. As the skew surge is an integrated measurement over a tidal cycle, the temporal evolution of the storm surge is lost by using this concept instead of the non-tidal residual. However, the temporal evolution of storm surges has been shown as an important factor to be considered in flood risk assessments because it can significantly affect the resulting volume of water flooding inland, producing therefore different flood extents and flood depths (Quinn et al., 2014; Santamaria-Aguilar et al., 2017a).

In this study, we explore the dependency between extreme skew surges and HW levels at 15 tide-gauge sites worldwide characterized by a mixed semidiurnal tidal regime. Our aim is to assess whether the water depth differences between HWs of mixed tidal regimes can also produce a tide-surge interaction similar to the interaction observed in semidiurnal regimes between LWs and HWs.

## **4.2. Tide-gauge data**

We use tide-gauge records from the Global Extreme Sea Level Analysis (GESLA-2) database (Woodworth et al., 2017) of 13 locations worldwide with a mixed tidal regime and more than 20 years of hourly data (Figure 4.1). We reference the tide-gauge series to their MSL, using the reference information of these tide-gauge stations provided by the Permanent Service of Mean Sea Level. We also use the tide-gauge series of Buenos Aires and Mar del Plata (Santamaria-Aguilar et al., 2017b) that are not included in the GESLA-2 database and were provided by the Servicio de Hidrografia Naval of Argentina. All tide-gauge series were checked for datum shifts, spikes, and erroneous values from earthquakes and tsunamis as indicated in the station information of the Permanent Service of Mean Sea Level. We find several spikes in the tide-gauge series of Antofagasta from 2010 onward and therefore decide to exclude these years from the analysis. In addition, we use reanalysis wind data from the NOAA-CIRES twentieth Century Reanalysis v2 data set (Compo et al., 2011) of the closest grid nodes to the tide-gauge stations for analyzing the monthly storminess of each location.

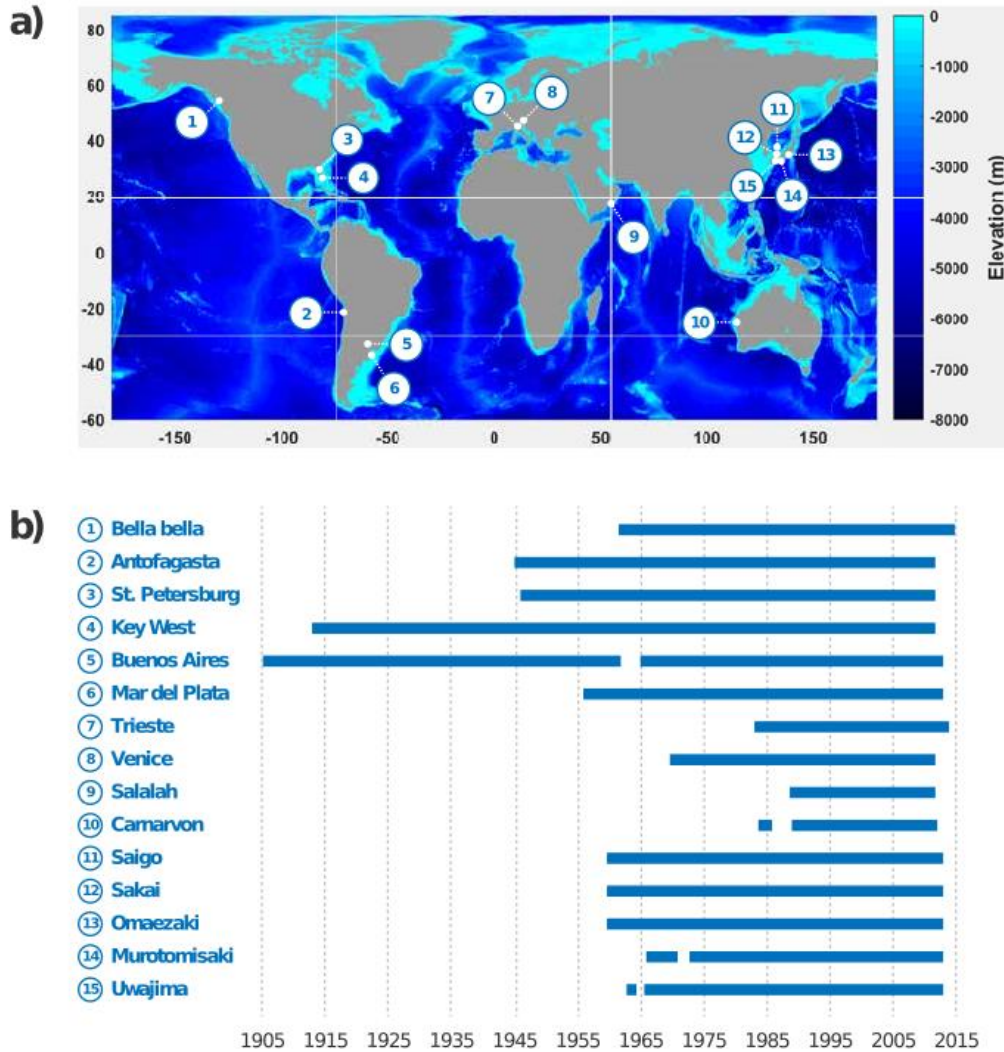


Figure 4.1 (a) Map showing the location of the tide-gauge sites and (b) length of the tide-gauge records

### 4.3. Methods

Tide-gauge records contain the contribution of MSL, astronomical tide, and the meteorological component commonly known as surge. In this study we are interested in the relationship between the astronomical and meteorological components, and therefore, in a first step, we remove the MSL signal by subtracting a 30-day moving average. In this way we remove long-term trends and seasonality of MSL as well as the contribution of vertical land movement (Mawdsley et al., 2015; Mawdsley and Haigh, 2016). It must be noted that part of the signal of the seasonal tidal constituents, such as  $S_A$  and  $S_{SA}$ , can also be included in the 30-day moving average (as they have the same frequency) and thus removed by the detrending process. In a second step, we perform a harmonic analysis of each calendar year of the detrended tide-gauge series that is at least 75% complete using the UTide Matlab package (Codiga, 2011),

obtaining those tidal constituents that have a value of signal-to-noise ratio of at least two for every year (between 59 and 67 constituents depending on the completeness and length of the year). As the  $S_A$  and  $S_{SA}$  signals cannot be distinguished from the seasonal climate variation signal, we quantify the effects of detrending the WL series on  $S_A$  and  $S_{SA}$  by also performing a harmonic analysis of the trended WL series. We produce the astronomical WLs of each calendar year of records based on these constituents. We extract all the HW peaks of the tidal series, classifying them in HHWs and LHWs, and then apply the method described in Mawdsley and Haigh, (2016) for calculating the skew surge associated to each HW peak. Therefore, we calculate skew surges by finding the largest local maxima of the observed water levels within a time window of  $\pm 3$  hr around the HW peaks (in case no local maxima are found we repeat the search by increasing the length of the time-window by 1 hr, to a maximum of 6 hr) and apply the following two criteria: (1) We discard those observed local maxima that occur between double LWs; (2) we discard those observed local maxima that are closer in time to other HW peaks than their associated HW peak.

We follow the statistical methods employed by Williams et al., (2016), described below, for analyzing dependency between the magnitude of extreme skew surges and their associated HWs in order to produce comparable results. However, in our analysis we define two extreme skew samples at each location using two different approaches in order to also assess the influence of the independence between successive extreme events. Our analysis focuses only on locations with a mixed tidal regime (i.e., with HWs of different magnitude per day), and thus, events that last for more than one HW peak can influence the results of the dependence analysis between the magnitude of extreme skew surges and their associated HWs. Therefore, we define one extreme sample as the highest 1% (hereafter Ex. Sample; Williams et al., 2016) and another extreme sample as the peaks over the 99% threshold with an independent time of 2 days between successive events (hereafter POT sample).

We assess dependence between extreme skew surges and their associated HWs by two statistical measurements. First, we calculate Kendall's tau correlations between the two extreme skew surge samples and their associated HWs. Kendall's tau is a nonparametric test that measures the strength and direction of the dependency between two variables. In a second analysis, we assess whether the HWs associated to the extreme skew surge samples are drawn from the distribution of all HWs of the studied period by applying the Anderson-Darling test (with a significance level of 0.05). If any extreme skew surge can occur at any HW level (i.e., if the magnitude of the

extreme skew surge does not depend on the HW level), the HWs associated to the extreme skew surge sample should follow the same distribution of all HWs, which is the null hypothesis of the Anderson-Darling test. We estimate the probability distribution function (hereafter PDF) of all HWs using normal kernel density with a bandwidth of  $1^{\text{th}}/35^{\text{th}}$  of the range of all HWs (Figures 4.2e and 4.2f, and similar figures in Appendix C). The value of the bandwidth was selected after performing a sensitivity analysis of several bandwidths, as bandwidth can highly affect the shape of the final PDF and thus the results of the Anderson-Darling test. Specifically, a large bandwidth can over smooth the PDF, thus hiding possible “true” peaks of the PDF, while a small bandwidth increases the statistical error due to the low data density in some bands. Therefore, we perform a sensitivity analysis of the Anderson-Darling test estimating the PDF for bandwidths from  $1^{\text{th}}/5^{\text{th}}$  to  $1^{\text{th}}/60^{\text{th}}$  of the HWs range and select a bandwidth of  $1^{\text{th}}/35^{\text{th}}$  of the HWs range as the optimal. Trends presented in any of the variables can also produce spurious correlations and affect the result of the Anderson-Darling test. Previous studies reported significant secular trends in tidal levels of most areas of the world, including the majority of the locations of this study (Mawdsley et al., 2015; Santamaria-Aguilar et al., 2017b), but skew surges do not show significant long-term trends in most regions of the world (Mawdsley and Haigh, 2016). In order to discard effects of trends in the dependence analysis, we have performed an analysis of covariance for all HWs, HHWs, and LHWs of the different data sets (i.e., all data of the study period and the two extreme samples) in each station. We find no significant differences between the linear trends of the different data sets, with exception of the LHWs of the Ex. Sample of Sakai.

Seasonality of tidal levels and storminess can also hide or show a dependency between the two variables because the stormiest months may not coincide with the months of larger HWs. Therefore, we also perform the second dependence analysis weighting the PDF of all HWs by the monthly storminess. Initially, we aimed to estimate monthly storminess based on the reanalysis wind data similar to Williams et al., (2016). However, after performing a crosscheck analysis between the extreme skew samples and the reanalysis wind data of the closest grid nodes to the tide-gauge stations, we found that less than 50% of extreme skew surges are linked to wind speeds higher than the 97<sup>th</sup> percentile in most of the stations (increasing to 65–100%, depending on the station, when reducing the wind threshold to the 80<sup>th</sup> percentile). Therefore, we calculate monthly PDFs and weigh them based on the relative number of extreme events of each month. The reason why we could not find a strong simultaneous connection between the extreme skew surges and strong winds at most of the

locations is probably because storms are generated far from the tide-gauge stations. For example, Santoro et al., (2013) showed that the storm surges observed in Buenos Aires and Mar del Plata are generated further south in the Argentinean continental shelf (Figure 4.3) and propagate northward as coastal trapped waves until they reach the estuary.

#### **4.4. Results and Discussion**

We find very low and not statistically significant correlation values (Kendall's tau) between both extreme skew samples and their associated HW levels for all tide-gauge stations (Table C.1 in Appendix C). From this first measurement, we can assume that the magnitude of extreme skew surges is independent of the HW level. However, results from the Anderson-Darling test do not lead to the same conclusion in all the stations. The null hypothesis of the Anderson-Darling test assumes that HWs associated to the extreme skew sample are drawn from the same distribution of all HWs. Our results show a rejection of the null hypothesis at around half of the stations from the analysis of both extreme samples and thus a dependency of extreme skew surges on the HW level at those places (see Figure 4.4 and Table C.3 in Appendix C). However, we observe that in some stations these results are very sensitive to some parameters of the methodology applied, such as the definition of the extreme sample and bandwidth of the kernel density estimator (Figure 4.4 and Table C.3 in Appendix C).

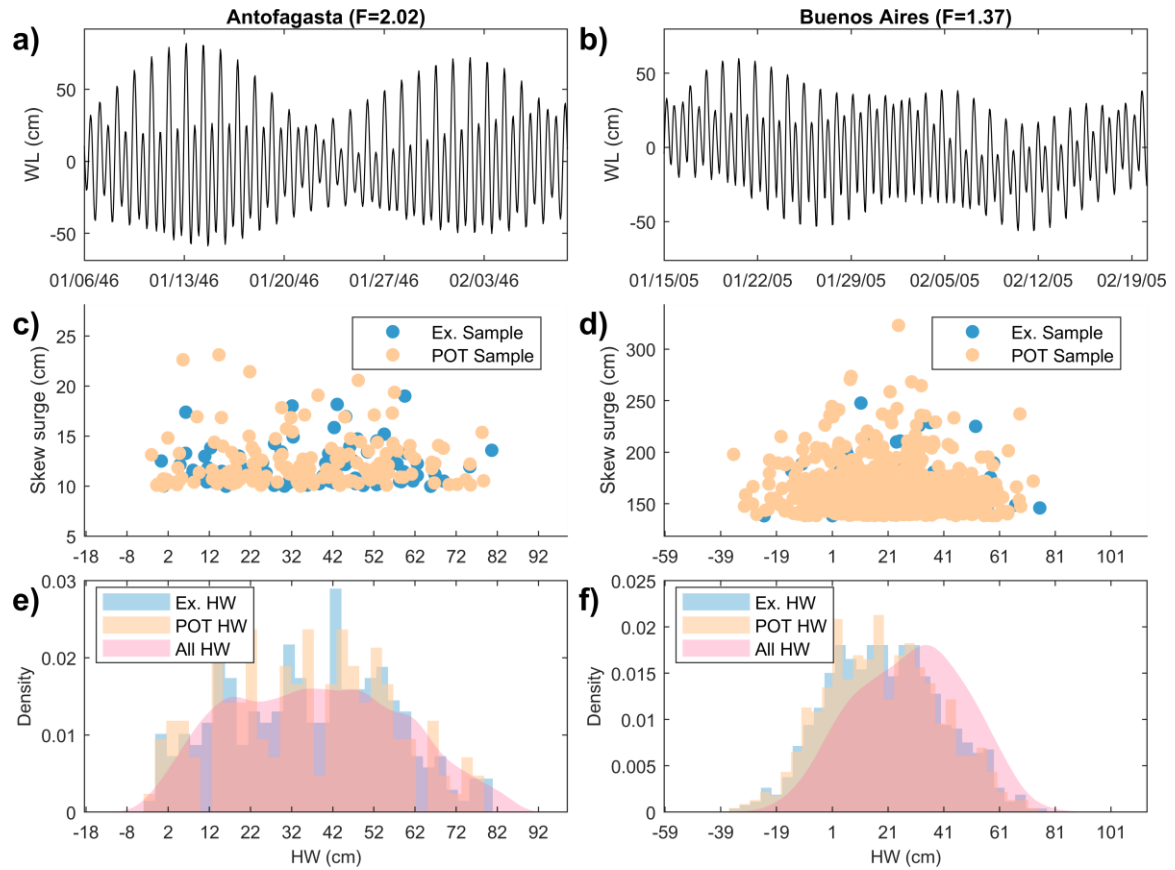


Figure 4.2 Tidal water levels of (a) Antofagasta and (b) Buenos Aires. Scatter plots of both samples of extreme skew surges (note that all values of the POT sample are also included in the Ex. Sample) and their associated high waters (HWs) for (c) Antofagasta and (d) Buenos Aires. Histograms of HWs associated to the two extreme skew samples and probability distribution function of all HWs of (e) Antofagasta and (f) Buenos Aires. Similar figures for the other tide-gauge sites can be found in Appendix C.

Although all the analyzed tide-gauge sites have a mixed tidal regime, we can observe in Figures 4.2a and 4.2b (and similar figures in Appendix C) that tidal levels as well as the HW PDFs (Figures 4.2e and 4.2f) differ from place to place. From a visual assessment, we observe that in some locations the HW PDF shows two peaks (such as St. Petersburg or Mar del Plata in Appendix C) while in others the shape of the HW PDF resembles a Gaussian distribution with skewness to one of the tails (e.g., Trieste or Saigo in Appendix C). We observe that these differences are not related to the relative importance of the amplitude of the main diurnal or semidiurnal constituents, which we assess by a commonly used form factor  $F$  (Pugh and Woodworth, 2014).

$$F = \frac{(H_{M2} + H_{S2})}{(H_{K1} + H_{O1})} \quad \text{Eq.5}$$

where  $H$  represents the amplitude for the  $M_2$ ,  $S_2$ ,  $K_1$ , and  $O_1$ . The value of  $F$  can be found in Figures 4.2a and 4.2b for Antofagasta and Buenos Aires, and in the same graphs in Appendix C for the other stations. The differences observed between HW PDFs of places with similar  $F$  ratio can be due to differences in the phases of those constituents. Differences in the shallow-water constituents between stations can also contribute to the observed differences in the HW PDFs because all the stations are located in coastal areas and some of them are situated in regions with a wide shallow continental shelf (such as the Argentinian and U.S. stations; Figure 4.3).

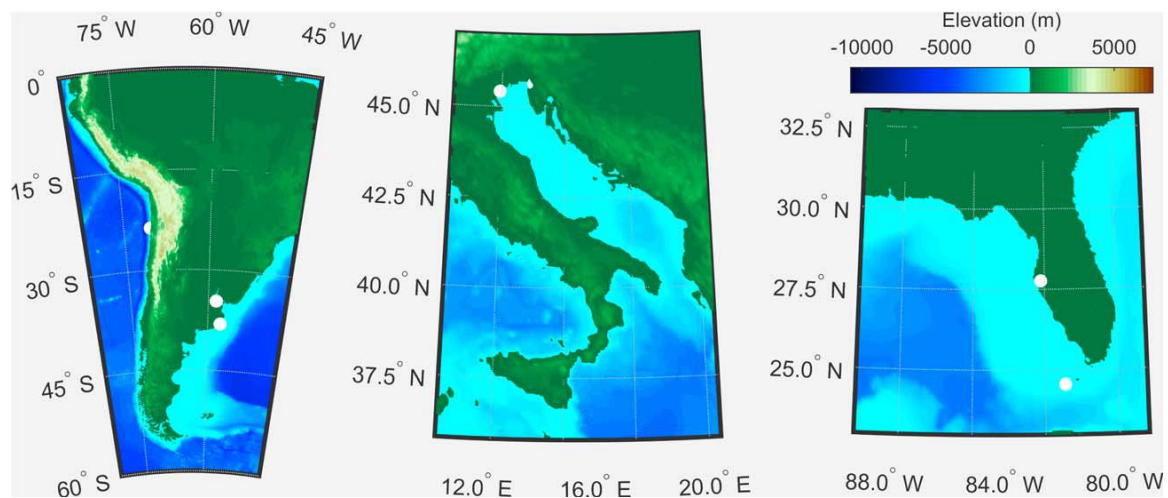


Figure 4.3 Regional maps showing the width of the continental shelf of the study areas.

Four of the stations analyzed, namely, St. Petersburg, Key West, Buenos Aires, and Mar del Plata, show a dependency between extreme skew surges and HW levels regardless of the definition of the extreme sample, bandwidth, and seasonality effects. In these four places, extreme skew surges tend to occur in smaller HW levels (e.g., Figure 4.2f for Buenos Aires) regardless of the differences observed in the shape of the HW PDFs and the histograms of the HWs associated to extreme skew surges. This supports the hypothesis that differences in water depth between HW peaks can also produce a tide-surge interaction, that is, wind stress is more effective in generating extreme surges in smaller HWs than in larger HWs. We also observe that the magnitude of extreme skew surges in these four locations is larger than in the sites where we find independence. In addition, these four tide gauges are located in places characterized by a shallow and wide continental shelf (Figures 4.1 and 4.3), which can contribute to an enhanced effect of the tide-surge interaction.

On the other hand, we find independence between extreme skew surges and HWs in six of the 15 tide-gauge sites (Bella bella, Antofagasta, Carnarvon, Saigo, Omaezaki, and Uwajima) regardless of the approaches used in the analysis. In these sites, maximum observed skew surges are between 70 and 50 cm, which are about half of the height observed in the locations where we find dependence, and these tide gauges are located in areas with a narrow continental shelf (Figure 4.3).

From the sensitivity analysis of the bandwidth used for the kernel density estimator, we observed that in some stations (Salalah, Saigo, and Sakai) the Anderson-Darling test is very sensitive to the bandwidth value selected. Although there are some automatic approaches to define the bandwidth, they do not ensure the definition of an optimal bandwidth, and therefore, the subjectivity in the definition of this parameter can bias the final results of this analysis.

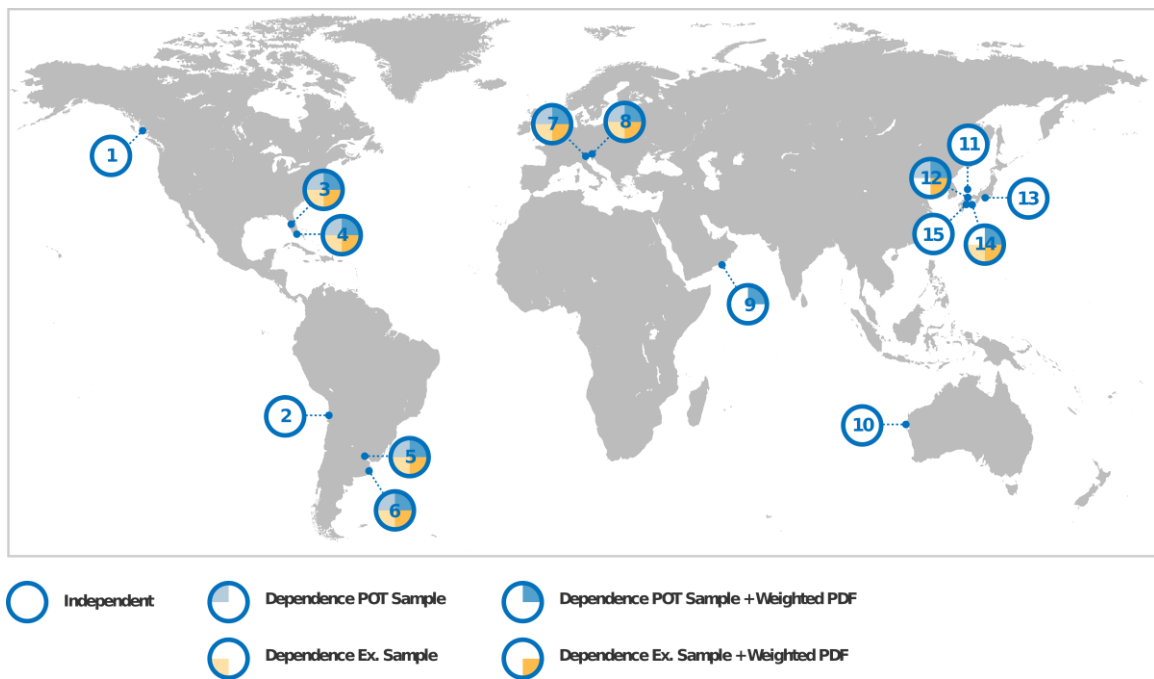


Figure 4.4 Results of the dependence analysis obtained for all tide-gauges and extreme samples. Dependent = rejection of the null hypothesis of the Anderson-Darling test (0.05 significant level. The results for  $\alpha = 0.01$  can be found in Figure C.8 in Appendix C). Independent = the null hypothesis cannot be rejected. The null hypothesis is that HWs associated to the extreme skew sample are drawn from the same distribution as all HWs. (These results can also be found in Table C.3 in Appendix C). HW = high water; PDF = probability distribution function.

The dependence analysis can be sensitive to the definition of the extreme sample in places with a mixed tidal regime because the effects of the tide-surge interaction due to differences of water depth between HWs can be “hidden” if the duration of an extreme surge event comprises more than one HW peak. However, we only observe that two stations show dependency for one of the extreme samples but independence

for the other extreme sample. Sakai shows dependency for the Ex. Sample but independence for the POT sample. The opposite is true in Murotomisaki where the POT sample shows a dependency of the HW level, but independence is observed for the Ex. sample. On the other hand, in Murotomisaki, the PDF of HWs associated to the POT sample shows three peaks (there are three bands of HW levels that are much more likely than other bands), while the PDF of HWs associated to the Ex. Sample is smoother (Figure C.1 to C.7 in Appendix C). Reducing the significant level of the Anderson-Darling test to 0.01, we find that Buenos Aires and Mar del Plata show dependence for the two extreme samples, while Venice and Sakai only for the Ex. Sample and St. Petersburg and Key West for the POT sample (Figure C.8 in Appendix C).

#### **4.4.1. Seasonal Effects**

Although we removed the effects of the MSL seasonality by detrending the tide-gauge series before the analysis, seasonality of extreme skew surges can produce a bias in the dependence analysis by skewing the sample of HWs associated to extremes to the HW values of the stormiest months. If these months coincide with the minimum declination of the Sun (equinoxes) and the Moon, the HWs associated to extremes can be biased to larger HWs and vice versa. In Figure 4.5, we can observe the PDF and the weighted PDF of all HWs together with the histograms of the HWs associated to the extreme skew surges of all the stations. In general, we do not observe large differences between the two PDFs probably due to the small tidal seasonal signal, as we discuss below. However, we find that the weighting of the HWs PDF of Trieste and Venice removes the dependency to the HW level obtained for the POT extreme sample but not for the Ex. Sample. Therefore, it is not clear if the dependence observed in these two locations can be caused by the seasonality, and further research is needed for addressing this issue. The reduction of seasonal effects in the HWs PDF also shows dependency to the HW level of both extreme samples in Sakai and Murotomisaki. As discussed before, these two places show dependence only of one extreme sample from the analysis with the non-weighted PDF, and thus, dependence can be hidden by seasonality effects. We must note that part of the signal attributed to the tidal seasonal terms is removed in the detrending process through aliasing. In addition, the  $S_A$  was only estimated from the harmonic analysis for the leap years because we performed the harmonic analysis over calendar years. The gravitational seasonality is very small compared to the MSL seasonality, and the amplitude of the  $S_A$  and  $S_{SA}$  is enhanced due to the MSL seasonality (Pugh and Woodworth, 2014).

Nevertheless, we have compared the effects of the detrending approach on the estimated mean amplitude of the  $S_{SA}$ , and we find differences of less than 3 cm, which is similar to the magnitude of the estimated confidence intervals of the amplitudes.

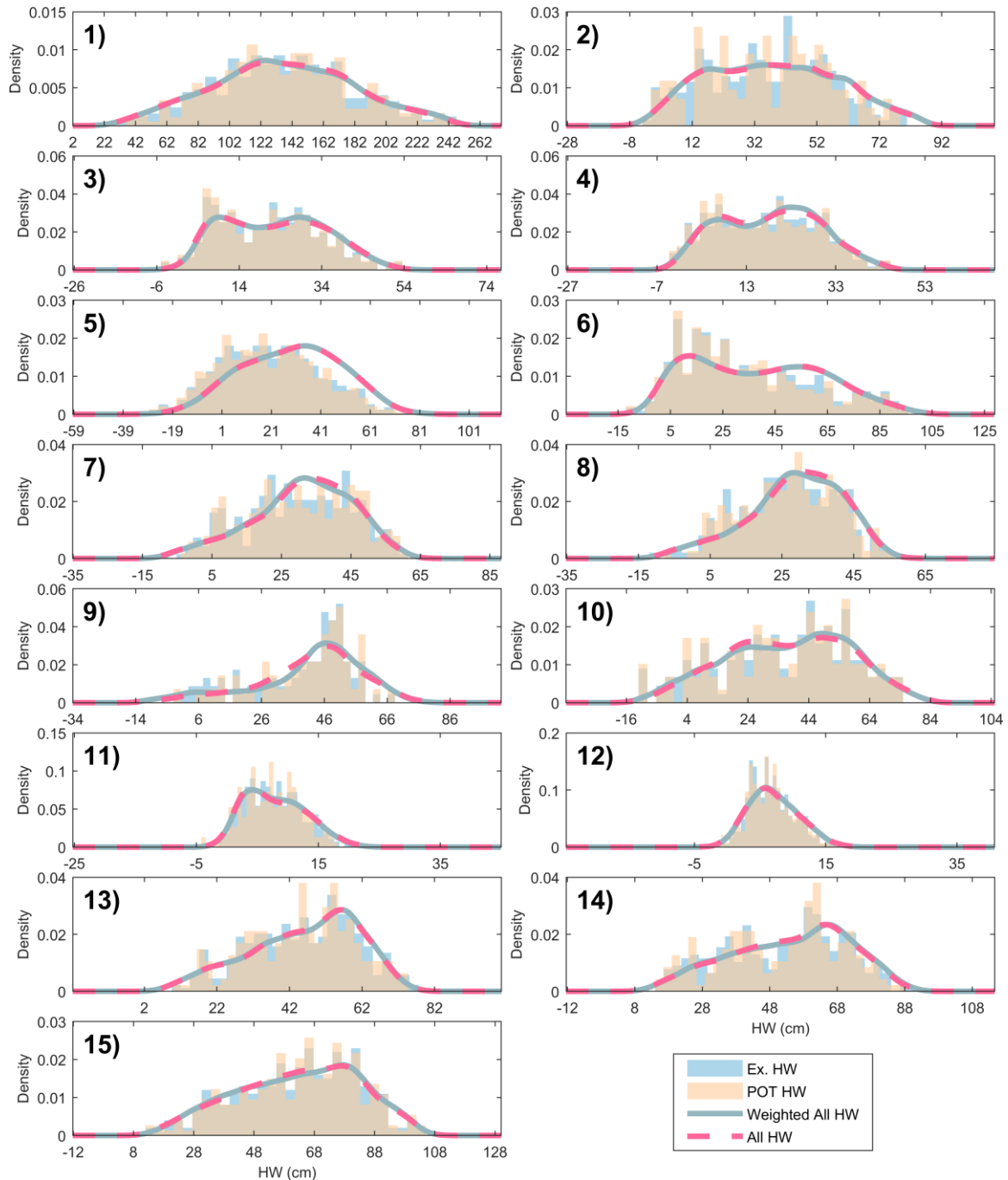


Figure 4.5 PDF and weighted PDF of all HWs, and histograms of HWs associated to the two extremes samples of (1) Bella bella, (2) Antofagasta, (3) St. Petersburg, (4) Key West, (5) Buenos Aires, (6) Mar del Plata, (7) Trieste, (8) Venice, (9) Salalah, (10) Carnarvon, (11) Saigo, (12) Sakai, (13) Omaezaki, (14) Murotomisaki, and (15) Uwajima. HW = high water; PDF = probability distribution function.

#### 4.4.2. Dependence Analysis for LHWs and HHWs

In order to further investigate if the dependency to the HW level obtained is related to the mixed tidal regime, we have calculated the relative frequency of both extreme skew surge samples at LHWs (Table 4.1). We observe that more of the 50% of extreme skew surges from both extreme samples occurred at LHWs at all stations (with the exception of the POT sample of Uwajima). We observe a high relative frequency (around 65–74%) of extreme skew surges occurring at LHWs at Buenos Aires and Mar del Plata, which supports the hypothesis that larger skew surges are generated at smaller HW levels and specifically at LHWs in mixed semidiurnal regimes. However, the relative frequency observed in other sites that showed dependency to the HW level is of a magnitude that is similar to, or even lower than, the relative frequency obtained for sites that showed independence. For example, we observe a similar relative frequency of extreme skew surges at LHWs at Bella bella or Antofagasta, which showed independence, than at the U.S. and Italian tide gauges, which showed dependence.

*Table 4.1 Relative Frequency (in Percentage) of Extreme Skew Surges at lower high water*

Station	Ex. Sample	POT Sample
Bella bella	57.06 %	58.82 %
Antofagasta	56.17 %	56.25 %
St. Petersburg	58.62 %	62.15 %
Key West	55.51 %	59.00 %
Buenos Aires	71.33 %	73.57 %
Mar del Plata	64.68 %	68.33 %
Trieste	53.38 %	52.96 %
Venice	56.23 %	56.45 %
Salalah	60.07 %	62.82 %
Carnarvon	52.21 %	52.38 %
Saigo	52.92 %	52.40 %
Sakai	56.84 %	55.17 %
Omaezaki	50.82 %	50.41 %
Murotomosaki	53.90 %	59.48 %
Uwajima	51.04 %	49.91 %

Williams et al., (2016) found a significant bias toward neap tides in few of the stations analyzed as, for example, Bournemouth and Harwich in the United Kingdom. They also carried out numerical model simulations to investigate differences in skew surge height between spring and neap conditions, finding that larger skew surges can be produced on neap tides, depending on the weather system. However, the spring-neap cycle is not clearly defined in mixed semidiurnal regimes, which can be observed in

Figures 4.2a and 4.2b (and Figures C.1–C.7 in Appendix C), as it is in semidiurnal regimes. Therefore, we cannot directly attribute the tendency observed in sites that show dependency but not a large number of extreme events in LHWs, to the spring-neap cycle. The differences between the distributions of HWs in the extreme samples and the total HWs can be related to a tendency of larger surges occurring at lower values of LHWs and/or HHWs. In order to analyze this tendency, we performed the Anderson-Darling test again but separated the two HW levels (i.e., for LHWs and HHWs) for those stations that showed dependence but not a large percentage of extreme skew surges at LHWs. The histograms of the extreme samples at the two HW levels as well as the PDF of all LHWs and HHWs are presented in Figure 4.6.

For the majority of these stations, we find a dependency of the extreme skew surge samples to one of the HW levels, although the pattern is not the same for the different regions. For example, we find a significant tendency of extreme skew surges occurring at the lower HHW values at St. Petersburg, while we do not observe this tendency in Key West. There, we observe the same pattern but only for the extreme skew surges associated to LHWs. Trieste also shows a larger frequency of extreme skew surges occurring during the lower LHW levels, but we do not find significant differences between the HW levels associated to extreme skew surges and the corresponding PDFs of all HW levels. For Sakai, we find dependence at both HW levels, but we observe a larger occurrence of extreme skew surges at smaller HHWs. Therefore, we observe a clear tendency of larger skew surges occurring at smaller HW values for some stations, but further research is needed in order to better characterize the dynamics of the tide-surge interaction (e.g., numerical modeling).

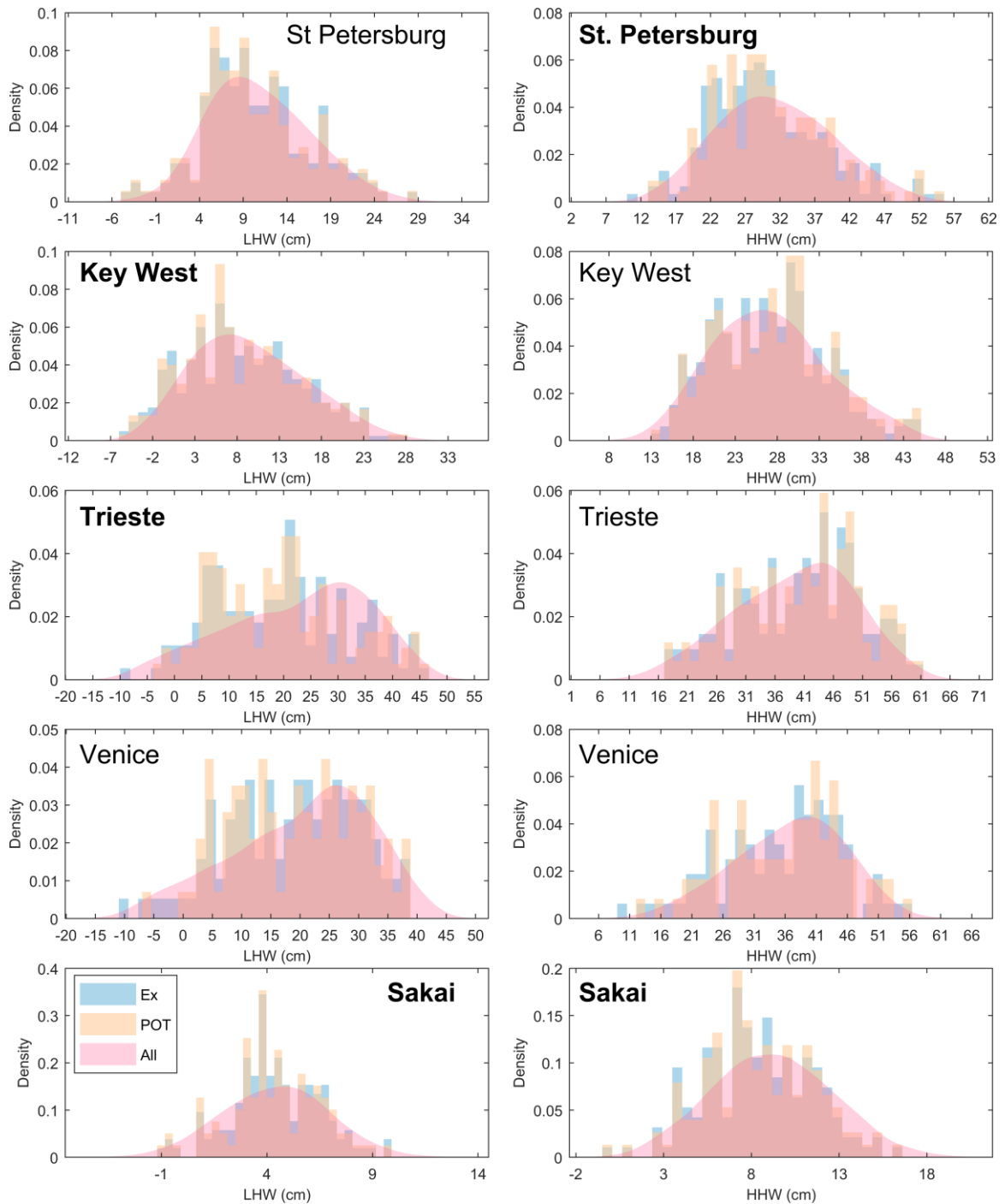


Figure 4.6 Histograms of the LHWs (left panels) and HHWs (right panels) associated to the two extreme skew surge samples and PDFs of all LHWs and HHWs. Stations' names that are in bold show a dependency (at 0.05 and 0.01 significant level, excluding both POT samples of Sakai, POT sample of St. Petersburg, and Key West that only show dependency at 0.05 level). HHW = higher high water; LHW = lower high water; PDF = probability distribution function.

## 4.5. Conclusions

Previous analyses have assumed extreme skew surges to be independent of HW levels worldwide. However, our results show that extreme skew surges are not always independent of the HW level in places with a mixed tidal regime, where one semidiurnal HW peak is larger than the next. The differences in water depth between HWs can also produce a tide-surge interaction, as we observe that extreme skew surges tend to occur during smaller HWs in tide gauges of regions with a wide shallow continental shelf, such as Buenos Aires and Key West. On the other hand, we find independence in those tide gauges located in regions with a narrow continental shelf. The places that show dependence of extreme skew surges and smaller HWs also experience storm surges of larger magnitude than those showing independence, which can be due to a contribution of the tide-surge interaction observed. Further research, involving numerical model simulations, is needed in order to better explore and quantify the dynamics of the tide-surge interaction at HWs in sites with mixed-tidal regimes, such as the ones included in this study.

The statistical comparison of the HWs PDFs seems to be more effective than correlation coefficients as a measure of dependence, as it shows the relationship between the two variables. However, spurious relationships can be found or can be hidden due to secular trends, inter-annual variability, and seasonality of both extreme skew surges and tidal levels, and therefore, these parameters also need to be taken into account. In addition, we observe that in some cases the results of the dependence analysis are sensitive to the definition of some subjective parameters of the methodology applied, such as the bandwidth of the kernel density estimator and the approach used to define the extreme sample.

The dependence of extreme skew surges to the HW level obtained in half of the analyzed tide-gauge stations leads to questioning the suitability of using the skew surge parameter instead of the non-tidal residual for flood assessments at those locations, as it offers no significant advantage and at the same time masks the storm evolution, which is a factor that can significantly affect flooding (Quinn et al., 2014; Santamaria-Aguilar et al., 2017a) and should not be neglected in flood assessments. Therefore, new approaches accounting both for the dependence between extreme surges and the tidal level as well as for the storm evolution would need to be developed for sites with mixed semidiurnal tidal regimes.

## **Acknowledgments**

S. Santamaria-Aguilar and A. T. Vafeidis were supported by the EU FP7 project RISES-AM (Grant 603396). We acknowledge the support of the Servicio de Hidrografia Naval (SHN) of Argentina for providing the tide-gauge series of Buenos Aires and Mar del Plata, which are available from SHN under request. All the other tide-gauge series are freely available from the GESLA-2 database (<http://gesla.org/>). In addition, the calculated skew surges time series and their associated HWs were made freely available from <https://doi.org/10.6084/m9.figshare.6455948.v1>. We are thankful to Maureen Tsakiris for helping with the design of Figure 4.4 and Table C.3. We would also like to thank Joanne Williams for providing constructive and valuable comments that helped to improve the paper. We would also like to acknowledge Jonathan Tawn for providing guidance on how to account for trends in the tidal levels with the methodology applied.



Chapter 5.

**Summary and general  
conclusions**



The main aim of this thesis has been to improve the understanding of the variability of the WL and its components (i.e. tides and surges), in order to reduce uncertainties associated with this variability when assessing extreme WLs for coastal flood assessments. The research and main findings have focused on two main temporal scales: 1) secular to inter-annual; 2) short-term (from hours to days).

### **1. Long-term trends and inter-annual variability of WLs, tides and surges**

In Chapter 2, the long-term trends and inter-annual variability of the WLs, tides and surges were analyzed for the case studies of two of the longest tide-gauge records of the southern hemisphere: Buenos Aires (1905-2013) and Mar del Plata (1956-2013; Argentina). In both locations, the WLs show significant long-term trends and inter-annual variability over the last century. The former originates from changes of the MSL over the study period, but also from changes in the tidal component. In this context, lower WLs rose faster than both the higher WLs and the MSL, which is caused by a rise of the low tidal levels. A detailed analysis of the changes in the tides at these two locations over the study period showed that significant long-term changes occurred in the main tidal constituents and thus translated to long-term changes in the tidal levels. Although these changes are not constant over the entire study period, a significant net decrease of the tidal amplitude is observed at both sites. In the case of Buenos Aires, this significant net decrease in the tidal amplitude is highly correlated to the long-term changes in the river discharge. Even though previous studies have claimed no influence of river discharge on WLs at Buenos Aires' tide-gauge due to the large size of the RdIP estuary (e.g., D'Onofrio et al., 1999), the results presented in Chapter 2 point to a dampening of the tidal wave during the wet periods of the river and vice versa. In addition to these long-term changes in the tides induced by river discharge, extreme NTRs of Buenos Aires seem to also be affected by extreme river discharge events, as a high correlation was found between the annual high percentile series of the two variables. Therefore, long-term changes in river discharge induced by climate change may in turn alter the tidal characteristics and extreme WLs in estuaries. These changes and interactions between river discharge, tides and extreme NTRs need to be analyzed and considered when assessing coastal flooding, especially in estuarine regions, as they have the potential to amplify or dampen flood impacts.

The results presented in Chapter 2 and previous studies (see Haigh et al., 2020 for a review) could not confirm that the rise of the MSL is the only driver of the observed changes in the tides over the last century, and pointed to several processes driving those changes in the tides. However, it is well known that changes in water depth

induce changes in the tides, and hydrodynamic modelling experiments point to tidal changes under different SLR scenarios (see e.g. Arns et al., 2015a; Pickering et al., 2017b). As shown in Arns et al., (2015a) and in Chapter 3, SLR has the potential to increase the tidal amplitude at the German Bight coastline, which will in turn exacerbate flooding. The amplification induced by SLR is not linear with the increase of the sea-level as relatively larger changes are simulated under low to moderate SLR scenarios than under a high end scenario. In addition, these induced changes are not spatially homogeneous, highlighting the importance of local shallow water dynamics and the non-linear effects of SLR.

## **2. Short-term variability of WLs**

This thesis has addressed two specific cases of the short-term variability: 1) the variability of the extreme WL curve (i.e. hydrograph); and 2) the tide-surge interaction.

These two factors are partly related because the tide-surge interaction causes a dependency between the surge and tidal levels, which complicates their separation and the extreme value analysis. In order to simplify the extreme value analysis, a common approach is to take only the peaks into account and to use the skew surge, which has been shown to be independent of the tidal level, instead of the NTR. However, these simplifications lead to a loss of the information related to the temporal evolution of the extreme WL events, which is required as input of flood models. This requirement leads to another simplification that is frequently addressed by using a single design hydrograph and thus neglecting the variability of the hydrographs of extreme WL events. The uncertainties related to neglecting the variability of the WL curve when assessing flooding were evaluated in terms of overflow and fullness for a case study at the German Bight coast in Chapter 3. The high variability found at times around the WL peaks introduces large uncertainties related to the total overflow volumes, because overflow/overtopping is more likely at these time steps, as the WLs can be of similar magnitude to the storm peak. This high historical variability of the hydrographs of extreme events can lead to a threefold increase of the total overflow volumes between events, which highlights the large uncertainties introduced in flood impact assessments when using a single design hydrograph. These large uncertainties increase when we account for the spatial variability of the storm hydrographs along the coastal stretch (~13 Km). The total overflow differences along the coastline can be of the same order as the difference between the overflow resulting from the T = 200 years and the T= 10,000 years event for the same location. As discussed before, SLR has the potential to increase the tidal range in this region, which

causes an increase of the WLs around the HW peaks and thus larger overflow volumes. However, the changes induced by SLR are not linear with the increase of the water depth and larger impacts can be expected from low to moderate SLR scenarios.

In Chapter 4, the dependency between the skew surge and the associated HW levels was assessed for places with a mixed semidiurnal regime. Results show that the extreme skew surges are not independent of the HW levels at all locations, thus not all extreme skew surges can occur with all HW levels. Therefore, extreme skew surges are not always independent of the tidal level, which leads to questioning the advantage of this parameter compared to the NTR. The NTR is also dependent on the tidal level but maintains the information of the storm evolution, which is a factor that can introduce large uncertainties when assessing flooding as discussed before.

## **5.1. Answers to Research Questions**

Specifically, the main objective of this thesis has been addressed by answering three research questions:

**1. Have the WLs and WL components at Buenos Aires and Mar del Plata (Argentina) shown any secular trend or inter-annual variability over the last century? Can these trends and variability be linked to large-scale climate patterns?**

The tide-gauge records of Buenos Aires (1905-2013) and Mar del Plata (1956-2013) are two of the longest records of the southern hemisphere, but these tide-gauge records are not included in global databases and have therefore not been included in previous variability studies. Secular trends and inter-annual variability were analyzed using a method frequently applied for this task, the percentile analysis method, in order to produce comparable results to previous assessments in other regions of the world (e.g. Marcos & Woodworth, 2107; Menendez & Woodworth, 2010). The percentile analysis allows assessing changes in the frequency distribution of WLs and whether these changes are similar to the changes of the MSL or caused by other factors. The percentile analysis of the tide-gauge records of Buenos Aires and Mar del Plata revealed that the WLs of these two locations showed significant long-term trends over the last century, which originate from the rise of the MSL but also from long-term trends occurring in the tidal component. At both locations, lower WLs showed larger increases

than the higher WLs and the MSL as a result of changes in the tide. When the tidal percentile series are removed, the residual or surge component showed no significant long-term trends at both locations.

A further analysis of the tidal component by a running harmonic analysis found significant long-term trends in the main tidal constituents (M2, S2, O1, K1 and M4) at both locations. Here, a net long-term decrease of the main semidiurnal constituents together with an increase of the main diurnal constituents was found. These changes in the main tidal constituents cause a net long-term decrease of the tidal range in the order of  $-0.62$  [mm  $y^{-1}$ ] at Buenos Aires and  $-0.43$  [mm  $y^{-1}$ ] at Mar del Plata. Although a net decrease of the tidal range is observed in Buenos Aires, both the tidal levels and constituents show an inter-annual to decadal variability which is highly correlated to the long-term variability of the river discharge. Therefore, the changes in river discharge are the main potential factor altering the tides at Buenos Aires. However, the river discharge does not seem to affect the tide at Mar del Plata, which is located outside the estuary at the open coast. Comparing the changes in the MSL over the studied period to the corresponding changes in the tides under SLR scenarios reported by other studies (e.g., Luz Clara et al., 2015; Carless et al., 2016), greater increases of the MSL will be required to produce the changes reported for Mar del Plata. Therefore, another process or multiple processes are responsible of the observed tidal changes at Mar del Plata.

## **2. How large are the uncertainties associated with not considering the spatial and temporal variability of storm surges at local scales? How would the rise of the sea-level affect the temporal and spatial evolution of extreme WLs and what are the implications for coastal flooding?**

In Chapter 3, the temporal and spatial variability of the extreme WL events from 1970 to 2009 were analyzed along a coastal stretch of 13 km at the German Bight. The WL curves of these events show large variability, which can lead to a two- to three-fold increase in total overflow volumes between events of equal storm peak level. Therefore, neglecting the temporal variability of extreme WL events by using a single design WL curve will introduce large uncertainties in the resulting flooding in this region. Neglecting the spatial variability of these extreme WL events along the stretch of coast analyzed will further increase the uncertainties of estimated overflow volumes, which can be in the same order as increasing the return WL by a factor of 50 (e.g. difference between the  $T = 200$  years and  $T = 10,000$  years for a single location).

In the German Bight, SLR has the potential of increasing the tidal range based on numerical simulations (Arns et al., 2015a). As shown in Chapter 3, this increase of the tidal range implies an increase of the WLs at the times near the HW peak and a decrease of the WLs at times around the LW peaks. However, this increase is not linear with SLR as low to moderate SLR scenarios (i.e. median values of RCP 4.5 and RCP 8.5) cause relatively greater changes than the RCP 8.5 HE. Changes to the WL curve of extreme events induced by SLR will increase the overflow volumes compared to the historical WL curves, therefore increasing the potential flooding. The changes induced by SLR are not spatially homogenous, which highlights the importance of local shallow water processes.

### **3. Are extreme skew surges independent of high water levels in a mixed semidiurnal tidal regime?**

Extreme skew surges are considered independent from the HW level worldwide based on previous studies performed in places with a semidiurnal tidal regime (e.g. Williams et al., 2016). However, the differences in water depth between HW levels can be larger in mixed semidiurnal regimes, where one HW peak is larger than the next, potentially causing a tide-surge interaction and therefore a dependency between them. The dependency between extreme skew surges and the associated HWs was statistically assessed at 15 locations with a mixed semidiurnal tidal regime worldwide in Chapter 4. As shown in this chapter, the differences in water depth between HW peaks in mixed tidal regimes can also lead to tide-surge interactions and as such larger extreme skew surges tend to coincide with smaller HW levels. This effect is statistically significant at locations with a wide shallow continental shelf, which also experienced larger extreme skew surges than those located in regions of narrower continental shelves.

The advantage of using the skew surge parameter over the NTR is that the skew surge is independent from the associated HW or tidal levels. However, the dependency between extreme skew surges and HW levels found in half of the analyzed locations leads to questions on the suitability of the parameter “skew surge” instead of the NTR for flood assessments, as the latter can also account for the time evolution of the storm, which was found to greatly affect flooding as shown in Chapter 3



Chapter 6.

**Implications for research and  
further work**



The main objectives of this thesis have been achieved based on the results summarized in the previous section. Nevertheless, the findings of this thesis also indicate some implications for research and other issues that require further research in order to increase the knowledge on WL variability and their associated uncertainties for assessing coastal flooding. Specifically, the main recommendations for research and further work are discussed in the following points:

### **1. Accounting for the variability of the WL curve when assessing flooding**

Significant effort is being directed to assess future SLR flood impacts and the uncertainties related to future SLR scenarios. However, as demonstrated in Chapter 3, the commonly applied approach of using a single “design” WL curve when simulating flooding with hydrodynamic models introduces large uncertainties in the total flood volumes. Although sophisticated multivariate extreme value models and stochastic models have been developed for producing joint probabilities and synthetic WL curves from historical extreme WL events (Wahl et al., 2011; MacPherson et al., 2019), most flood impact assessments are still only considering a single design WL curve (e.g. Vousdoukas et al., 2018a). The high computational effort required to run several events using hydrodynamic flood models is one of the main reasons why the variability of the WL curve is not accounted for. However, the methodology (presented in Chapter 3) for normalizing the WL curve of a large number of events and estimating the bounds of those WL curves can be used to reduce the number of events required. In this context, the simulation of the median, the 5<sup>th</sup> percentile and the 95<sup>th</sup> percentile WL curves would be sufficient for providing an estimation of the flooding and the uncertainties related to the WL curve.

### **2. Modelling the dependency between extreme NTR and tidal levels**

Following the discussion of the previous point, the dependency of the NTR to the tidal level is another factor limiting the analysis of several WL curves when assessing flooding. The NTR is the only parameter which defines the surge component that also includes information on the temporal evolution of the storm, however the magnitude of the NTR is dependent on the tidal level due to tide-surge interaction. On the other hand, the skew surge parameter, which does not contain information on the temporal evolution of the surge, was assumed to be independent of HWs worldwide, but as shown in Chapter 4, extreme skew surges show a dependency in some locations with a mixed semidiurnal tidal regime. Therefore, future research should be directed to modelling the dependency of the NTR curve to the tidal levels. In this context, the study of Arns et al., (2020) has begun modelling of the dependency between the NTR and

tidal levels of extreme WL peaks, however the temporal information of the event is still not included in the model.

### **3. Interactions between river discharge, storm surges and tides**

Recently, the analysis of compound events from river and coastal drivers has become a popular topic in research as compound flooding can exacerbate the flood impacts compared to the occurrence of single/separate events. In addition, the co-occurrence of events such as storm surges and extreme river discharge can be expected because in many cases both are driven by the same atmospheric phenomena. This effect has been observed at Buenos Aires, where the upper percentile Residual series showed a high positive correlation with river discharge (Chapter 2). However, the analysis performed in Chapter 2 as well as most of the recent studies addressing compound events are focused on the statistical dependency between the drivers (see e.g. Couasnon et al., 2020 for a global assessment) and the physical interactions between those drivers (e.g. interactions between river discharge, storm surges and tides) are still poorly understood. As the co-occurrence of compound river and coastal flooding is statistically possible, the interactions between the drivers need to be further explored, by using e.g. numerical models, for a more precise characterization of areas at risk from compound flooding.

### **4. Effects of river discharge long-term trends on tidal characteristics**

Tides showed secular trends in both tidal levels and their constituents over the last century in most coastal regions of the world, including Buenos Aires and Mar del Plata (Chapter 2), but the drivers of these changes are still unknown. However, the secular changes in the tide at Buenos Aires are highly correlated with the secular changes in the river discharge, indicating that the river discharge might be a potential driver of these changes despite the large size of the RdIP estuary. This factor needs to be accounted for when analyzing the historical tidal changes in other estuaries, but also for projecting future changes in the tides. Climate induced changes in river discharge can also alter the tidal characteristics in estuaries, dampening or exacerbating SLR impacts on the tides. Therefore, projections of river discharge need to be included when assessing future SLR impacts on the tides in estuarine regions.

### **5. Accounting for tidal changes in flood impact assessments**

SLR has the potential to produce non-linear amplifications in the tides, but also reductions for the majority of coastal regions (see e.g., Pickering et al., 2012). However, these potential future changes are not included when assessing coastal

flooding. The only studies that have assessed future tidal changes are the studies of Vousdoukas et al., (2017, 2018b), but in both cases the changes were averaged by regions and were considered negligible. However, tidal amplifications can exacerbate flooding at local to regional scales as shown in Chapter 3 and in Arns et al., (2015a), and these amplifications will also affect wave propagation by reducing wave dissipation due to friction and allowing larger waves to reach the coastline. Therefore, ignoring these potential amplifications of the tides can lead to underestimating flood risk in some coastal regions.



## References

- Arns, A., Dangendorf, S., Jensen, J., Talke, S., Bender, J., Pattiaratchi, C., et al. (2017). Sea-level rise induced amplification of coastal protection design heights. *Sci. Rep.* 7, 40171. doi:10.1038/srep40171.
- Arns, A., Wahl, T., Dangendorf, S., and Jensen, J. (2015a). The impact of sea level rise on storm surge water levels in the northern part of the German Bight. *Coast. Eng.* 96, 118–131. doi:10.1016/j.coastaleng.2014.12.002.
- Arns, A., Wahl, T., Haigh, I. D. D., and Jensen, J. (2013a). Determining extreme water return levels at un-gauged sites: a case study of the Schleswig-Holsteins coastline and Islands in north-west Germany. *Coast. Dyn.*, 127–138. Available at: [http://www.coastaldynamics2013.fr/pdf\\_files/012\\_Arns\\_arne.pdf](http://www.coastaldynamics2013.fr/pdf_files/012_Arns_arne.pdf).
- Arns, A., Wahl, T., Haigh, I. D. D., Jensen, J., and Pattiaratchi, C. (2013b). Estimating extreme water level probabilities: A comparison of the direct methods and recommendations for best practise. *Coast. Eng.* 81, 51–66. doi:10.1016/j.coastaleng.2013.07.003.
- Arns, A., Wahl, T., Haigh, I. D., and Jensen, J. (2015b). Determining return water levels at ungauged coastal sites: a case study for northern Germany. *Ocean Dyn.* 65, 539–554. doi:10.1007/s10236-015-0814-1.
- Arns, A., Wahl, T., Wolff, C., Vafeidis, A. T., Haigh, I. D., Woodworth, P., et al. (2020). Non-linear interaction modulates global extreme sea levels, coastal flood exposure, and impacts. *Nat. Commun.* 11, 1–9. doi:10.1038/s41467-020-15752-5.
- Artana, C., Ferrari, R., Koenig, Z., Saraceno, M., Piola, A. R., and Provost, C. (2016). Malvinas Current variability from Argo floats and satellite altimetry. *J. Geophys. Res. Ocean.* 121, 4854–4872. doi:10.1002/2016JC011889.
- Batstone, C., Lawless, M., Tawn, J., Horsburgh, K., Blackman, D., McMillan, A., et al. (2013). A UK best-practice approach for extreme sea-level analysis along complex topographic coastlines. *Ocean Eng.* 71, 28–39. doi:10.1016/j.oceaneng.2013.02.003.
- Bilskie, M. V., Hagen, S. C. C., Alizad, K., Medeiros, S. C. C., Passeri, D. L. L.,

- Needham, H. F. F., et al. (2016). Dynamic simulation and numerical analysis of hurricane storm surge under sea level rise with geomorphologic changes along the northern Gulf of Mexico. *Earth's Futur.*, n/a--n/a.  
doi:10.1002/2015EF000347.
- Bouwer, L. M., and Jonkman, S. N. (2018). Global mortality from storm surges is decreasing. *Environ. Res. Lett.* 13. doi:10.1088/1748-9326/aa98a3.
- Bruss, G., Gönner, G., and Mayerle, R. (2010). Extreme scenarios at the German North Sea coast. A numerical model study. *Coast. Eng.* 32, 1–13.
- Carless, S. J., Green, J. A. M., Pelling, H. E., and Wilmes, S. B. (2016). Effects of future sea-level rise on tidal processes on the Patagonian Shelf. *J. Mar. Syst.* 163, 113–124. doi:10.1016/j.jmarsys.2016.07.007.
- Church, J. A., and Gregory, J. M. (2013). Sea level change. *Encycl. Ocean Sci.*, 493–499. doi:10.1016/B978-0-12-409548-9.10820-6.
- Cid, A., Menéndez, M., Castanedo, S., Abascal, A. J., Méndez, F. J., and Medina, R. (2015). Long-term changes in the frequency, intensity and duration of extreme storm surge events in southern Europe. *Clim. Dyn.* doi:10.1007/s00382-015-2659-1.
- Codiga, D. L. (2011). Unified Tidal Analysis and Prediction Using the UTide Matlab Functions. doi:10.13140/RG.2.1.3761.2008.
- Coles, S. (2001). *An introduction to statistical modeling of extreme values*. London: Springer-Verlag.
- Colosi, J. A., and Munk, W. (2006). Tales of the Venerable Honolulu Tide Gauge. *J. Phys. Oceanogr.* 36, 967–996. doi:10.1175/JPO2876.1.
- Combes, V., and Matano, R. P. (2014). Trends in the Brazil/Malvinas Confluence region. *Geophys. Res. Lett.* 41, 8971–8977.  
doi:10.1002/2013GL058987.Received.
- Compo, G. P., Whitaker, J. S., Sardeshmukh, P. D., Matsui, N., Allan, R. J., Yin, X., et al. (2011). The Twentieth Century Reanalysis Project. *Q. J. R. Meteorol. Soc.* 137, 1–28. doi:10.1002/qj.776.
- Couasnon, A., Eilander, D., Muis, S., Veldkamp, T. I. E. E., Haigh, I. D., Wahl, T., et

- al. (2020). Measuring compound flood potential from river discharge and storm surge extremes at the global scale. *Nat. Hazards Earth Syst. Sci.* 20, 489–504. doi:10.5194/nhess-20-489-2020.
- D'Onofrio, E. E., Fiore, M. M. E., and Pousa, J. L. (2008). Changes in the Regime of Storm Surges at Buenos Aires, Argentina. *J. Coast. Res.* 1, 260–265. doi:10.2112/05-0588.1.
- D'Onofrio, E. E., Fiore, M. M. E., and Romero, S. I. (1999). Return periods of extreme water levels estimated for some vulnerable areas of Buenos Aires. *Cont. Shelf Res.* 19, 1681–1693. doi:10.1016/S0278-4343(98)00115-0.
- Dangendorf, S., Arns, A., Pinto, J. G., Ludwig, P., and Jensen, J. (2016). The exceptional influence of storm "Xaver" on design water levels in the German Bight. *Environ. Res. Lett.* 11, 1–10. doi:10.1088/1748-9326/11/5/054001.
- Dangendorf, S., Calafat, F. M., Arns, A., Wahl, T., Haigh, I. D., and Jensen, J. (2014). Mean sea level variability in the North Sea: Processes and implications. *J. Geophys. Res. Ocean.* 119, 6820–6841. doi:10.1002/jgrc.20224.
- Dangendorf, S., Marcos, M., Wöppelmann, G., Conrad, C. P., Frederikse, T., and Riva, R. (2017). Reassessment of 20th century global mean sea level rise. *Proc. Natl. Acad. Sci.*, 201616007. doi:10.1073/pnas.1616007114.
- Dangendorf, S., Mudersbach, C., Jensen, J., Anette, G., and Heinrich, H. (2013). Seasonal to decadal forcing of high water level percentiles in the German Bight throughout the last century. *Ocean Dyn.* 63, 533–548. doi:10.1007/s10236-013-0614-4.
- Dawson, R. J., Hall, J. W., Bates, P. D., and Nicholls, R. J. (2005). Quantified Analysis of the Probability of Flooding in the Thames Estuary under Imaginable Worst-case Sea Level Rise Scenarios. *Int. J. Water Resour. Dev.* 21, 577–591. doi:10.1080/07900620500258380.
- Devlin, A. T., Jay, D. A., Talke, S. A., and Zaron, E. (2014). Can tidal perturbations associated with sea level variations in the western Pacific Ocean be used to understand future effects of tidal evolution? *Ocean Dyn.*, 1093–1120. doi:10.1007/s10236-014-0741-6.
- Doyle, M. E., and Barros, V. R. (2011). Attribution of the river flow growth in the Plata

- Basin. *Int. J. Climatol.* 31, 2234–2248. doi:10.1002/joc.2228.
- Feng, X., Tsimplis, M. N., and Woodworth, P. L. (2015). Nodal variations and long-term changes in the main tides on the coasts of China. *J. Geophys. Res. Ocean.*, 1–17. doi:10.1002/2014JC010320. Received.
- Fiore, M. E., D'Onofrio, E. E., Grismeyer, W. H., and Mediavilla, D. G. (2008). El ascenso del nivel del mar en la costa de la provincia de Buenos Aires. *Cienc. Hoy* 18, 50–57.
- Fiore, M. M. E., D'Onofrio, E. E., Pousa, J. L., Schnack, E. J., and Bértola, G. R. (2009). Storm surges and coastal impacts at Mar del Plata, Argentina. *Cont. Shelf Res.* 29, 1643–1649. doi:10.1016/j.csr.2009.05.004.
- Garner, A. J., Weiss, J. L., Parris, A., Kopp, R. E., Horton, R. M., Overpeck, J. T., et al. (2018). Evolution of 21st Century Sea Level Rise Projections. *Earth's Futur.* 6, 1603–1615. doi:10.1029/2018EF000991.
- Gillett, N. P., Kell, T. D., and Jones, P. D. (2006). Regional climate impacts of the Southern Annular Mode. *Geophys. Res. Lett.* 33, L23704. doi:10.1029/2006GL027721.
- Gönnert, G., and Gerkenmeier, B. (2015). A Multi-Method Approach to Develop Extreme Storm Surge Events to Strengthen the Resilience of Highly Vulnerable Coastal Areas. *Coast. Eng. J.* 57, 1. doi:10.1142/S0578563415400021.
- Grinsted, A., Jevrejeva, S., Riva, R. E. M., and Dahl-Jensen, D. (2015). Sea level rise projections for Northern Europe under RCP8.5. *Clim. Res.* 64, 15–23. doi:10.3354/cr01309.
- Haigh, I. D., MacPherson, L. R., Mason, M. S., Wijeratne, E. M. S., Pattiaratchi, C. B., Crompton, R. P., et al. (2014). Estimating present day extreme water level exceedance probabilities around the coastline of Australia: tropical cyclone-induced storm surges. *Clim. Dyn.* 42, 139–157. doi:10.1007/s00382-012-1653-0.
- Haigh, I. D., Nicholls, R., and Wells, N. (2010a). A comparison of the main methods for estimating probabilities of extreme still water levels. *Coast. Eng.* 57, 838–849. doi:10.1016/j.coastaleng.2010.04.002.

- Haigh, I. D., Pickering, M. D., Green, J. A. M., Arbic, B. K., Arns, A., Dangendorf, S., et al. (2020). The Tides They Are A-Changin': A Comprehensive Review of Past and Future Nonastronomical Changes in Tides, Their Driving Mechanisms, and Future Implications. *Rev. Geophys.* 58, 1–39. doi:10.1029/2018RG000636.
- Haigh, I. D., Wadey, M. P., Wahl, T., Ozsoy, O., Nicholls, R. J., Brown, J. M., et al. (2016). Spatial and temporal analysis of extreme sea level and storm surge events around the coastline of the UK. 1–14.
- Haigh, I., Nicholls, R., and Wells, N. (2010b). Assessing changes in extreme sea levels: Application to the English Channel, 1900–2006. *Cont. Shelf Res.* 30, 1042–1055. doi:10.1016/j.csr.2010.02.002.
- Hill, D. F. (2016). Spatial and Temporal Variability in Tidal Range : Evidence , Causes , and Effects. *Curr. Clim. Chang. Reports*, 232–241. doi:10.1007/s40641-016-0044-8.
- Hinkel, J., Jaeger, C., Nicholls, R. J., Lowe, J., Renn, O., and Peijun, S. (2015). Sea-level rise scenarios and coastal risk management. *Nat. Clim. Chang.* 5, 188–190. doi:10.1038/nclimate2505.
- Hinkel, J., Lincke, D., Vafeidis, A. T., Perrette, M., Nicholls, R. J., Tol, R. S. J., et al. (2014). Coastal flood damage and adaptation costs under 21st century sea-level rise. *Proc. Natl. Acad. Sci. U. S. A.* 111, 3292–7. doi:10.1073/pnas.1222469111.
- Ho, M., Kiem, A. S., and Verdon-Kidd, D. C. (2012). The Southern Annular Mode: A comparison of indices. *Hydrol. Earth Syst. Sci.* 16, 967–982. doi:10.5194/hess-16-967-2012.
- Höffken, J., Vafeidis, A. T., MacPherson, L. R., and Dangendorf, S. (2020). Effects of the Temporal Variability of Storm Surges on Coastal Flooding. *Front. Mar. Sci.* 7, 1–14. doi:10.3389/fmars.2020.00098.
- Horsburgh, K. J., and Wilson, C. (2007). Tide-surge interaction and its role in the distribution of surge residuals in the North Sea. *J. Geophys. Res.* 112, C08003. doi:10.1029/2006JC004033.
- Idier, D., Bertin, X., Thompson, P., and Pickering, M. D. (2019). Interactions Between Mean Sea Level, Tide, Surge, Waves and Flooding: Mechanisms and Contributions to Sea Level Variations at the Coast. *Surv. Geophys.* 40, 1603–

1630. doi:10.1007/s10712-019-09549-5.
- Idier, D., Paris, F., Cozannet, G. Le, Boulahya, F., and Dumas, F. (2017). Sea-level rise impacts on the tides of the European Shelf. *Cont. Shelf Res.* doi:10.1016/j.csr.2017.01.007.
- Jaime, P. (2002). Analisis del regimen hidrológico de los rios Parana y Uruguay. Ezeiza doi:10.1017/CBO9781107415324.004.
- Jay, D. A. (2009). Evolution of tidal amplitudes in the eastern Pacific Ocean. *Geophys. Res. Lett.* 36, 1–5. doi:10.1029/2008GL036185.
- Jonathan, P., and Ewans, K. (2013). Statistical modelling of extreme ocean environments for marine design: A review. *Ocean Eng.* 62, 91–109. doi:10.1016/j.oceaneng.2013.01.004.
- Kaiser, G., and Kortenhaus, A. (2008). Pilot Study “ German Bight Coast .”
- Kay, M. (2007). *Practical Hydraulics*. Second. , ed. Taylor & Francis doi:10.1017/CBO9781107415324.004.
- Kortenhaus, A., Lambrecht, H.-J., Flood, I., Analysis, R., Methodologies, M., and Number, R. (2006). Preliminary reliability analysis of flood defences in the pilot site : German Bight.
- Letetrel, C., Marcos, M., Martín Míguez, B., and Woppelmann, G. (2010). Sea level extremes in Marseille (NW Mediterranean) during 1885-2008. *Cont. Shelf Res.* 30, 1267–1274. doi:10.1016/j.csr.2010.04.003.
- Luz Clara, M., Simionato, C. G., D’Onofrio, E., Fiore, M., and Moreira, D. (2014). Variability of tidal constants in the Río de la Plata estuary associated to the natural cycles of the runoff. *Estuar. Coast. Shelf Sci.* 148, 85–96. doi:10.1016/j.ecss.2014.07.002.
- Luz Clara, M., Simionato, C. G., D’Onofrio, E., and Moreira, D. (2015). Future Sea Level Rise and Changes on Tides in the Patagonian Continental Shelf. *J. Coast. Res.* 313, 519–535. doi:10.2112/JCOASTRES-D-13-00127.1.
- MacPherson, L. R., Arns, A., Dangendorf, S., Vafeidis, A. T., and Jensen, J. (2019). A Stochastic Extreme Sea Level Model for the German Baltic Sea Coast. *J. Geophys. Res. Ocean.* 124, 2054–2071. doi:10.1029/2018JC014718.

- Marcomini, S. C., and Lopez, R. A. (2006). Evolution of a beach nourishment project at Mar del Plata. *J. Coast. Res.* 2004, 834–837.
- Marcos, M., Calafat, F. M., Berihuete, Á., and Dangendorf, S. (2015). Long-term variations in global sea level extremes. *J. Geophys. Res. Ocean.*, n/a-n/a. doi:10.1002/2015JC011173.
- Marcos, M., Tsimplis, M. N., and Shaw, A. G. P. (2009). Sea level extremes in southern Europe. *J. Geophys. Res. Ocean.* 114, 1–16. doi:10.1029/2008JC004912.
- Marcos, M., and Woodworth, P. L. (2017). Spatiotemporal changes in extreme sea levels along the coasts of the North Atlantic and the Gulf of Mexico. *J. Geophys. Res. Ocean.*, 7031–7048. doi:10.1002/2017JC013065. Received.
- Marcos, M., Wöppelmann, G., Matthews, A., Ponte, R. M., Birol, F., Arduin, F., et al. (2019). Coastal Sea Level and Related Fields from Existing Observing. *Surv. Geophys.* doi:10.1007/s10712-019-09513-3.
- Mawdsley, R., and Haigh, I. D. (2016). Spatial and temporal variability and long-term trends in skew surges globally. *Front. Mar. Sci.* 3, 1–17. doi:10.3389/fmars.2016.00029.
- Mawdsley, R. J., Haigh, I. D., and Wells, N. C. (2015). Global secular changes in different tidal high water, low water and range levels. *Earth's Futur.*, 66–81. doi:10.1002/2014EF000282.
- McMillan, A. M., Batstone, C. P., Worth, D., Tawn, J. A., Horsburgh, K., and Lawless, M. (2011). Coastal flood boundary conditions for UK mainland and islands. Project SC060064/TR2: Design sea levels.
- Meccia, V. L. L., Simionato, C. G. G., Fiore, M. E. E., D'Onofrio, E. E. E., and Dragani, W. C. C. (2009). Sea surface height variability in the Rio de la Plata estuary from synoptic to inter-annual scales: Results of numerical simulations. *Estuar. Coast. Shelf Sci.* 85, 327–343. doi:10.1016/j.ecss.2009.08.024.
- Menéndez, M., and Woodworth, P. L. (2010). Changes in extreme high water levels based on a quasi-global tide-gauge data set. *J. Geophys. Res. Ocean.* 115, 1–15. doi:10.1029/2009JC005997.

- Ministerium für Energiewende, L. U. und ländliche R. des L., and Schleswig-Holstein (2012). Generalplan Küstenschutz des Landes Schleswig-Holstein. Available at: <http://www.schleswig-holstein.de/DE/Fachinhalte/K/kuestenschutz/generalplanKuestenschutz.html>.
- Mudersbach, C., Wahl, T., Haigh, I. D., and Jensen, J. (2013). Trends in high sea levels of German North Sea gauges compared to regional mean sea level changes. *Cont. Shelf Res.* 65, 111–120. doi:10.1016/j.csr.2013.06.016.
- Müller, M. (2011). Rapid change in semi-diurnal tides in the North Atlantic since 1980. *Geophys. Res. Lett.* 38, 1–6. doi:10.1029/2011GL047312.
- Müller, M., Arbic, B. K., and Mitrovica, J. X. (2011). Secular trends in ocean tides: Observations and model results. *J. Geophys. Res. Ocean.* 116, 1–19. doi:10.1029/2010JC006387.
- Müller, M., Cherniawsky, J. Y., Foreman, M. G. G., and Von Storch, J. S. (2014). Seasonal variation of the M 2 tide. *Ocean Dyn.* 64, 159–177. doi:10.1007/s10236-013-0679-0.
- Nagy, G. J., Severov, D. N., Pshennikov, V. A., De los Santos, M., Lagomarsino, J. J., Sans, K., et al. (2008). Rio de la Plata estuarine system: Relationship between river flow and frontal variability. *Adv. Sp. Res.* 41, 1876–1881. doi:10.1016/j.asr.2007.11.027.
- Neumann, B., Vafeidis, A. T., Zimmermann, J., and Nicholls, R. J. (2015). Future coastal population growth and exposure to sea-level rise and coastal flooding - A global assessment. *PLoS One* 10. doi:10.1371/journal.pone.0118571.
- Nicholls, R. J., Hanson, S. E., Lowe, J. a., Warrick, R. a., Lu, X., and Long, A. J. (2014). Sea-level scenarios for evaluating coastal impacts. *Wiley Interdiscip. Rev. Clim. Chang.* 5, 129–150. doi:10.1002/wcc.253.
- Nnamchi, H. C., Li, J., and Anyadike, R. N. C. (2011). Does a dipole mode really exist in the South Atlantic Ocean? *J. Geophys. Res. Atmos.* 116, 1–15. doi:10.1029/2010JD015579.
- Palma, E. D., Matano, R. P., and Piola, A. R. (2008). A numerical study of the Southwestern Atlantic Shelf circulation: Stratified ocean response to local and offshore forcing. *J. Geophys. Res. Ocean.* 113, 1–22.

doi:10.1029/2007JC004720.

Parker, B. B. (2007). *Tidal analysis and prediction*.

doi:10.1017/cbo9781139235778.007.

Pasquini, A. I., and Depetris, P. J. (2007). Discharge trends and flow dynamics of South American rivers draining the southern Atlantic seaboard: An overview. *J. Hydrol.* 333, 385–399. doi:10.1016/j.jhydrol.2006.09.005.

Pasquini, A. I., and Depetris, P. J. (2010). ENSO-triggered exceptional flooding in the Paraná River: Where is the excess water coming from? *J. Hydrol.* 383, 186–193. doi:10.1016/j.jhydrol.2009.12.035.

Perez Garcia, R. (2012). MESA 2 : Rellenos en la Ribera de la Ciudad Metropolitana. in *18° Congreso de Saneamiento y Medio Ambiente, IV Feria Internacional de Tecnologías del Medio Ambiente y en Agua (FITMA)* (Buenos Aires: Fundacion Ciudad), 1–20.

Pickering, M. D. D., Wells, N. C. C., Horsburgh, K. J. J., and Green, J. a. M. (2012). The impact of future sea-level rise on the European Shelf tides. *Cont. Shelf Res.* 35, 1–15. doi:10.1016/j.csr.2011.11.011.

Pickering, M. D., Wells, N. C., Horsburgh, K. J., and Green, J. A. M. (2017). The impact of future sea-level rise on the global tides. *Cont. Shelf Res.* 35, 1–15. doi:10.1016/j.csr.2011.11.011.

Piola, A. R., Campos, E. J. D., Möller, O. O., Charo, M., and Martinez, C. (2000). Subtropical Shelf Front off eastern South America. *J. Geophys. Res. Ocean.* 105, 6565–6578. doi:10.1029/1999JC000300.

Prime, T., Brown, J. M., and Plater, A. J. (2016). Flood inundation uncertainty: The case of a 0.5% annual probability flood event. *Environ. Sci. Policy* 59, 1–9. doi:10.1016/j.envsci.2016.01.018.

Pugh, D. (2004). *Changing sea levels : effects of tides, weather, and climate*.

Cambridge University Press Available at:

[https://books.google.de/books?id=Ysa4yymmEotYC&printsec=frontcover&hl=es&source=gbs\\_ge\\_summary\\_r&cad=0#v=onepage&q&f=false](https://books.google.de/books?id=Ysa4yymmEotYC&printsec=frontcover&hl=es&source=gbs_ge_summary_r&cad=0#v=onepage&q&f=false) [Accessed June 2, 2017].

- Pugh, D., and Woodworth, P. (2014). *Sea-level science: Understanding tides, surges, tsunamis and mean sea-level changes*. doi:10.1017/CBO9781139235778.
- Quinn, N., Lewis, M., Wadey, M. P., and Haigh, I. D. D. (2014). Assessing the temporal variability in extreme storm-tide time series for coastal flood risk assessment. *J. Geophys. Res. Ocean.* 119, 4983–4998. doi:10.1002/2014JC010197.
- Ramirez, J. A., Lichter, M., Coulthard, T. J., and Skinner, C. (2016). Hyper-resolution mapping of regional storm surge and tide flooding: comparison of static and dynamic models. *Nat. Hazards*. doi:10.1007/s11069-016-2198-z.
- Rasheed, A. S., and Chua, V. P. (2014). Secular Trends in Tidal Parameters along the Coast of Japan. *Atmosphere-Ocean* 52, 155–168. doi:10.1080/07055900.2014.886031.
- Ray, R. D. (2009). Secular changes in the solar semidiurnal tide of the western North Atlantic Ocean. *Geophys. Res. Lett.* 36, 1–5. doi:10.1029/2009GL040217.
- Rhein, M., Rintoul, S. R., Aoki, S. (Japan), Campos, E. (Brazil), Chambers, D. (USA), Feely, R. A. (USA) (USA), et al. (2013). Climate Change 2013: The Physical Science Basis(Ch3). *Clim. Chang. 2013 Phys. Sci. Basis. Contrib. Work. Gr. I to Fifth Assess. Rep. Intergov. Panel Clim. Chang.*, 62. doi:10.1017/CBO9781107415324.010.
- Salecker, D., Gruhn, A., and Schlamkow, C. (2011). Statistical analysis of hydrodynamic impacts for risk assessment of coastal areas. *J. Coast. Res.*, 1906–1910.
- Santamaria-Aguilar, S., Arns, A., and Vafeidis, A. T. A. T. (2017a). Sea-level rise impacts on the temporal and spatial variability of extreme water levels: A case study for St. Peter-Ording, Germany. *J. Geophys. Res. Ocean.* 122, 1–22. doi:10.1002/2016JC012579.
- Santamaria-Aguilar, S., Schuerch, M., Vafeidis, A. T. A. T., and Carretero, S. C. S. C. (2017b). Long-Term Trends and Variability of Water Levels and Tides in Buenos Aires and Mar del Plata, Argentina. *Front. Mar. Sci.* 4, 1–15. doi:10.3389/fmars.2017.00380.

- Santoro, P. E., Fossati, M., and Piedra-Cueva, I. (2013). Study of the meteorological tide in the Río de la Plata. *Cont. Shelf Res.* 60, 51–63.  
doi:10.1016/j.csr.2013.04.018.
- Schuerch, M., Scholten, J., Carretero, S., García-Rodríguez, F., Kumbier, K., Baechtiger, M., et al. (2016). The effect of long-term and decadal climate and hydrology variations on estuarine marsh dynamics: An identifying case study from the Río de la Plata. *Geomorphology* 269, 122–132.  
doi:10.1016/j.geomorph.2016.06.029.
- Seneviratne, S. I., Nicholls, N., Easterling, D., Goodess, C. M., Kanae, S., Kossin, J., et al. (2012). Changes in climate extremes and their impacts on the natural physical environment. *Manag. Risks Extrem. Events Disasters to Adv. Clim. Chang. Adapt. Spec. Rep. Intergov. Panel Clim. Chang.* 9781107025, 109–230.  
doi:10.1017/CBO9781139177245.006.
- Silvestri, G., and Vera, C. (2009). Nonstationary impacts of the southern annular mode on Southern Hemisphere climate. *J. Clim.* 22, 6142–6148.  
doi:10.1175/2009JCLI3036.1.
- Slangen, A. B. A., Carson, M., Katsman, C. A., van de Wal, R. S. W., Köhl, A., Vermeersen, L. L. A., et al. (2014). Projecting twenty-first century regional sea-level changes. *Clim. Change* 124, 317–332. doi:10.1007/s10584-014-1080-9.
- Studenmund, A. H. (1997). “Using Econometrics: A practical Guide,” in (Reading, Mass.: Addison-Wesley), 259–328.
- Ulm, M., Arns, A., Wahl, T., Meyers, S. D., Luther, M. E., and Jensen, J. (2016). The Impact of a Barrier Island Loss on Extreme Events in the Tampa Bay. *Front. Mar. Sci.* 3. doi:10.3389/fmars.2016.00056.
- Visbeck, M. (2009). A station-based southern annular mode index from 1884 to 2005. *J. Clim.* 22, 940–950. doi:10.1175/2008JCLI2260.1.
- Vitousek, S., Barnard, P. L., Fletcher, C. H., Frazer, N., Erikson, L., and Storlazzi, C. D. (2017). Doubling of coastal flooding frequency within decades due to sea-level rise. *Sci. Rep.* 7, 1–9. doi:10.1038/s41598-017-01362-7.
- Vousdoukas, M. I., Mentaschi, L., Feyen, L., and Voukouvalas, E. (2017). Extreme sea levels on the rise along Europe’s coasts. *Earth’s Futur.* 5, 1–20.

doi:10.1002/eff2.192.

- Vousdoukas, M. I., Mentaschi, L., Voukouvalas, E., Bianchi, A., Dottori, F., and Feyen, L. (2018a). Climatic and socioeconomic controls of future coastal flood risk in Europe. *Nat. Clim. Chang.* 8, 776–780. doi:10.1038/s41558-018-0260-4.
- Vousdoukas, M. I., Mentaschi, L., Voukouvalas, E., Verlaan, M., Jevrejeva, S., Jackson, L. P., et al. (2018b). Global probabilistic projections of extreme sea levels show intensification of coastal flood hazard. *Nat. Commun.* 9, 1–12. doi:10.1038/s41467-018-04692-w.
- Vousdoukas, M. I., Voukouvalas, E., Mentaschi, L., Dottori, F., Giardino, A., Bouziotas, D., et al. (2016). Developments in large-scale coastal flood hazard mapping. *Nat. Hazards Earth Syst. Sci.* 16, 1841–1853. doi:10.5194/nhess-16-1841-2016.
- Wadey, M. P., Cope, S. N., Nicholls, R. J., McHugh, K., Grewcock, G., and Mason, T. (2015). Coastal flood analysis and visualisation for a small town. *Ocean Coast. Manag.* 116, 237–247. doi:10.1016/j.ocecoaman.2015.07.028.
- Wahl, T. (2017). sea-level rise and storm surges, relationship status: complicated! *Environ. Res. Lett.* 12, 0–21. doi:10.1088/1748-9326/aa8eba.
- Wahl, T., and Chambers, D. P. (2015). Climate controls multidecadal variability in U. S. extreme sea level records. *J. Geophys. Res. C Ocean.* 121, 1527–1544. doi:10.1002/2014JC010443.
- Wahl, T., Haigh, I. D., Nicholls, R. J., Arns, A., Dangendorf, S., Hinkel, J., et al. (2017). Understanding extreme sea levels for broad-scale coastal impact and adaptation analysis. *Nat. Commun.* 8, 16075. doi:10.1038/ncomms16075.
- Wahl, T., Mudersbach, C., and Jensen, J. (2011). Assessing the hydrodynamic boundary conditions for risk analyses in coastal areas: a stochastic storm surge model. *Nat. Hazards Earth Syst. Sci.* 11, 2925–2939. doi:10.5194/nhess-11-2925-2011.
- Wahl, T., Mudersbach, C., and Jensen, J. (2012). Assessing the hydrodynamic boundary conditions for risk analyses in coastal areas: a multivariate statistical approach based on Copula functions. *Nat. Hazards Earth Syst. Sci.* 12, 495–510. doi:10.5194/nhess-12-495-2012.

- Williams, J., Horsburgh, K. J., Williams, J. A., and Proctor, R. N. F. (2016). Tide and skew surge independence: New insights for flood risk. *Geophys. Res. Lett.* 43, 6410–6417. doi:10.1002/2016GL069522.
- Wong, P. P., Losada, I. J., Gattuso, J.-P., Hinkel, J., Khattabi, A., McInnes, K. L., et al. (2014). *Climate Change 2014: Impacts, Adaptation, and Vulnerability. Part A: Global and Sectoral Aspects. Contribution of Working Group II to the Fifth Assessment Report of the Intergovernmental Panel of Climate Change.*
- Woodworth, P. L. (2010). A survey of recent changes in the main components of the ocean tide. *Cont. Shelf Res.* 30, 1680–1691. doi:10.1016/j.csr.2010.07.002.
- Woodworth, P. L., and Blackman, D. L. (2004). Evidence for systematic changes in extreme high waters since the mid-1970s. *J. Clim.* 17, 1190–1197. doi:10.1002/joc.761.
- Woodworth, P. L., Hunter, J. R., Marcos, M., Caldwell, P., Menéndez, M., and Haigh, I. (2017). Towards a global higher-frequency sea level dataset. *Geosci. Data J.* 3, 50–59. doi:10.1002/gdj3.42.
- Woodworth, P. L., Melet, A., Marcos, M., Ray, R. D., Wöppelmann, G., Sasaki, Y. N., et al. (2019). Forcing Factors Affecting Sea Level Changes at the Coast. *Surv. Geophys.* 40, 1351–1397. doi:10.1007/s10712-019-09531-1.



# Appendix A

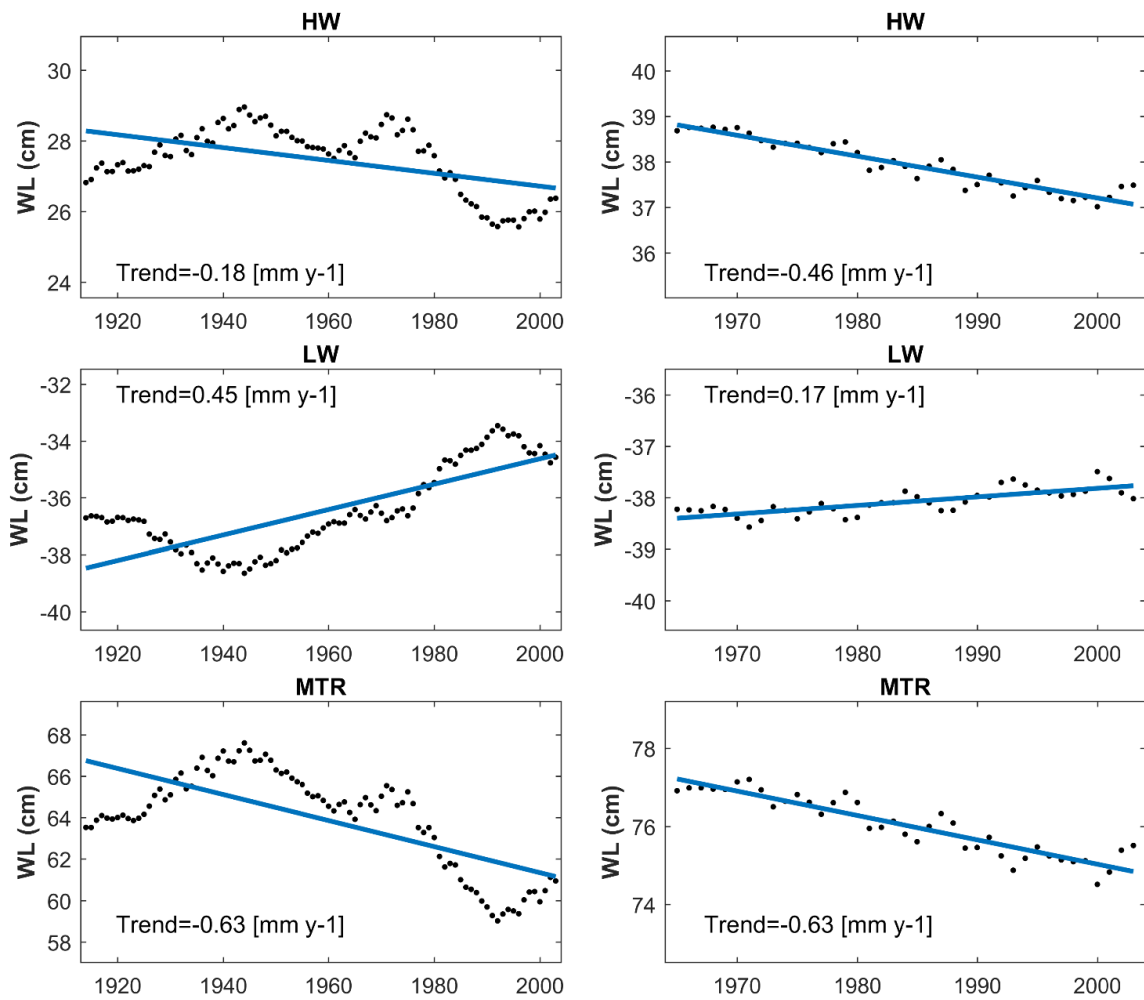


Figure A. 1 Linear trends of Annual MHW, MLW and MTR of Buenos Aires (left panels) and Mar del Plata (right panels).

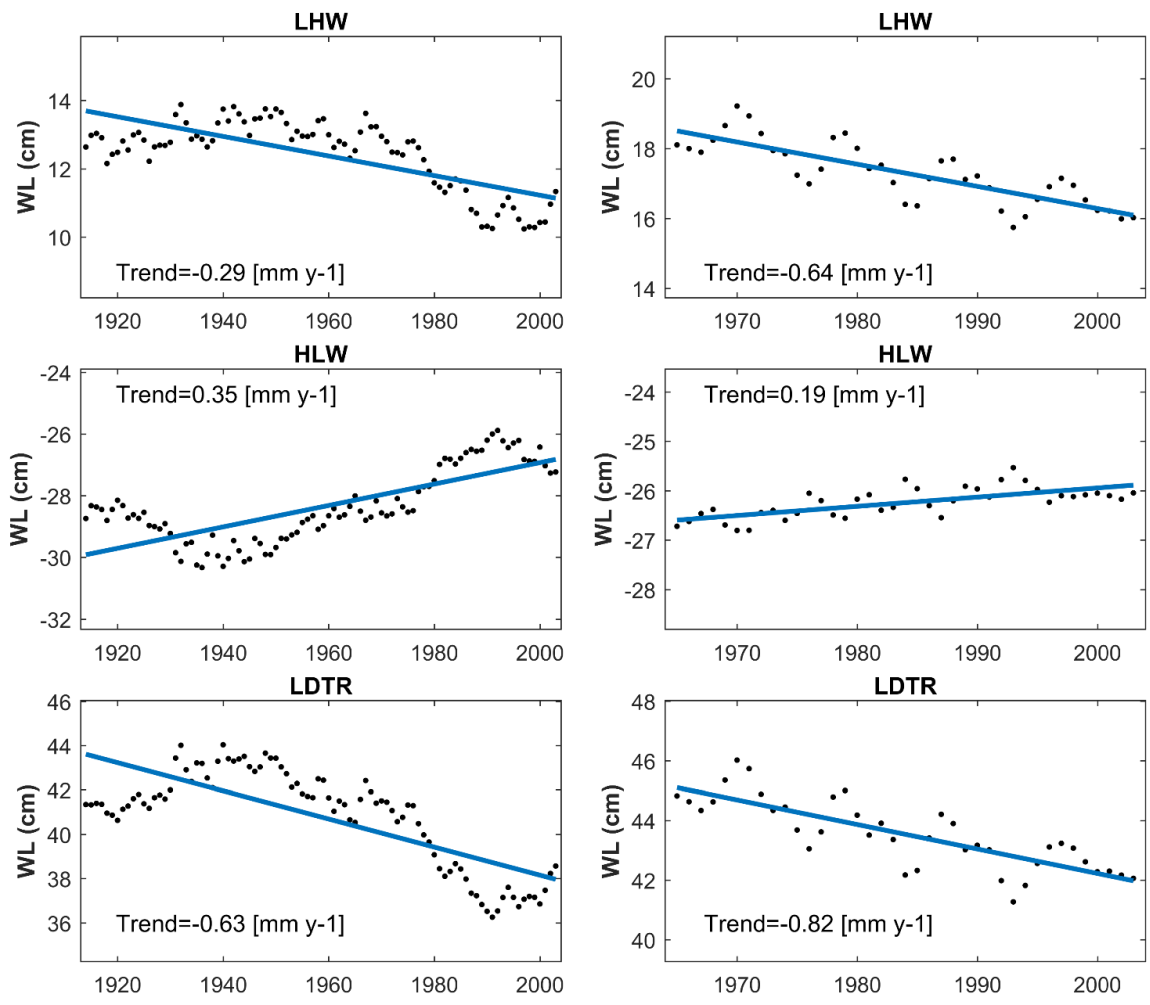


Figure A. 2 Linear trends of Annual LHW, HLW and LDTR of Buenos Aires (left panels) and Mar del Plata (right panels).

## Appendix B

### Sensitivity test of the multi-linear regression model to different data sampling methods.

We test the performance of the multi-linear regression model constructed using different data sampling methods, namely simultaneous scatter data, equally spaced quantiles and equally spaced quantiles in double logarithmic scale. The test is performed using the simulated and observed WLs of the three tide-gauge stations, assuming two of them as predictor variables and the third one as response variable.

$$S_3 = a \cdot S_1 + b \cdot S_2 \quad (1)$$

Where  $S_1$  and  $S_2$  denote the two tide-gauge stations used as predictor variables,  $S_3$  denotes the station used as response variable,  $a$  and  $b$  are the regression coefficients of the model.

The simultaneous scatter data comprises the use of all simultaneous data of the three stations to fit the model, while the other two sampling methods select a number of WLs according to their probability in linear scale (i.e. equally spaced in probability) and double logarithmic scale (i.e.  $-\log(-\log(\text{Probability}))$ ) [e.g., *Tomas, 2009*]. We select in both cases 2000 WLs in order to cover the entire range of WL values.

Therefore, multiple-linear regression models are fitted to the simulated WL sampled by the three methods mentioned above, and used to transfer the observed WLs to the response site. The performance of the models is assessed by several goodness of fit measurements such as the root mean squared error, coefficient of determination, residual scatter index and index of agreement [see e.g. *Krause et al. 2005* for further information], which are calculated using the “transferred” and observed WLs of the response gauged site.

As it can be seen in Table B.1, the best model performance is found for the regression model constructed with the quantile WLs equally space in double logarithmic scale. This is probable because a better representation of both the highest and lowest WLs is obtained by fitting the regression model using the WLs of equally spaced quantiles in double logarithmic scale as it can be seen in Figure B.1. Therefore, this sampling method is also employed to construct the linear regressions used to correct the simulated data.

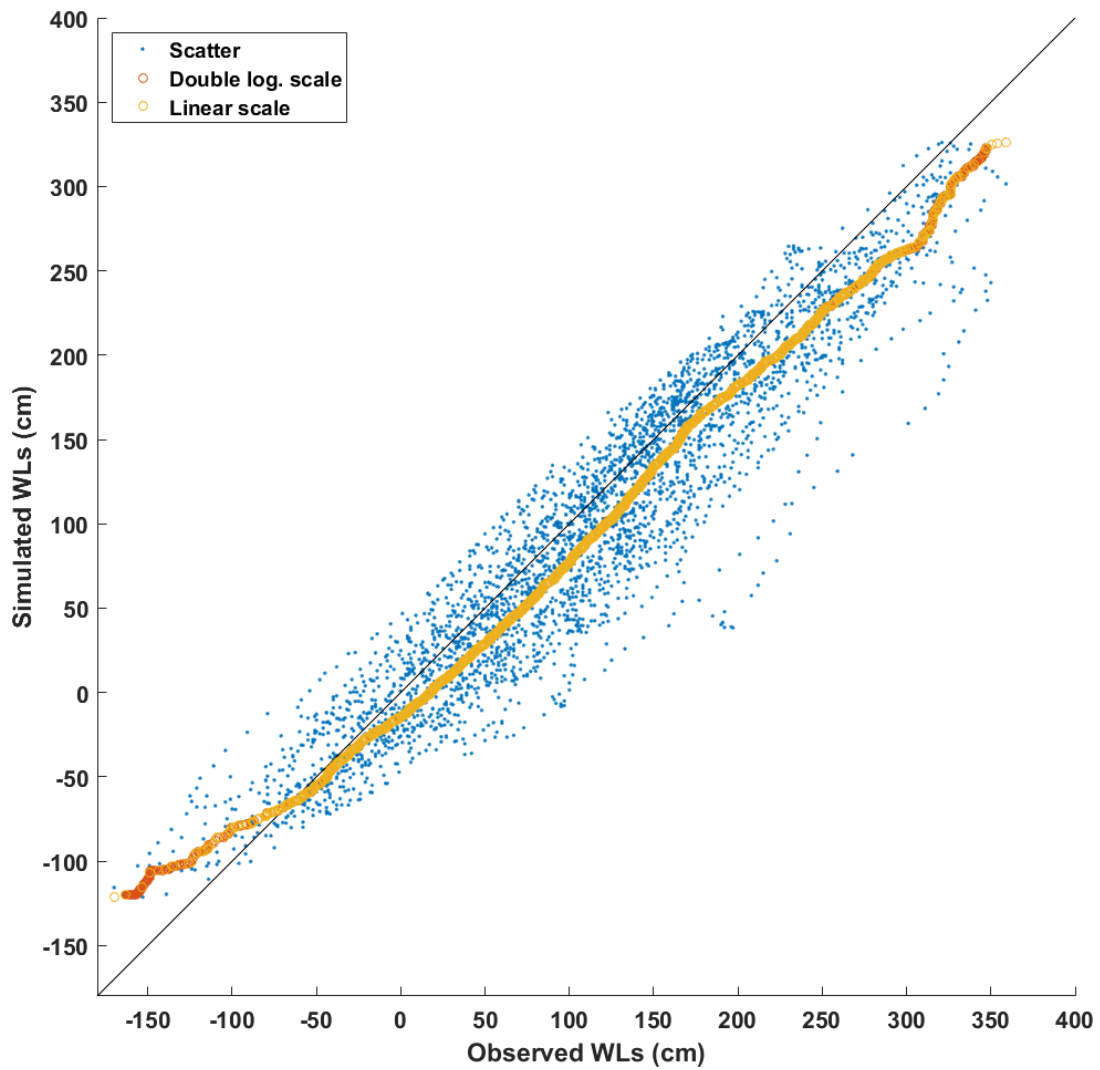


Figure B. 1 Example of the data selected by the three sampling methods tested to construct the regression models.

Table B. 1 Goodness of fit of the multiple-linear regression models constructed using the three sampling methods

Model	BIAS	RMS	R <sup>2</sup>	RSI	IA
Scatter WLs	9.4376	38.2288	0.9086	0.3365	0.9734
Linear Scale	-8.6472	34.9190	0.9225	0.3074	0.9762
Double Log Scale	-9.2379	23.0441	0.9647	0.9822	0.2028

## Appendix C

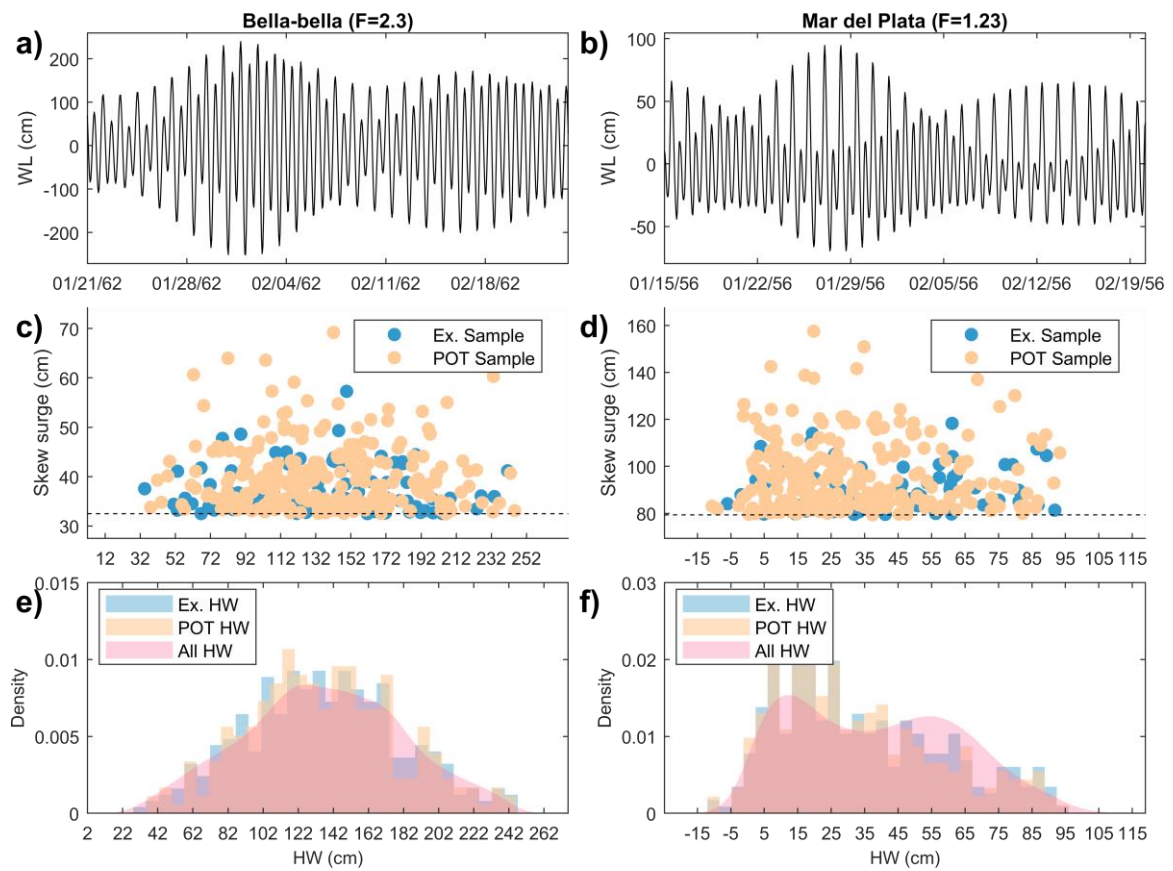


Figure C. 1 Tidal water levels of a) Bella bella and b) Mar del Plata. Scatter plots of both samples of extreme skew surges and their associated HWs for c) Bella bella and d) Mar del Plata. Histograms of HWs associated to the two extreme skew samples and PDF of all HWs of e) Bella bella and f) Mar del Plata.

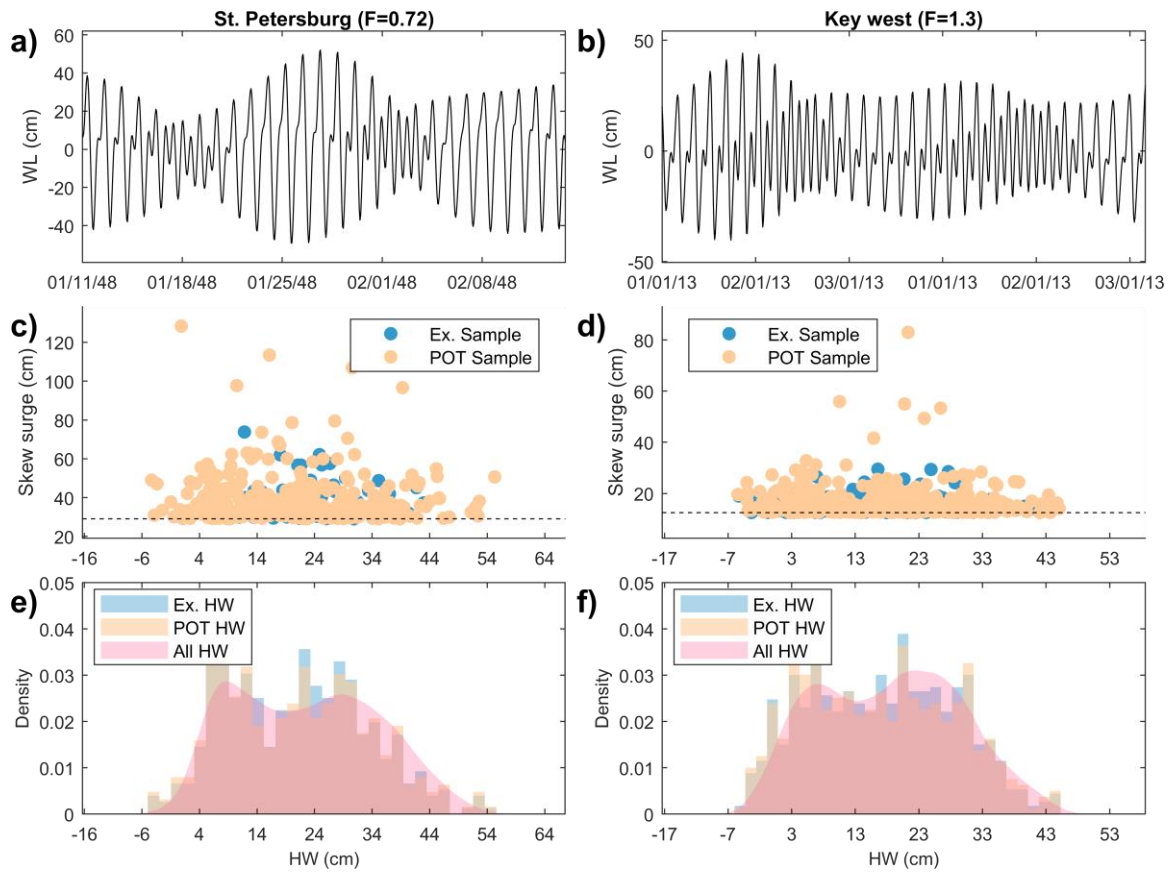


Figure C. 2 Tidal water levels of a) St. Petersburg and b) Key west. Scatter plots of both samples of extreme skew surges and their associated HWs for c) St. Petersburg and d) Key west. Histograms of HWs associated to the two extreme skew samples and PDF of all HWs of e) St. Petersburg and f) Key west.

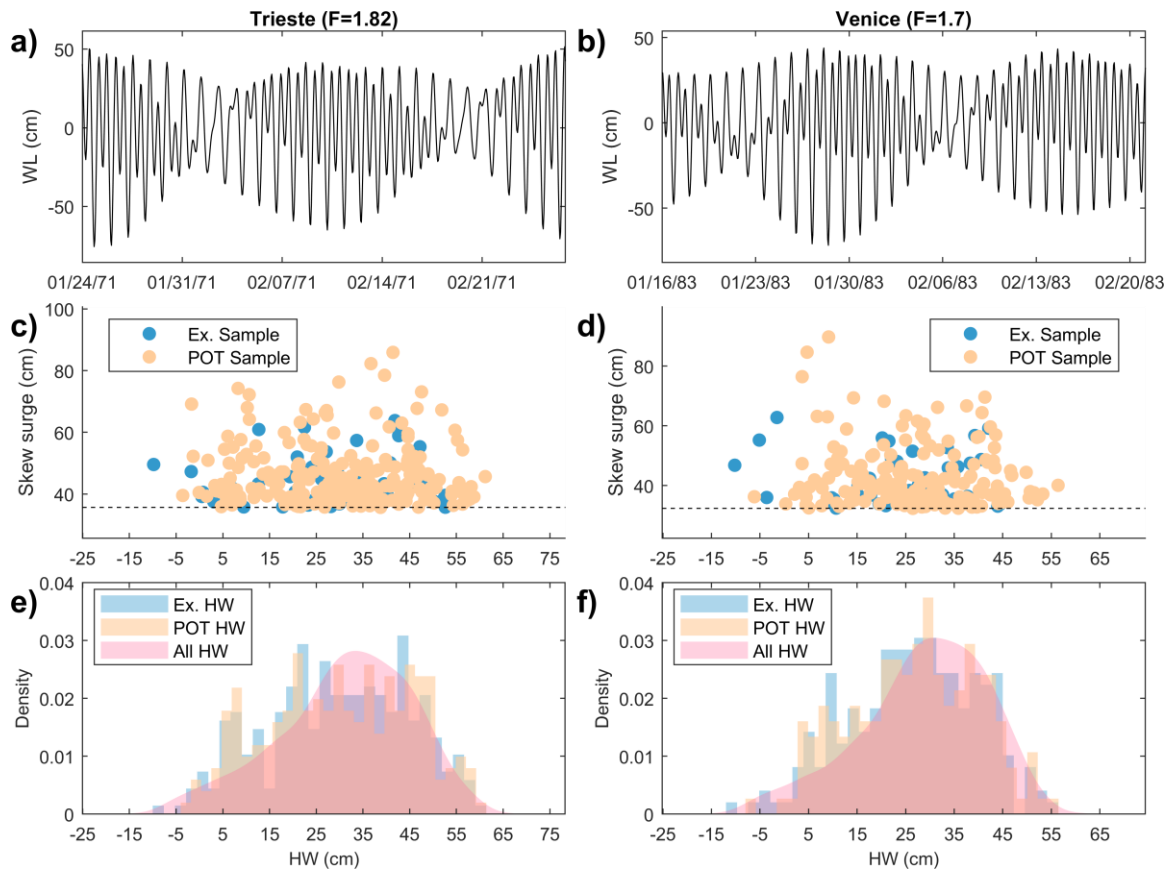


Figure C. 3 Tidal water levels of a) Trieste and b) Venice. Scatter plots of both samples of extreme skew surges and their associated HWs for c) Trieste and d) Venice. Histograms of HWs associated to the two extreme skew samples and PDF of all HWs of e) Trieste and f) Venice.

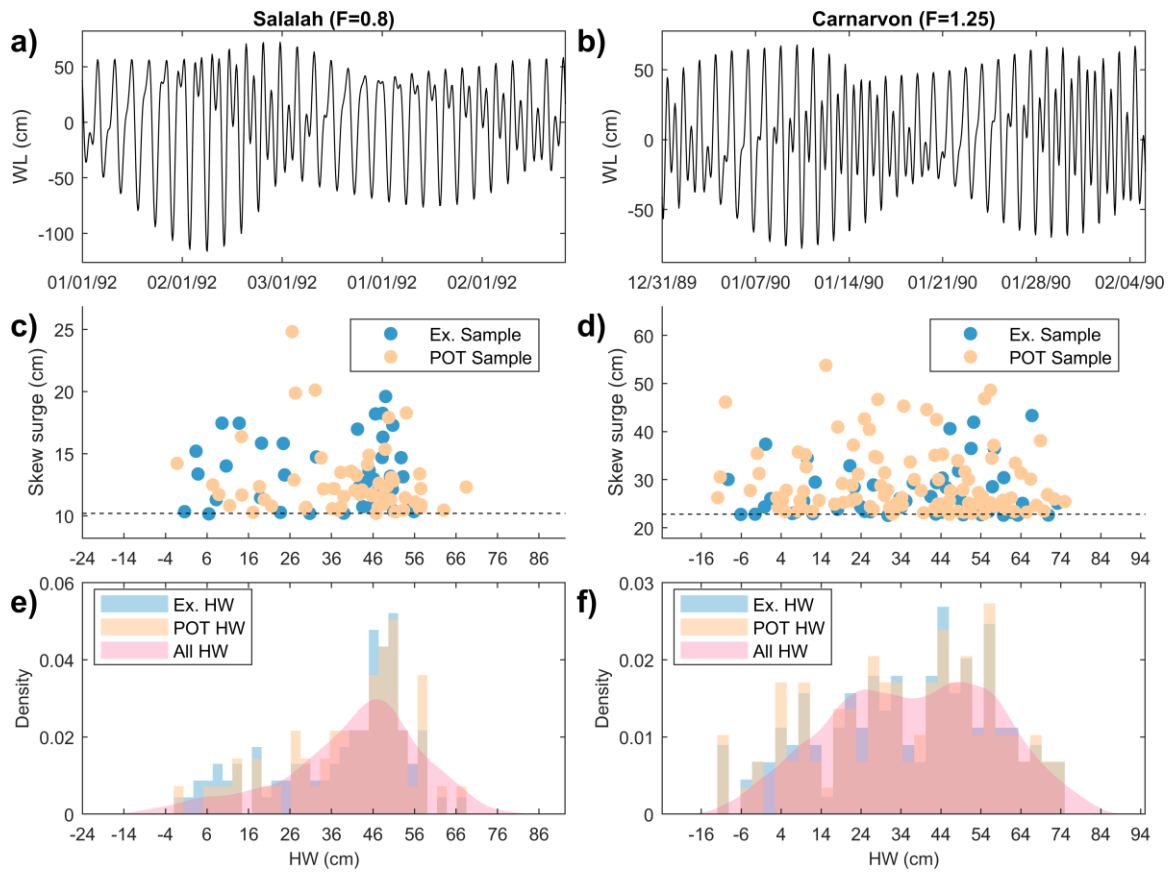


Figure C. 4 Tidal water levels of a) Salah and b) Carnarvon. Scatter plots of both samples of extreme skew surges and their associated HWs for c) Salah and d) Carnarvon. Histograms of HWs associated to the two extreme skew samples and PDF of all HWs of e) Salah and f) Carnarvon.

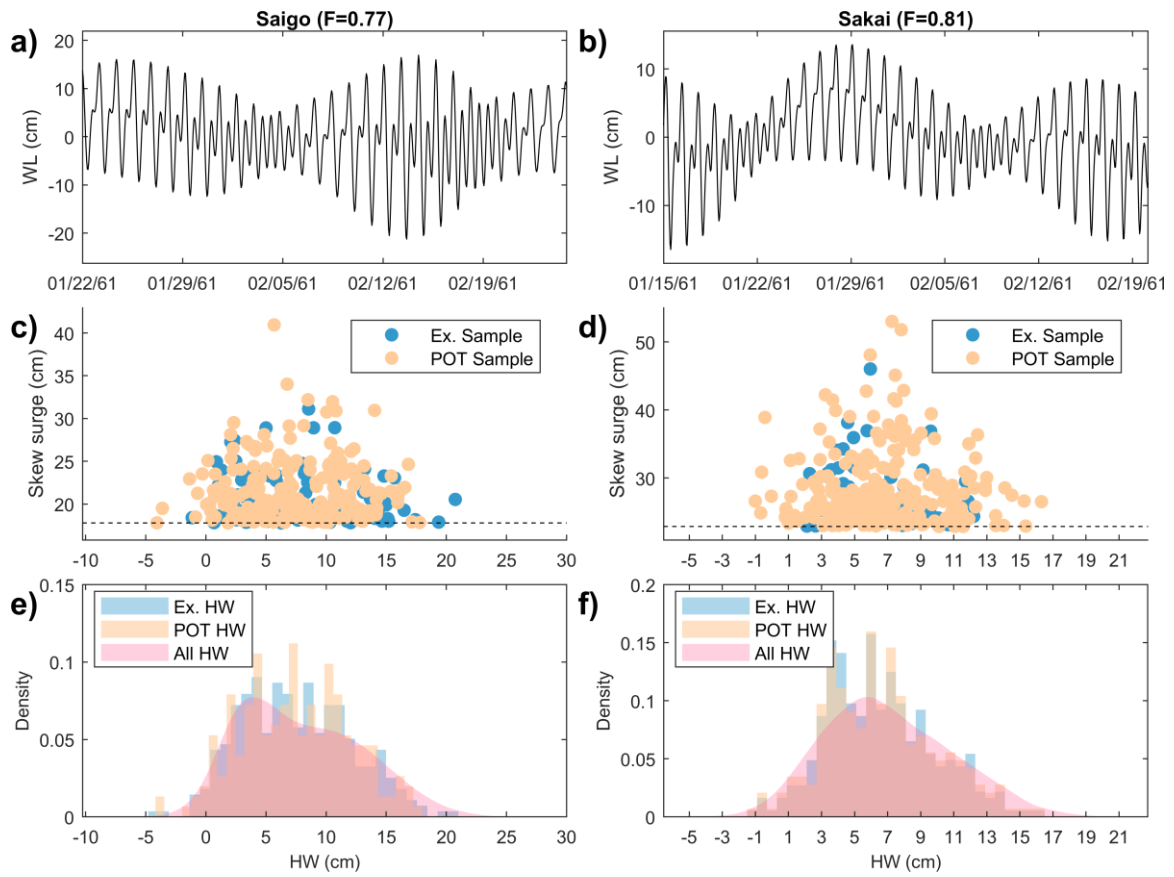


Figure C. 5 Tidal water levels of a) Saigo and b) Sakai. Scatter plots of both samples of extreme skew surges and their associated HWs for c) Saigo and d) Sakai. Histograms of HWs associated to the two extreme skew surge samples and PDF of all HWs of e) Saigo and f) Sakai.

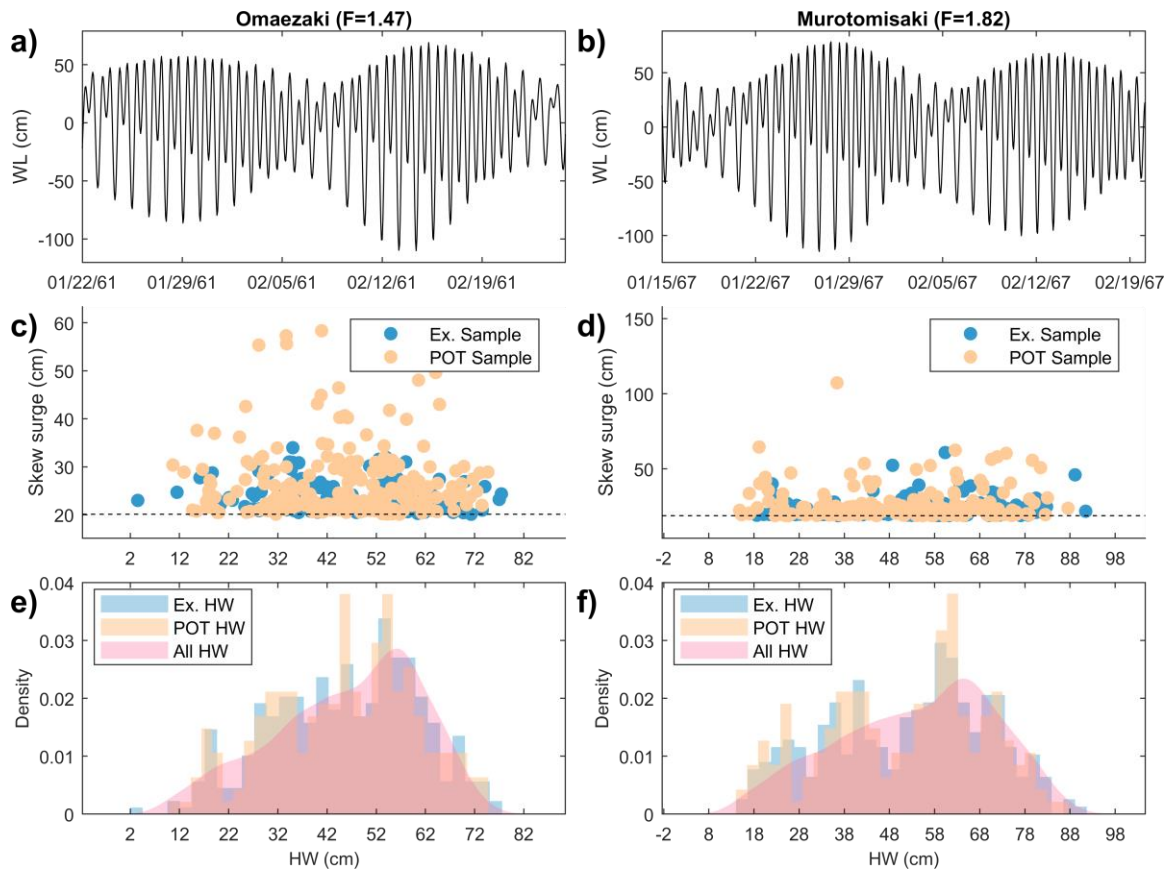


Figure C. 6 Tidal water levels of a) Omaezaki and b) Murotomisaki. Scatter plot of both samples of extreme skew surges and their associated HWs for c) Omaezaki and d) Murotomisaki. Histograms of HWs associated to the two extreme skew surge samples and PDF of all HWs of e) Omaezaki and f) Murotomisaki.

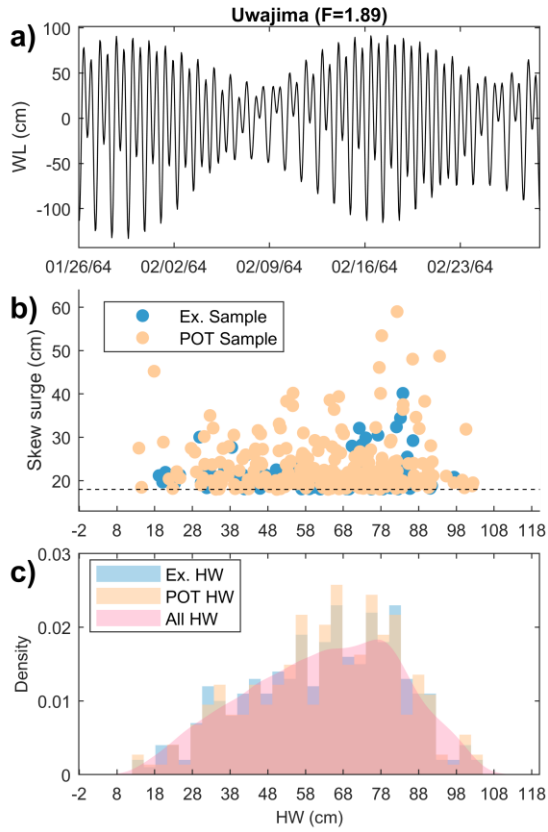


Figure C. 7 a) Tidal water levels of Uwajima. b) Scatter plots of both samples of extreme skew surges and their associated HWs. c) Histograms of HWs associated to the two extreme skew surge samples and PDF of all HWs.

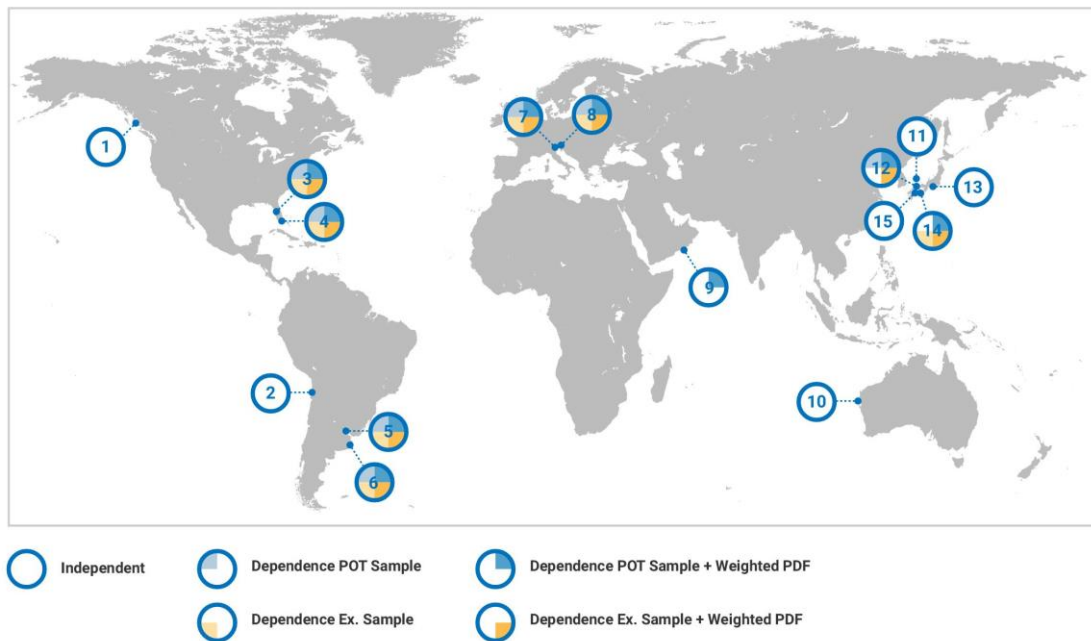


Figure C. 8 Results of the dependence analysis obtained for all tide-gauges and extreme samples. Dependent = Rejection of the null hypothesis of the Anderson-Darling test (0.01 significance level).

*Independent = The null hypothesis cannot be rejected. The null hypothesis is that HWs associated to the extreme skew sample are drawn from the same distribution as all HWs.*

*Table C. 1 Correlation (Kendall tau and p-values) between the skew surge Ex. Sample and its associated HWs for all the stations.*

<b>N°</b>	<b>Station</b>	<b>Kendall tau</b>	<b>P value</b>
1	Bella bella	-0.0160	0.6594
2	Antofagasta	0.0693	0.1072
3	St. Petersburg	-0.0450	0.1932
4	Key West	-0.0150	0.5641
5	Buenos Aires	0.0027	0.9141
6	Mar del Plata	-0.0022	0.9529
7	Trieste	-0.0190	0.6321
8	Venice	-0.0398	0.3847
9	Salalah	-0.0570	0.4073
10	Carnarvon	-0.0410	0.4514
11	Saigo	-0.0062	0.8692
12	Sakai	0.0359	0.3482
13	Omaezaki	-0.0417	0.2431
14	Murotomosaki	0.0444	0.2520
15	Uwajima	-0.0127	0.7329

*Table C. 2 Correlation (Kendall tau and p-values) between the skew surge POT sample and its associated HWs for all the stations.*

<b>N°</b>	<b>Station</b>	<b>Kendall tau</b>	<b>P value</b>
1	Bella bella	-0.0133	0.7529
2	Antofagasta	0.0798	0.1436
3	St. Petersburg	-0.0568	0.1354
4	Key West	-0.0405	0.1918
5	Buenos Aires	-0.0043	0.8723
6	Mar del Plata	0.0007	0.9871
7	Trieste	-0.0325	0.4628
8	Venice	-0.0548	0.2835
9	Salalah	-0.0929	0.3015
10	Carnarvon	-0.0867	0.1998
11	Saigo	0.0165	0.7253
12	Sakai	0.0532	0.2199
13	Omaezaki	0.0162	0.7218
14	Murotomosaki	0.0426	0.3803
15	Uwajima	-0.0285	0.5136

Table C. 3 Results of the dependence analysis ( $\alpha = 0.05$ ) obtained for all tide-gauges and extreme samples. *Dependent* = Rejection of the null hypothesis of the Anderson-Darling test. *Independent* = The null hypothesis cannot be rejected. The null hypothesis is that HWs associated to the extreme skew sample are drawn from the same distribution that all HWs.

STATION	Ex. Sample	POT Sample	Ex. Sample + Weighted PDF	POT Sample + Weighted PDF
① Bella bella	Independent	Independent	Independent	Independent
② Antofagasta	Independent	Independent	Independent	Independent
③ St. Petersburg	Dependent	Dependent	Dependent	Dependent
④ Key West	Dependent	Dependent	Dependent	Dependent
⑤ Buenos Aires	Dependent	Dependent	Dependent	Dependent
⑥ Mar del Plata	Dependent	Dependent	Dependent	Dependent
⑦ Trieste	Dependent	Dependent	Dependent	Independent
⑧ Venice	Dependent	Dependent	Dependent	Independent
⑨ Salalah	Independent	Independent	Dependent	Independent
⑩ Carnarvon	Independent	Independent	Independent	Independent
⑪ Saigo	Independent	Independent	Independent	Independent
⑫ Sakai	Dependent	Independent	Dependent	Dependent
⑬ Omaezaki	Independent	Independent	Independent	Independent
⑭ Murotomisaki	Independent	Dependent	Dependent	Dependent
⑮ Uwajima	Independent	Independent	Independent	Independent